NASA Contractor Report 181922

Heat Pipes for Wing Leading Edges of Hypersonic Vehicles

B.L. Boman, K.M. Citrin, E.C. Garner, and J.E. Stone

McDonnell Aircraft Company
St. Louis Missouri 63166

Contract NAS1-18144
January 1990

National Aeronautics and
Space Administration

Langley Research Center
Hampton, Virginia 23665

FINAL REPORT

HEAT PIPES FOR WING LEADING EDGES OF HYPERSONIC VEHICLES

by

B. L. Boman, K. M. Citrin, E. C. Garner, and J. E. Stone

December 1989

Prepared under Contract No. NAS1-18144

for

NATIONAL AERONAUTICS AND SPACE ADMINISTRATION

Langley Research Center, Hampton, VA 23665

by

McDonnell Aircraft Company (MCAIR)

McDonnell Douglas Corporation, St. Louis, MO 63166

FOREWORD

This report presents the results of a program to develop a full scale, sodium/Hastelloy X wing leading edge heat pipe. The work was performed from March 1986 through July 1989 under National Aeronautics and Space Administration (NASA) Contract NAS1-18144 by McDonnell Aircraft Company (MCAIR), St. Louis, Missouri, a division of McDonnell Douglas Corporation (MDC).

The program was sponsored by the NASA Langley Research Center (NASA LaRC) Thermal Structures Branch of the Loads and Aeroelasticity Division. The NASA technical monitor was Mr. Charles J. Camarda.

Mr. James E. Stone was the MCAIR Program Manager, with Mr. Bret L. Boman as Principal Investigator. Mr. Kenneth M. Citrin was responsible for the structural analysis. Mr. Edward C. Garner was responsible for manufacturing development and heat pipe fabrication. Special acknowledgement is given to Mr. Calvin C. Silverstein, CCS Associates, who provided guidance as program consultant.

Additional MCAIR and MDC personnel that provided valuable contributions to the program were:

Bob Calkins	- Test Stand Design, Fabrication
Ray Geckler	- Heat Pipe Design
Ralph Herring	- Technical Advisor
Marion Peeples	- Heat Pipe Conceptual Design
Chip Tefft	- Heat Pipe Wick Development

In addition, those involved in the heat pipe and test stand manufacture were: Bill Coffey, John Kozup, Angelo Lucido, Tom Pleimman, and Dan Tafft.

The program was conducted in accordance with the requirements and instructions of NASA LaRC request for proposal 1-96-2210.0014 and MCAIR Technical Proposal, Report MDC A9200, with revisions as mutually agreed upon by NASA and MCAIR. The program was conducted using customary units for the principal measurements and calculations.

TABLE OF CONTENTS

LIST OF ILLUSTRATIONS

LIST OF ILLUSTRATIONS - Continued

LIST OF ILLUSTRATIONS - Continued

LIST OF ILLUSTRATIONS - Continued

LIST OF SYMBOLS

Symbol	Equation No.(s)	Description	Units
A_e	12	Evaporator Area	ft^2
A_v	4,5	Vapor Space Area	ft^2
A_w	8,13,14	Wick Cross-Sectional Area	ft^2
C_0, C_1, C_2 C_3, C_4, C_5	2	Constants Used in Heating Rate Distribution Around the Wing Leading Edge	--
D_h	9	Vapor Space Hydraulic Diameter	ft
dx	8	Incremental Heat Pipe Length	ft
dw	fig.6	Wire diameter	in
E	15	Young's Modulus	psi
f	9,10,11	Friction factor (Darcy Weisbach)	--
f_{max}	15	Maximum Stress	psi
g	4,14	Gravitational Acceleration	ft/s^2
g_c	5,14	Gravitational Constant 32.174	$(ft \cdot lbm)/(lb_f \cdot S^2)$
h_o	fig. 5	Reference heat transfer coefficient to a one-foot radius sphere	$Btu/(ft^2 \cdot s \cdot °R)$
h_θ	fig. 5	Heat transfer coefficient at angle θ from the stagnation line	$Btu/(ft^2 \cdot s \cdot °R)$
K_e	12	Effective thermal conductivity of the wick	$Btu/(ft \cdot s \cdot °R)$
K_w	8,13,14	Wick Permeability	ft^2
L	13,14	Heat pipe length	ft
M	4	Molecular weight of the working fluid	$lbm/(lbm \cdot mol)$
$\dot{m}_L(x)$	8,13	Liquid or vapor mass flow rate	lbm/s
ΔP_c	6,7	Capillary pumping power	psf
ΔP_L	6,8,13	Liquid pressure loss	psf
ΔP_v	6,9	Vapor pressure loss	psf
ΔP_b	6	Body force pressure loss (acceleration and gravitational)	psf
$\dot{Q}$	14	Heat pipe heat transfer capability	Btu/s

Symbol	Equation No.(s)	Description	Units
$\dot{Q}_{ENTRAINMENT}$	5	Heat transfer limit based on entrainment of the liquid by vapor flow	Btu/s
$\dot{Q}_{SONIC}$	4	Heat transfer limit based on sonic vapor flow	Btu/s
q_o	1	Reference heating rate to a one-foot radius sphere	$Btu/(ft^2 \cdot s)$
q_{SL}	1	Wing leading edge stagnation line heating rate	$Btu/(ft^2 \cdot s)$
q_θ	2	Heating rate at angle θ from the stagnation line	$Btu/(ft^2 \cdot s)$
Re_v	10,11	Vapor flow Reynolds number (axial)	--
R_{LE}	1	Wing leading edge radius	ft
R_o	1	Reference heating rate radius	1.0 ft
R_u	4	Gas constant	1545 $(ft \cdot lb_f/)(lbm \cdot mol \cdot {}^\circ R)$
r_c	5,7,14	Capillary radius	ft
r_n	12	Nucleation cavity radius	ft
T_v	4,12	Vapor temperature	$^\circ R$
T_w	3	Heat pipe wall temperature (external)	$^\circ R$
$V_v(x)$	9	Vapor velocity	ft/s
Δx	fig. 6	Screen thickness	in.
Δx	fig. 32	Heat pipe spacing	in.
Δx_w	12	Wick thickness	ft
α	--	Angle-of-attack	deg
Λ	--	Wing sweep angle	deg
Λ_e	1	Effective wing sweep angle = $\sin^{-1}$ (sin Λ cos α)	deg
ϵ	3	Heat pipe surface emissivity	--
ε	fig. 6	Wick porosity	
$\Delta\epsilon$	15	Strain amplitude	in/in
ϵ_{eff}	15	Effective strain	in/in
γ	4	Ratio of specific heats	--

Symbol	Equation No.(s)	Description	Units
λ	4,5,12,14	Working fluid latent heat of vaporization	Btu/lbm
μ_L	8,13,14	Liquid viscosity	$(lb_f \cdot s)/ft^2$
ρ_L	8,13,14	Liquid density	lbm/ft^3
ρ_v	4,5,9,12	Vapor density	lbm/ft^3
σ	3	Stefan-Boltzman constant for radiation heat transfer	4.76×10^{-13} $Btu/(ft^2 \cdot s \cdot {}^\circ R^4)$
σ	5,7,12,14	Working fluid's surface tension	lb_f/ft
θ	2	Angle from wing stagnation line	radians

1.0 SUMMARY

High temperature, liquid metal heat pipes are an attractive thermal protection system option for the wing leading edges of hypersonic vehicles. Heat pipes reduce peak temperatures such that durable metallic materials can be used instead of ablative or ceramic materials. Heat pipes have no moving parts and offer improved reliability over active systems. In addition, heat pipes, because of their nearly isothermal operation, reduce steady-state temperature gradients and resulting thermal stresses.

Sodium/superalloy and lithium/refractory metal heat pipes were conceptually designed for the wing leading edges of three types of vehicles: an entry research vehicle, aerospace plane, and advanced shuttle. Since the primary program goal was to fabricate an internally instrumented heat pipe for testing and subsequent validation of design methodologies, a sodium/superalloy heat pipe for the advanced shuttle wing leading edge was selected for detailed design, analysis, and fabrication in order to insure program success. This sodium/Hastelloy X heat pipe was designed to reduce peak leading edge temperatures from 3500°F (uncooled radiation equilibrium) to 1800°F (superalloy limit). For this application, a 0.5 x 0.375 x 69.4 in. long Hastelloy X case, bent to a leading edge radius of 2.0 in., was designed. The stainless steel, diffusion bonded wick employs a variable thickness design in which the wick tapers from 10 layers in the condenser region to 4 layers in the evaporator. Thermal and structural analyses for steady-state, startup, and failure operation were performed.

Manufacturing techniques were developed for case forming, wick installation and case sealing. Installation of the wick uses an innovative technique in which a superplastically deformed titanium tube is used to apply the required pressure for diffusion bonding. The full scale heat pipe was fabricated using these techniques and was instrumented externally (thermocouples) and internally (thermocouples and pressure transducers). To verify the test article's structural integrity and measure its startup characteristics a test stand was developed to simulate reentry heating and cooling conditions. Radiant graphite heaters, evaporator region absorbers to prevent excessive side wall heat leakage, and condenser region absorbers to simulate radiation-to-sky cooling were incorporated.

2.0 INTRODUCTION

Future hypersonic vehicles will be designed to permit a large cross range during entry, synergetic plane change maneuvers, and sustained high speed flight. Such vehicles must withstand severe heating, particularly at wing leading edge and nose cap stagnation regions. These vehicles must also be designed for extensive reuse and rapid turnaround between flights. Therefore, efficient stagnation region thermal structural design concepts are needed which can accommodate high heating rates with minimal refurbishment.

Previous development efforts have shown that high temperature metallic heat pipes may be suited to meet these requirements (References 1 through 4). Heat pipes can effectively reduce structural temperatures in stagnation regions rapidly by transferring heat aft to cooler regions on the vehicle. This capability was demonstrated by radiant heating and aerothermal testing (References 1 and 2), where structural temperatures in the stagnation region were reduced from 2300°F to below 1200°F. The heat pipes used in these previous studies were one-half scale and externally instrumented to measure case temperatures. To avoid scaling considerations and to validate state-of-the-art heat pipe modeling computer codes, such as Reference 5, test data from full scale, internally instrumented liquid metal heat pipes are needed.

The prime objective of this program was to help determine the feasibility of incorporating heat pipes into the wing leading edges of hypersonic vehicles by designing and fabricating a full scale, internally instrumented heat pipe which can be used for testing and validation of relevant design methodologies. The program plan used to fulfill these objectives is shown in Figure 1. The design requirements, conceptual designs, detailed design analyses for the selected design and fabrication challenges for the heat pipe are summarized in this report. Supporting details, conclusions and recommendations are also provided.

In this study, MCAIR defined heat pipe design requirements for three hypersonic vehicle applications and conceptually designed heat pipes for their wing leading edges as described in Section 3.0. Then, with NASA's

guidance, the design concept for an advanced shuttle configuration was selected for detailed design. Designs were developed for both production and a test article. The test article, which incorporates available material gages and minimizes tooling development, represents a compromise between the optimum design and fabrication time. These designs are discussed in Section 4.0. Manufacturing techniques development and subsequent fabrication and instrumentation of the heat pipe are described in Section 5.0. Evaluation of the heat pipe during startup is presented in Section 6.0 along with the wing leading edge's ability to withstand heat pipe failure.

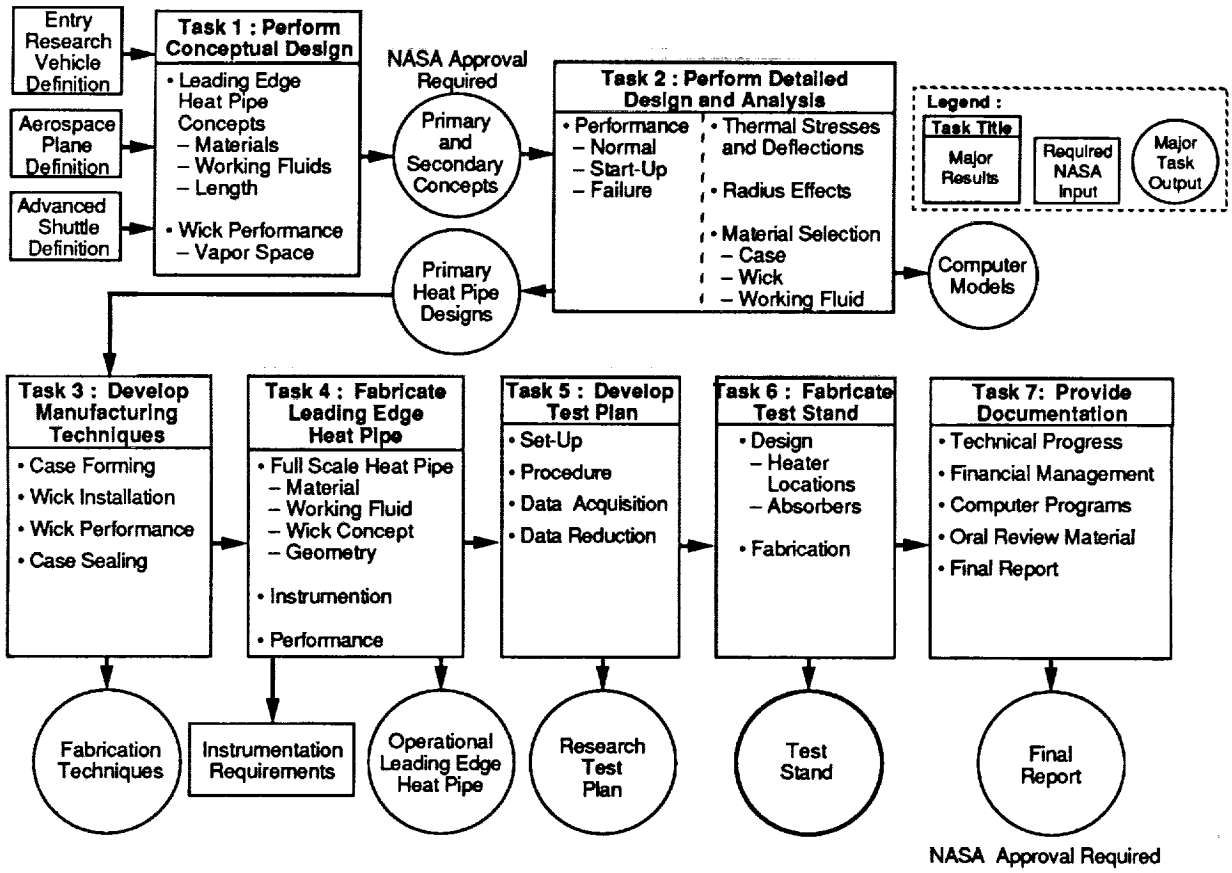

Figure 1. Program Study Plan

GP93-0239-1-D

In addition to developing and fabricating the heat pipe, plans were formulated for comprehensively testing the resultant test article and for testing a heat pipe assembly (to be possibly developed in a subsequent program) to evaluate the impact of a single heat pipe failure. A test stand was designed and fabricated to facilitate this testing. This test stand supports the heat pipe and provides the heating input and cooling capabilities necessary to accurately simulate the projected thermal environment for which the heat pipe is designed. The heat pipe test plans and test stand are discussed in Section 7.0. Program conclusions and recommendations are presented in Section 8.0.

3.0 HEAT PIPE CONCEPTUAL DESIGNS

Three hypersonic vehicle configurations were evaluated for potential application of wing leading edge heat pipes. The NASA specified configurations (Figure 2) were an Entry Research Vehicle (ERV), an aero-space (National Aero-Space Plane (NASP) type) plane, and an advanced space shuttle configuration. These vehicles represent a wide range of leading edge geometry, heating rates, and operating characteristics which can significantly effect leading edge heat pipe design.

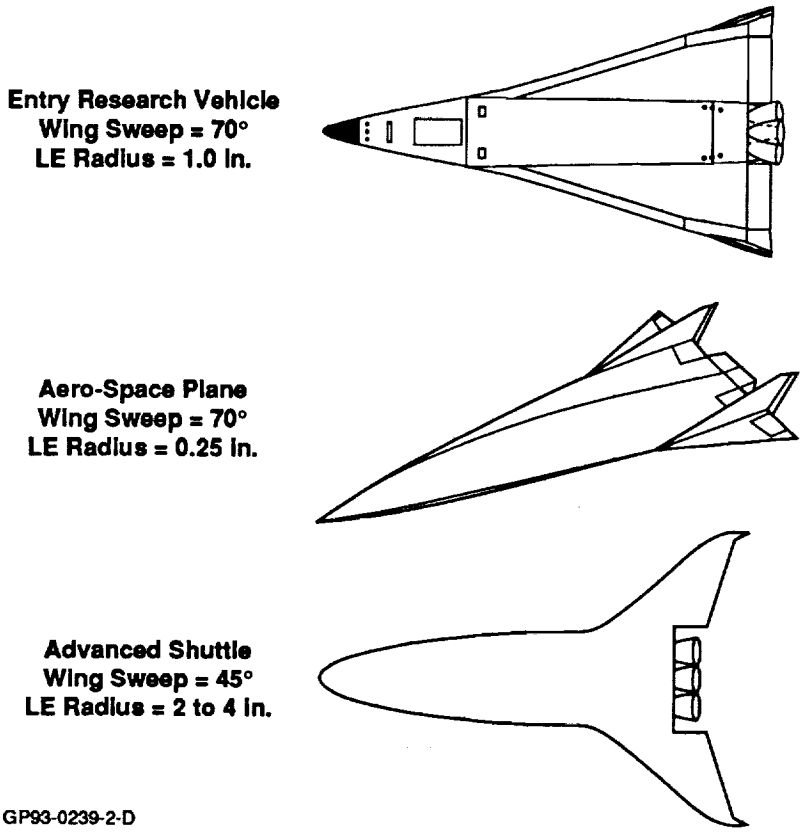

Figure 2. Hypersonic Vehicle Geometries Used for Conceptual Designs

Two classes of heat pipes were evaluated: sodium/superalloy heat pipes operating at 1800°F and lithium/refractory metal heat pipes operating at 2400°F. At the expected wing leading edge heat pipe operating temperatures (> 1500°F), liquid metals (e.g., sodium and lithium) are used for the working fluid because of their low vapor pressures, high thermal conductivity, and good transport properties at high temperatures. It is the vapor pressure that drives the case (pressure vessel) wall thickness and, hence, weight.

The purpose of the conceptual design effort was to assess the feasibility of incorporating heat pipes in these vehicles and to obtain an understanding of sensitivities to variations in design requirements. No attempts to optimize the design, conduct stress analysis, or provide detailed dimensions were made during this phase of the program. Heat pipe lengths, heat transfer vapor space, and wicking requirements were determined for each configuration using the approach described below.

3.1 METHODOLOGIES

One program objective was to develop a rapid, yet comprehensive analytical tool for preliminary heat pipe sizing studies. As described in this section, existing methodologies were assembled and integrated into an IBM PC based heat pipe sizing computer code to define length, vapor space, and wicking requirements for a given wing leading edge geometry and trajectory point.

Heat pipe lengths were determined by balancing the integrated aerothermal convective heating rates around the wing leading edge with the radiative cooling for a given heat pipe operating temperature (see Figure 3).

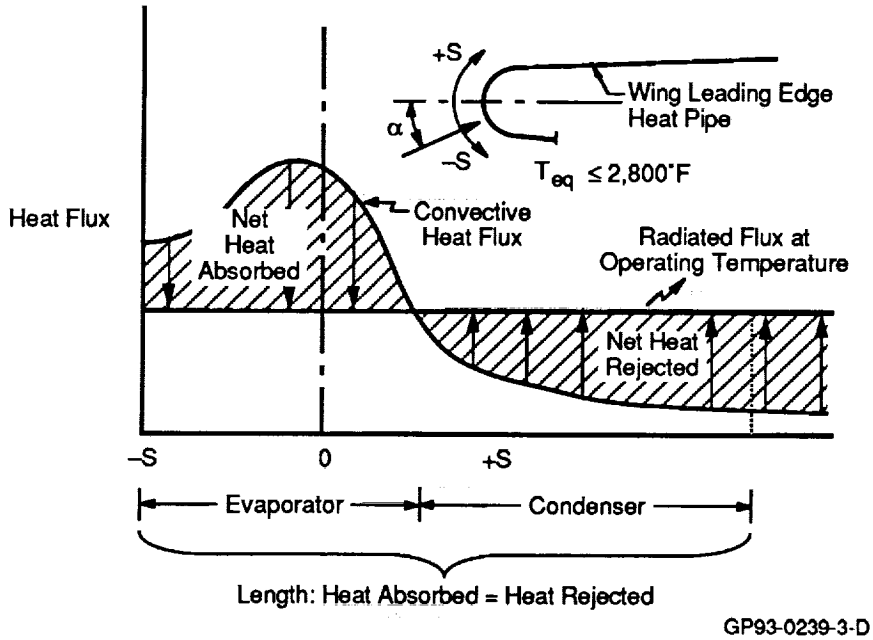

Figure 3. Heat Pipe Length Determined From Heat Balance

The heat pipe was assumed, with NASA's concurrence, to begin on the wing lower surface at a point where the radiation equilibrium temperature is equal to 2800°F (aft of this point on the lower surface, carbon-carbon or other hot structure would be employed). The heat pipe continues around the leading edge and ends on the upper wing surface when the net heat rejected in the condenser (radiation less convection) equals the net heat absorbed in the evaporator (convection less radiation).

Thus, the length is determined when the areas above and below the radiative heat flux line shown in Figure 3 are equal. As the heat pipe operating temperature increases, the radiative cooling increases significantly and the aerothermal heat load decreases slightly. Obviously, this reduces the required heat pipe length.

To calculate and then integrate the aerothermal convective heating rates, the leading edge was divided into three areas as shown in Figure 4: stagnation line; cylindrical region from the stagnation line to the radius tangency point; and the flat plate region beyond the tangency point. Heating rates in each area were determined using the relationships described below.

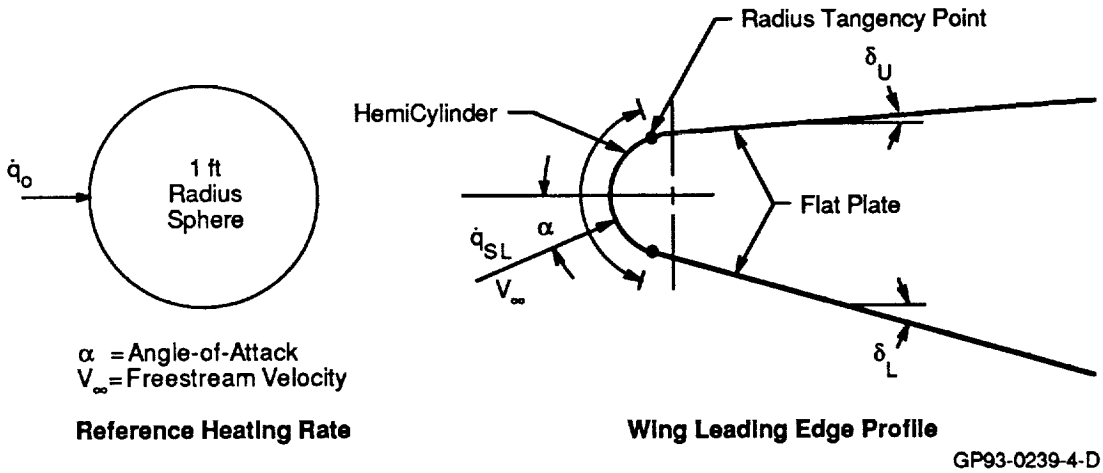

Figure 4. Reference Nomenclature for Wing Leading Edge Heating Calculations

The stagnation line heating rates were calculated using the following swept cylinder relationship from Reference 6.

$$\dot{q}_{SL} = \dot{q}_o \frac{1}{\sqrt{2}} \left(\frac{R_o}{R_{LE}}\right)^{0.5} \cos^{1.1} \Lambda_e \qquad (1)$$

The reference heating rates for a one-foot radius sphere, $\dot{q}_o$, were evaluated using the MINIVER computer code (Reference 7) for the trajectory velocities and altitudes.

The heating rate distribution around the leading edge, between the stagnation line and the radius tangency point (See Figure 4) was determined by curve fitting the swept infinite cylinder laminar heating distributions obtained from Reference 8 and shown in Figure 5. The resulting curve fit is shown below.

$$\frac{\dot{q}_\theta}{\dot{q}_{SL}} = C_o + C_1\theta + C_2\theta^2 + C_3\theta^3 + C_4\theta^4 + C_5\theta^5 \qquad (2)$$

where

$C_0 = 0.995605$; $C_1 = 9.3695 \times 10^{-2}$; $C_2 = 0.735023$;

$C_3 = 4.35835 \times 10^{-3}$; $C_4 = 0.230707$; $C_5 = 5.7874 \times 10^{-2}$

Heating rates aft of the cylinder/flat surface tangency point were assumed to decrease with the square root of the distance from this point (laminar flow) and were limited to a minimum $0.025\ \dot{q}_{SL}$.

The radiation heat transfer rate from the heat pipe surface to the sky was calculated as:

$$\dot{q} = \sigma\ \varepsilon\ (Tw^4) \qquad (3)$$

Once the heat pipe heat transfer requirement (i.e., net heat absorbed in the evaporator and transferred to the condenser) and required length were determined, the vapor space and wick requirements were determined using steady-state heat pipe limits.

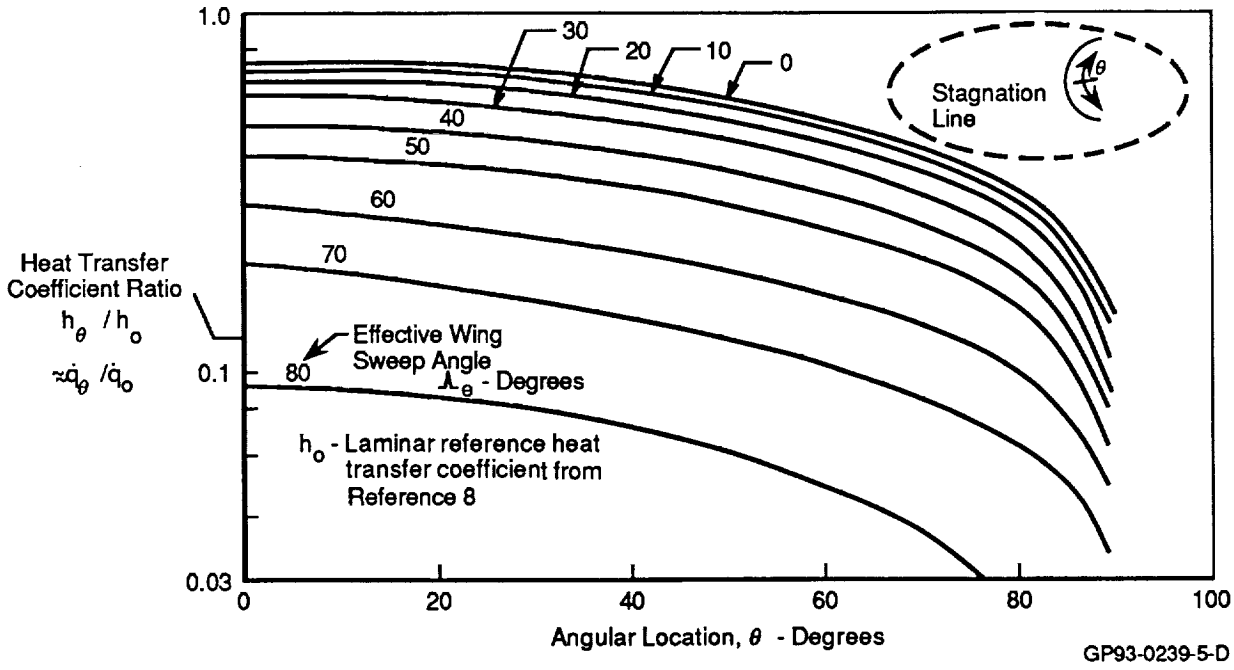

Figure 5. Swept Infinite Cylinder Laminar Heating Rate Distribution

The vapor space must be sized such that the vapor velocities are less than sonic flow and do not result in removing or entraining the counter-current, liquid flow in the wick structure. (The exception to this is during startup when sonic vapor flow is tolerable. This is discussed in Section 6.0).

Reference 9 and other general heat pipe theory texts (e.g., Reference 10) provide the following expressions for determining the maximum heat pipe heat transfer capacities based on sonic flow and entrainment considerations.

$$\dot{Q}_{SONIC} = \frac{A_V \rho_V \lambda \left(\frac{\gamma g_c R_u T}{M}\right)^{1/2}}{(2(\gamma+1))^{1/2}} \qquad (4)$$

$$\dot{Q}_{ENTRAINMENT} = A_V \lambda \left(\frac{\sigma \rho_V g_c}{2 r_c}\right)^{1/2} \qquad (5)$$

Where A_V = vapor space area

Thus, the minimum vapor space can be determined by substituting the heat pipe's required heat transfer capability into the above equations and solving for A_V.

The wick requirements were determined from the heat pipe pressure balance and prevention of boiling in the wick structure. The wick provides the pumping power, via capillary forces, for the liquid flow through the wick but is also is responsible for the pressure losses through the wick. The governing pressure balance is:

$$\Delta P_c = \Delta P_L + \Delta P_v + \Delta P_b \tag{6}$$

Again, Reference 9 and other heat pipe texts provide expressions for these pressure terms. The capillary pumping power of the wick, ΔP_c, is a function of wick capillary radius, r_c, and is expressed as:

$$\Delta P_c = \frac{2\sigma}{r_c} \tag{7}$$

While general wick characteristic values, such as the capillary radius (r_c), are tabulated in many sources, accurate values must be determined experimentally. Recognizing this limitation, Figure 6 which lists characteristic values for screen wick was used as a guide in wick preliminary design.

Pressure loss through the wick due to liquid flow is given by:

$$\Delta P_L = \frac{1}{K_w A_w} \frac{\mu_L}{\rho_L} \int \dot{m}\,(x)\, dx \tag{8}$$

Again, wick characteristic values such as the permeability-area product ($K_w A_w$) must be determined experimentally. The representative values ($K_w A_w$) used for preliminary design are also provided in Figure 6.

Pressure loss through the vapor space due to vapor flow is given by:

$$\Delta P_v = \frac{\rho_v f}{2 D_h} \int V_v^2(x)\, dx \tag{9}$$

where the friction factor, f, is evaluated based on boundary layer status as follows:

$$f = \frac{64}{Re} \text{ for } Re \leq 2000 \text{ (Laminar Flow)} \quad (10)$$

$$f = .184\ Re^{-0.2} \text{ for } Re > 2000 \text{ (Turbulent Flow)} \quad (11)$$

Parameter	Mesh Size – No. of Wires/in.			
	400	200	100	50
r_c ~Nominal Pore Radius ~ ft	1.04E-4	2.08E-4	4.17E-4	8.40E-6
r_c ~Maximum Pore Radius ~ft	1.35E-4	2.57E-4	5.02E-4	9.48E-4
K_w~ Permeability *~ft ^{2}	1.57E-10	5.84E-10	2.08E-9	9.24E-9
ϵ ~ Porosity	0.6701	0.6536	0.6289	0.6510
dw ~ Wire Diameter ~ in	0.0010	0.0021	0.0045	0.0085
ΔX ~ Screen Thickness ~ in	0.0023	0.0047	0.0094	0.0192

$^{*} K_w = dw^2\ \epsilon^3/(122\ (1-\epsilon)^2)$ GP93-0239-6-D

Figure 6. Typical Screen Wick Characteristics

From equations 7 and 8, it is evident that the wick must be designed to maximize the pumping power and minimize the liquid pressure loss. An additional consideration for wick design is that the wick in the evaporator region must be sized to prevent boiling within the wick structure. Normally, boiling occurs at the wick/vapor interface. Should boiling occur in the wick, the liquid will not be replenished and the case and wick structure will experience a sudden temperature increase potentially resulting in heat pipe failure. An expression for the maximum heat pipe heat transfer capacity to prevent boiling the the wick is provided by Reference 9, as a function of wick thickness, ΔX_w.

$$\dot{Q}_{BOILING} = \frac{2\sigma K_e A_e T_v}{\Delta X_w\ \lambda\ \rho_v} \left[\frac{1}{r_n} - \frac{1}{r_c}\right] \quad (12)$$

As part of this program, the aforementioned methodologies for calculating leading edge heat pipe heat limits, lengths, vapor space area, and wicking requirements were incorporated into an interactive,

stand-alone computer code. The code logic flow is shown in Figure 7. User inputs of wing geometry, heat pipe operating temperature, case emissivity, and the reference heating rate (obtained using the trajectory and MINIVER) are used in the heat balance to calculate the heat pipe length and heat transfer requirements. Initial estimates of the vapor space and wick structure are input by the user. The heat pipe heat transfer requirements is compared with the sonic flow and entrainment based heat transfer limits. Should the heat transfer requirement exceed these limits, the user must increase the vapor space. Once the vapor space is acceptable, the heat transfer requirement is compared to the boiling limit (based on the evaporator wick thickness). Should the boiling limit be exceeded the user must decrease the evaporator wick thickness. Next, a pressure balance is performed based on the user's wick input. Should the pressure losses exceed the pumping power, an additional wick-permeability area product (i.e., hydraulic conductance) is calculated which would balance the pressures. Then, the wick design is altered to provide this additional term. The end results of the code are the heat pipe length, vapor space and wicking requirements.

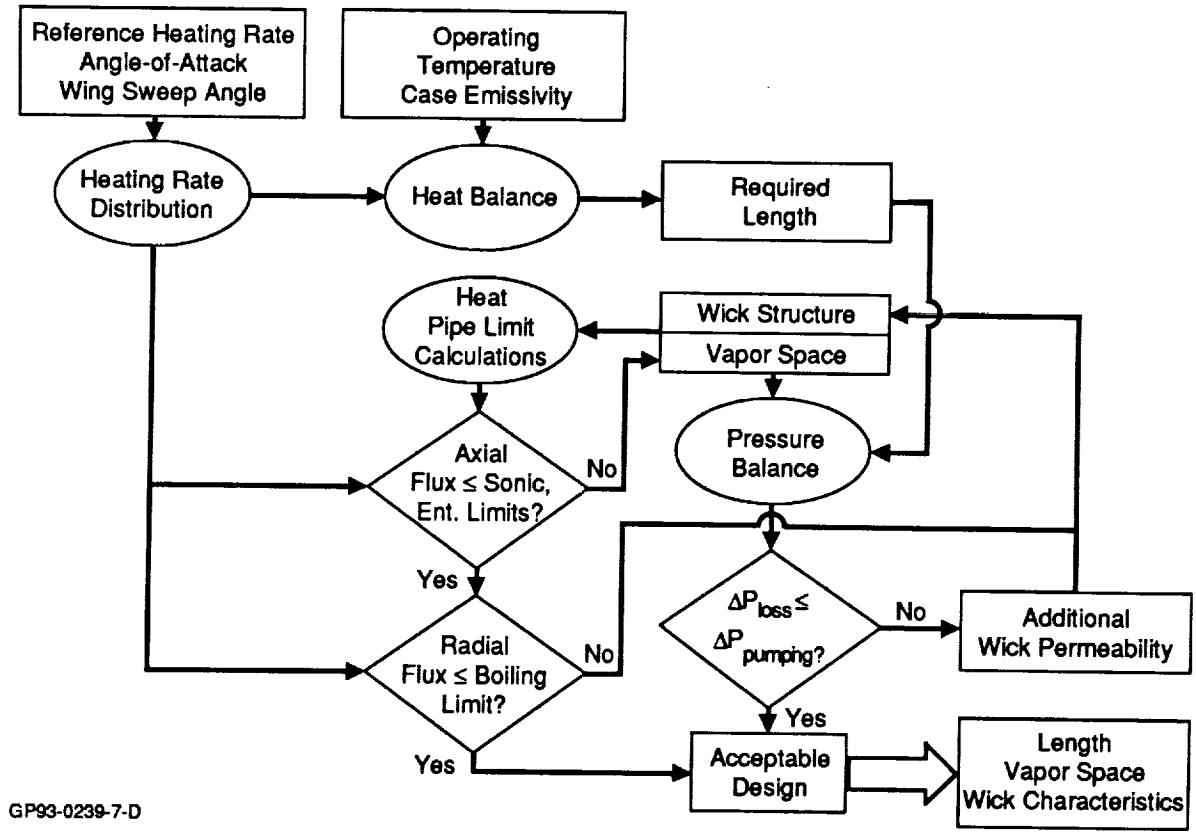

Figure 7. Heat Pipe Sizing Program

3.2 VEHICLE WING LEADING EDGE APPLICATIONS

Wing leading edge heat pipes were conceptually designed for: an ERV, an aerospace plane, and an advanced space shuttle, using the heat pipe sizing computer code. Some parametric studies were performed around each conceptual design to increase the understanding of heat pipe design sensitivities and limitations.

3.2.1 Entry Research Vehicle - The ERV, shown in Figure 8, has a leading edge radius of 1.0 in. and a wing sweep angle of 70°. Two trajectories, an earth atmospheric re-entry and a synergetic plane change (Figures 9 and 10), were used to determine the heat pipe design point. Both trajectories have a maximum reference heating rate of 125 Btu/(ft^2•s) (see Figures 11 and 12). However, because of its higher angle-of-attack operation, the synergetic plane change results in higher stagnation line heating. This higher heating rate was selected as the ERV leading edge heat pipe design point.

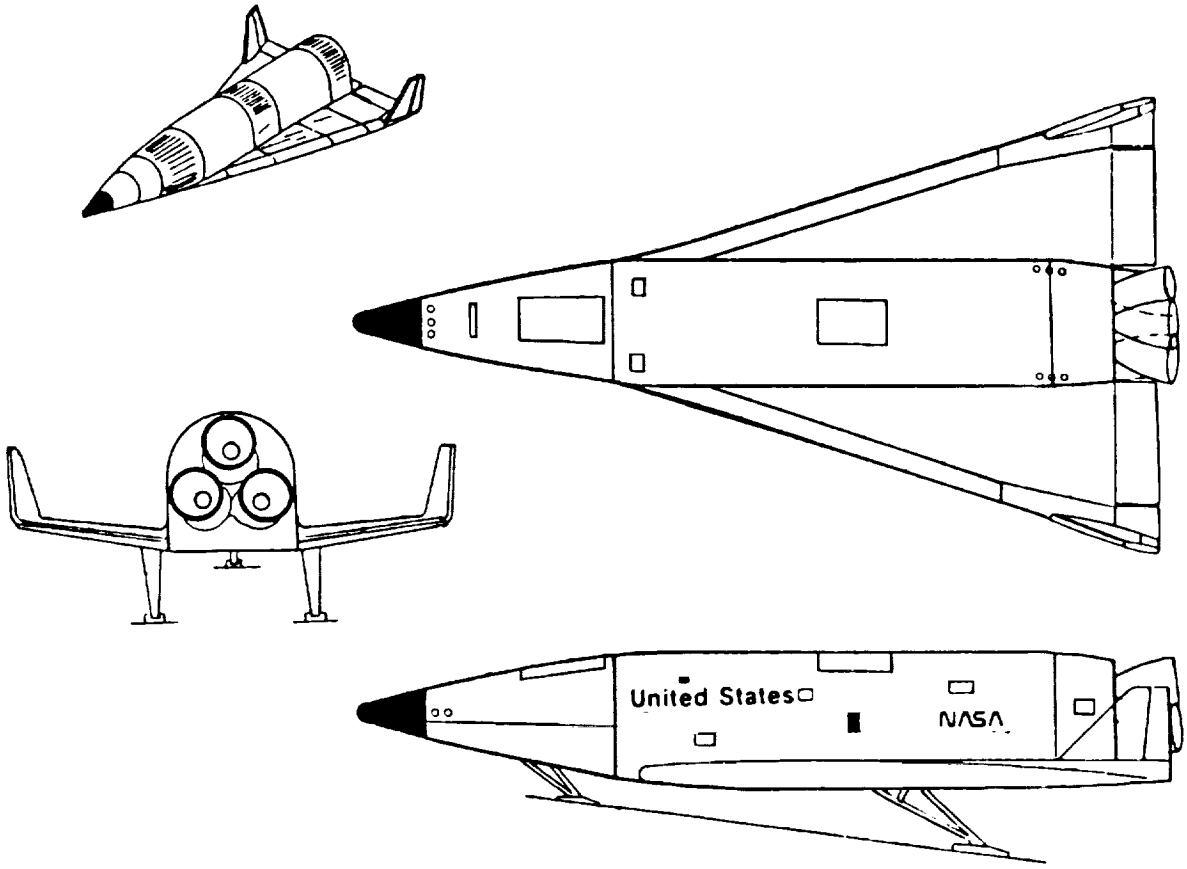

GP93-027

Figure 8. Entry Research Vehicle

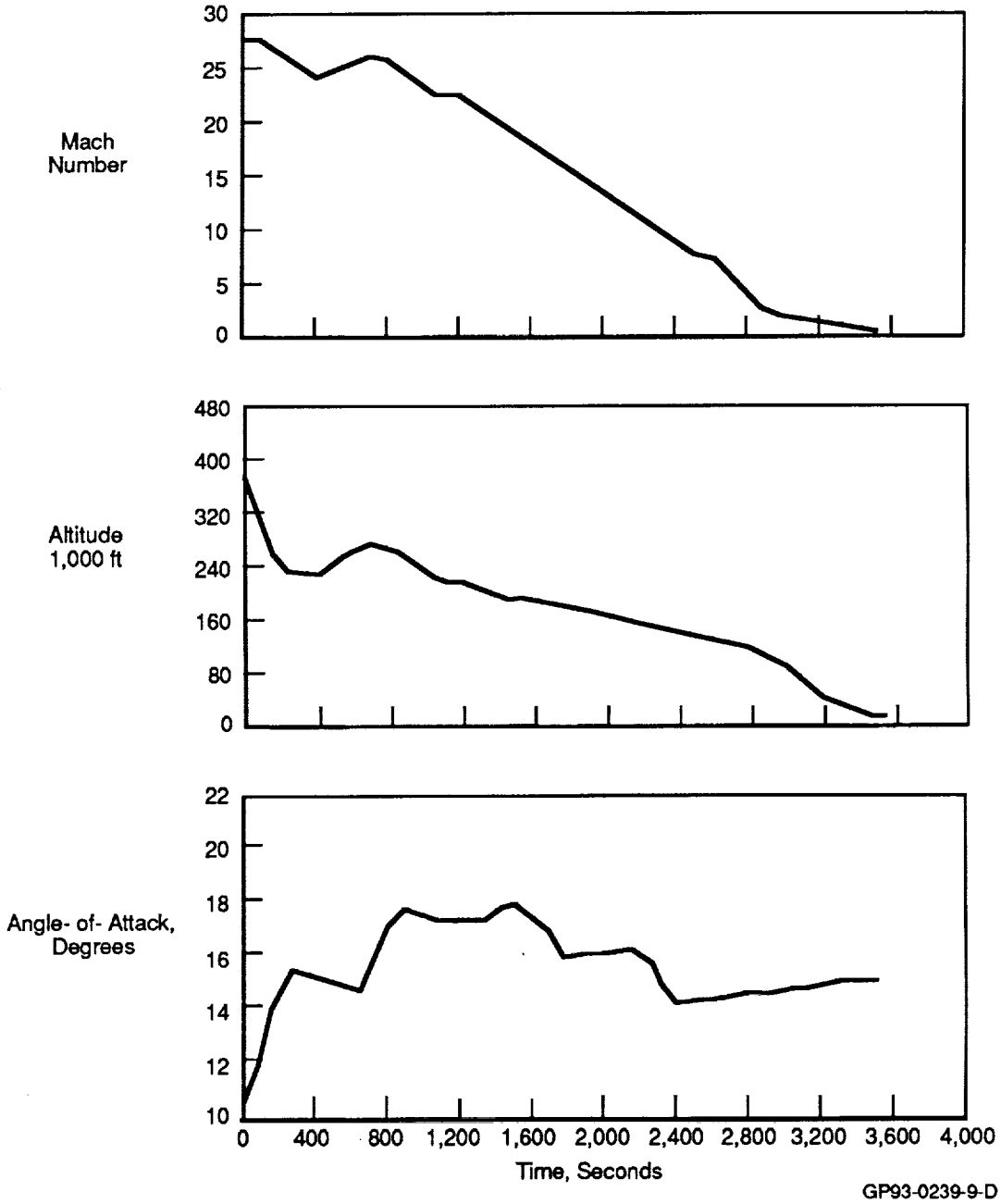

Figure 9. Entry Research Vehicle Re-Entry Trajectory

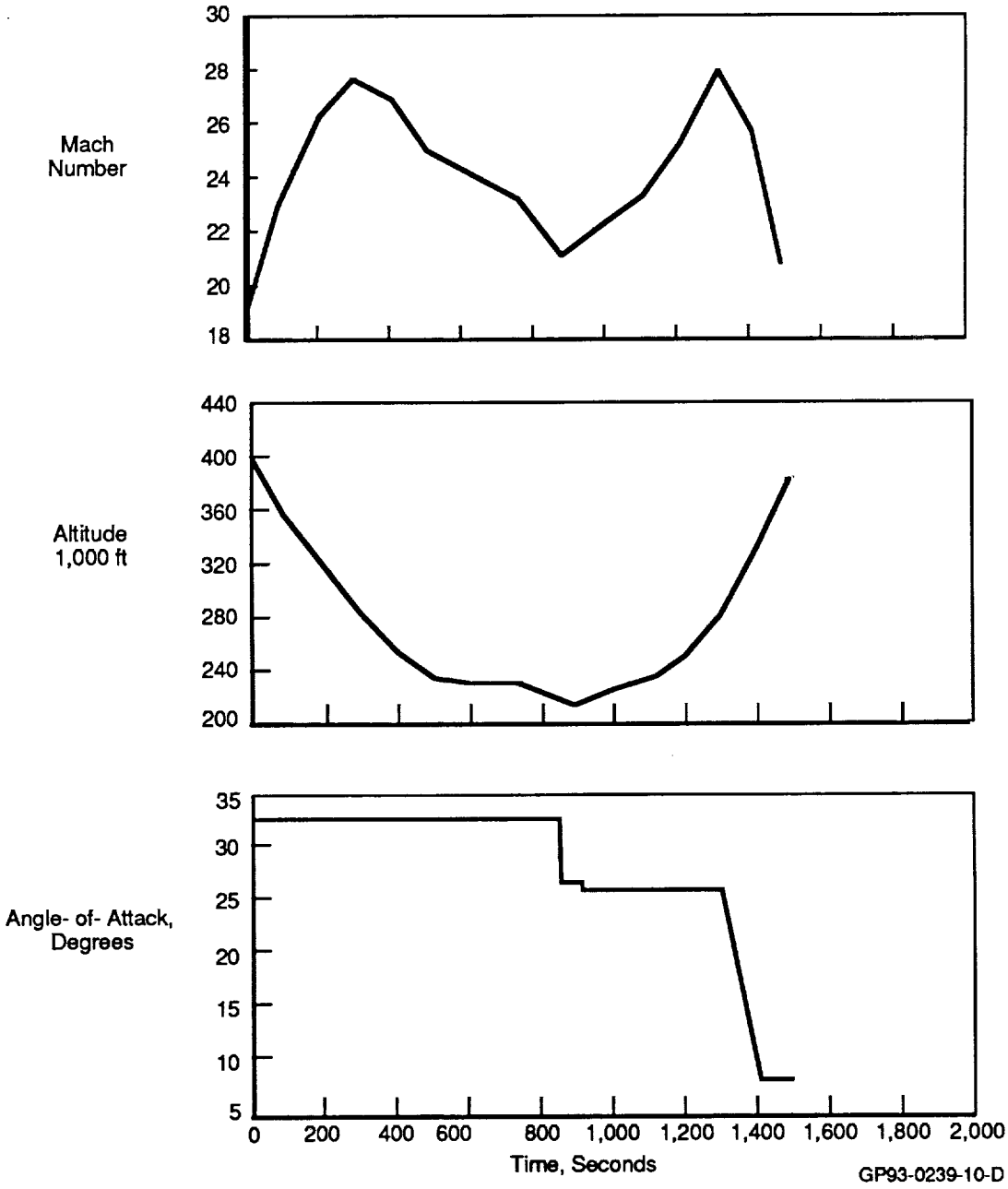

Figure 10. Entry Research Vehicle Synergetic Plane ChangeTrajectory

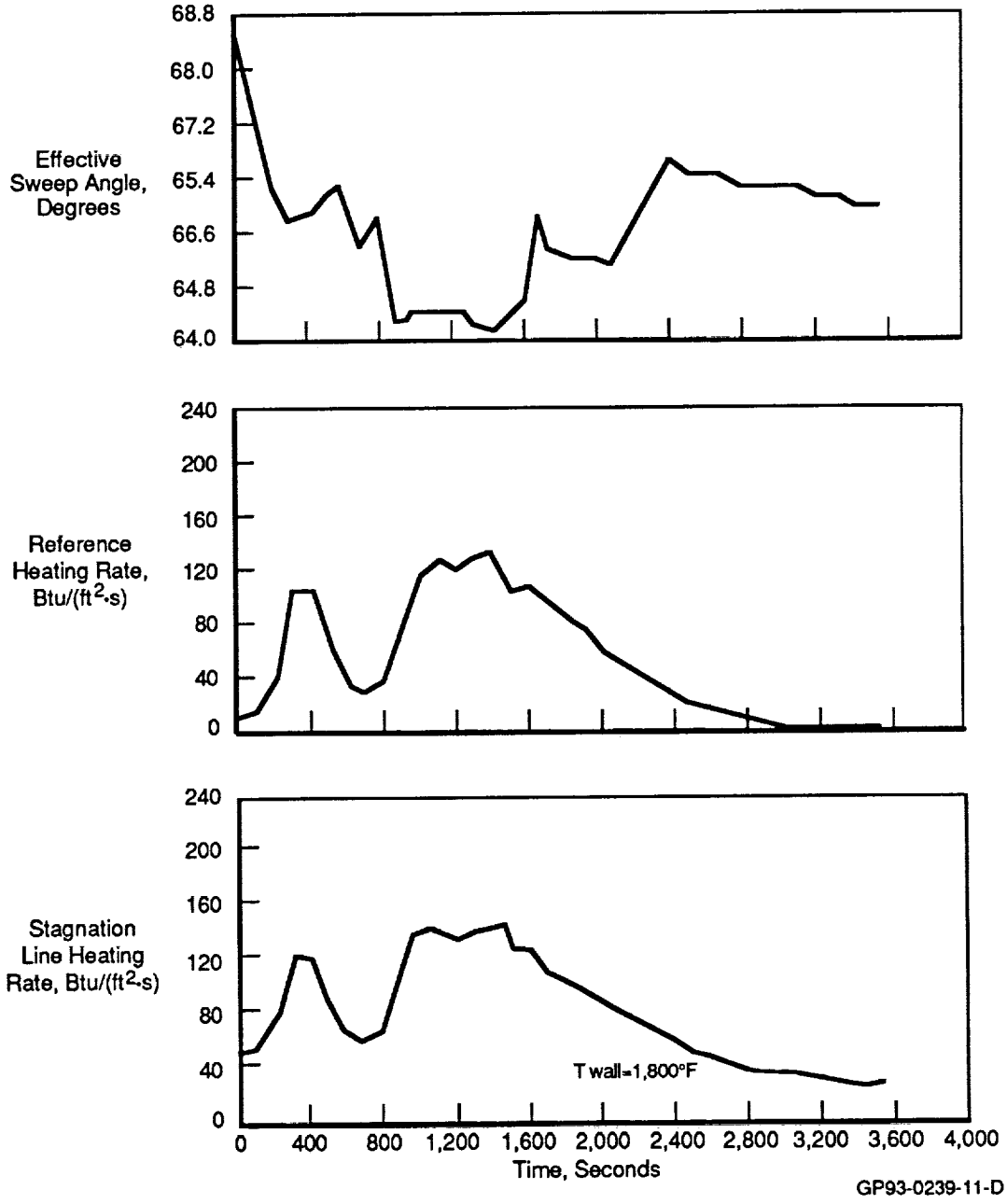

Figure 11. Entry Research Vehicle Heating Rates (Re-Entry Trajectory)

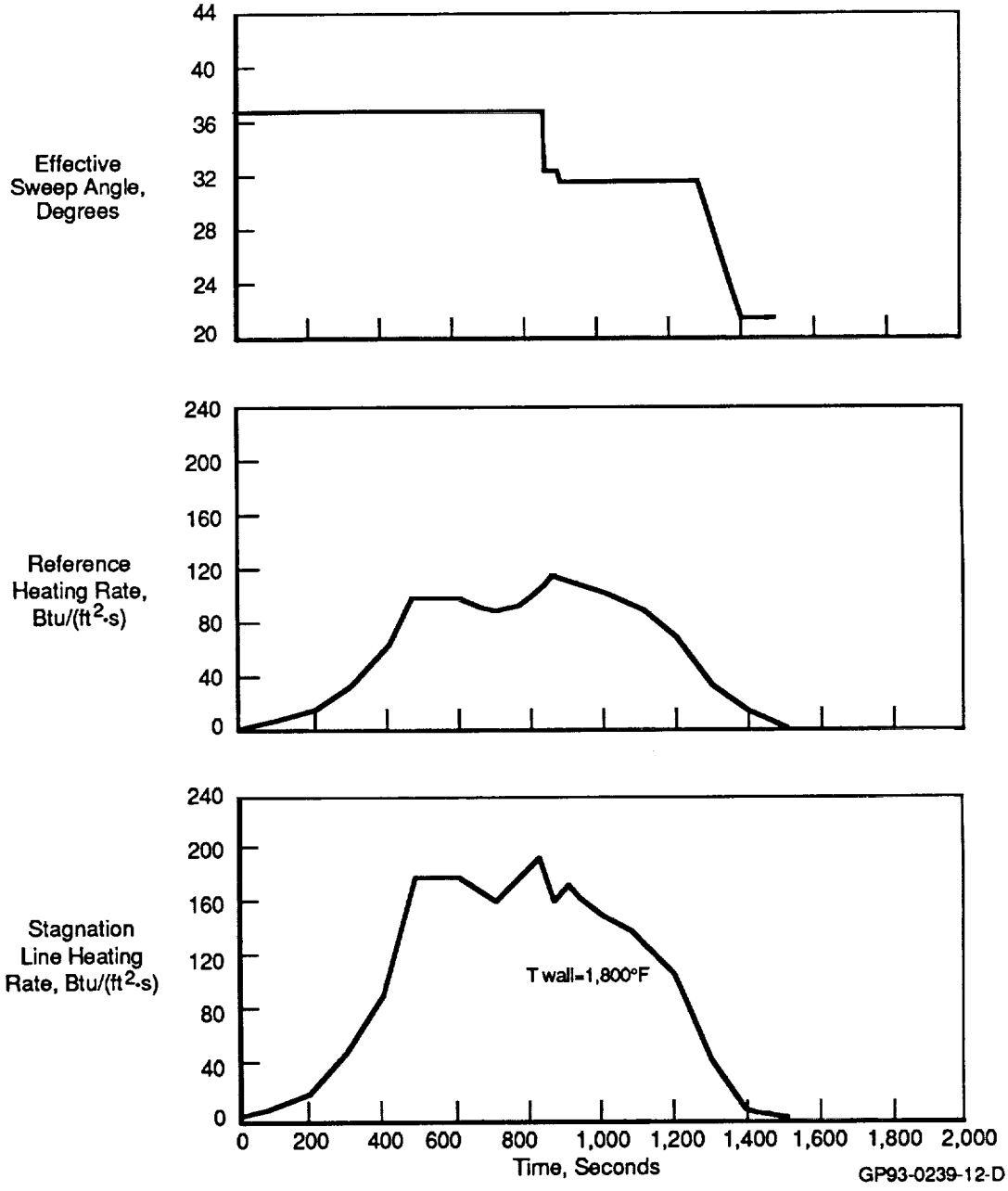

Figure 12. Entry Research Vehicle Heating Rates (Synergetic Plane Change Trajectory)

Heat pipe lengths required to isothermalize the wing leading edge were calculated as a function of operating temperature using the heat pipe sizing program described in Section 3.1. The results are shown in Figure 13. Heat pipe design requirements are presented in Figure 14 for a sodium/superalloy heat pipe operating at 1800°F and a lithium/refractory metal heat pipe operating at 2400°F. In both designs, the condenser was assumed to be only radiation cooled (as opposed to being augmented with an active cooling system).

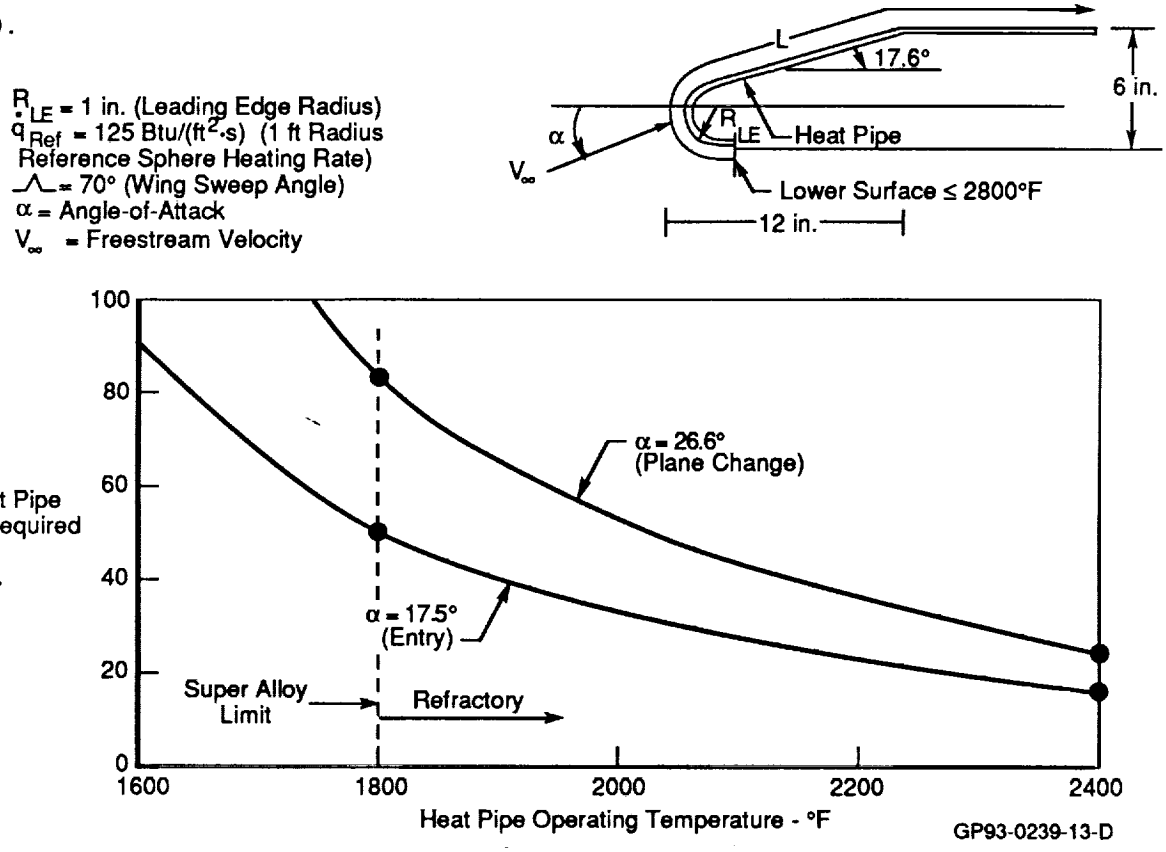

Figure 13. Refractory Heat Pipe Length Requirements are Much Less Than Those for Superalloy Heat Pipes

Since the ERV maximum wing surface length (normal to the leading edge) is 55 inches, the lithium/refractory metal heat pipe, with its required length of 24 inches, could be integrated into the wing leading edge. The required refractory metal heat pipe heat transfer capability, referenced to the axial and radial areas, are shown (Figure 14) to be well within the sonic, entrainment, and boiling limits. The additional wick permeability-area product (K_wA_w) required to provide total pressure losses below the capillary pumping limit provided by the assumed 200 mesh screen wick structure is also shown in Figure 14. This K_wA_w could be supplied by arteries, grooves, or other special features.

$(\dot{q}_o)_{ref}$ = 125 Btu/(ft^2·s)
Λ = 70° (Sweep Angle)
α = 26.6° (Angle-of-Attack)
$\dot{q}_{SL}$ = 156 Btu/(ft^2·s) (R_{LE} = 1 in.)
V_∞ = Freestream Velocity
ϵ = 0.8

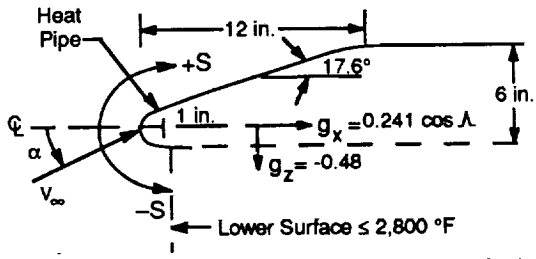

Design Parameters and Limits		Superalloy Heat Pipe	Refractory Heat Pipe
Heat Pipe Material		Hastelloy X	Molybdenum
Working Fluid		Sodium	Lithium
Operating Temperature	(°F)	1,800	2,400
Leading Edge Radius	(in.)	1	1
Heat Pipe Length	(in.)	86.4	24.3
• −S and +S Lengths	(in.)	(6.2 and 80.2)	(6.2 and 18.1)
• Evap and Cond Lengths	(in.)	(7.6 and 78.8)	(6.8 and 17.5)
Axial Heat Transfer	(Btu/sec/in. of Span)	3.32	2.57
Max Radial Heat Flux	Btu/(ft^2·s)	146	130
• Boiling Limit(1)	Btu/(ft^2·s)	536	3,271
Max Axial Heat Flux	Btu/(ft^2·s)	2,064	1,600
• Sonic Limit	Btu/(ft^2·s)	59,945	53,723
• Entrainment Limit(2)	Btu/(ft^2·s)	6,712	14,259
Wick Capillary Pumping Limit(2)	(psf)	56.5	116.3
Net Adverse Gravity Head	(psf)	12.2	−3.6
• Liquid + Vapor ΔP Limit	(psf)	44.2	120
Required Minimum Wick(2) Permeability * Area	(ft^4/in. of Span)	1.18E−11	3.13E−13
Maximum ΔT Between Fluid and External Surface @ Stagnation Line(3)	(°F)	72	21
Fluid Vapor Pressure	(psia)	35	13
Reference Stagnation Line Equilibrium Temperature for Uncooled Leading Edge	(°F)	4,040	4,040

(1) Based on 3 micron nucleation site radius and 2 layers 200 mesh screen @ wall
(2) Based on 200 mesh screen
(3) Based on 2 layers 200 mesh screen and 0.020 in. wall

GP93-0239-14

Figure 14. ERV Wing Leading Edge Heat Pipe Design Requirements
Superalloy and Refractory Metal Designs

While the required heat transfer capability of the sodium/superalloy heat pipe is also well within the heat pipe limits (Figure 14), its required length exceeds the available ERV wing surface length (86.4 in. vs. 55 in.). Thus, this design is not feasible unless its design requirements are relaxed. There are methods for reducing the required heat pipe length (and corresponding wick requirements) that would merit consideration for the ERV wing leading edge application. For example:

- Reducing the reference heating rate from 125 Btu/(ft^2•s) to 100 Btu/(ft^2•s) by altering the trajectory would reduce the superalloy heat pipe length to 50 inches (Figure 15).

- Reducing the angle of attack from 26.6 degrees to 18 degrees would reduce the heat pipe length to 50 inches (Figure 16).

The ramifications of altering the ERV trajectory to make sodium/superalloy heat pipes feasible for this configuration were not investigated in detail though one would expect some degradation in vehicle performance (e.g., reduced cross-range).

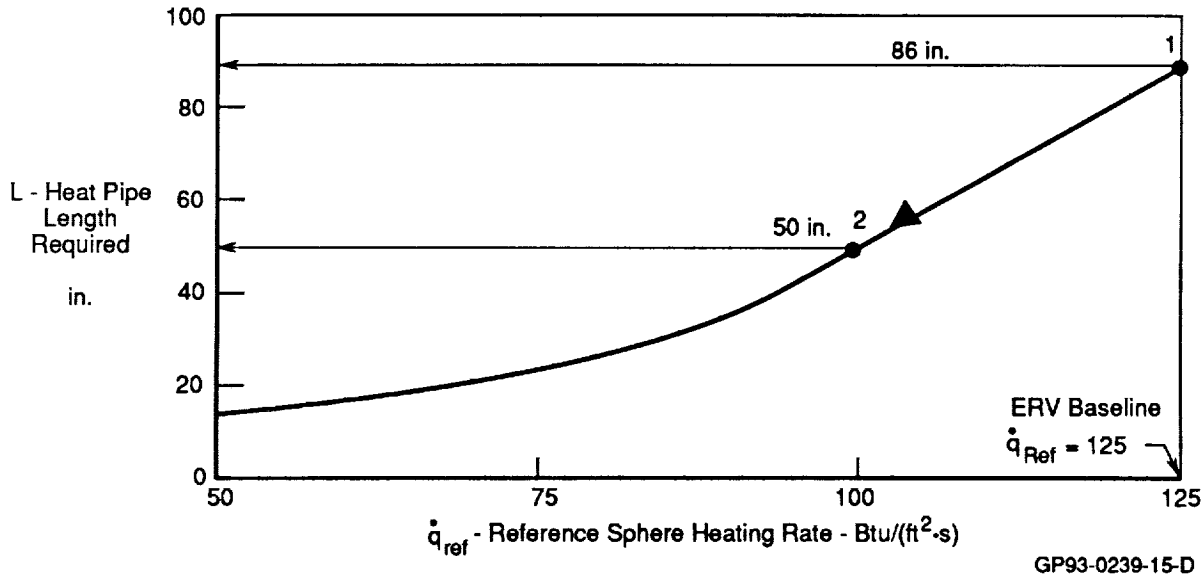

Figure 15. Altering ERV Trajectory Could Allow Use of Superalloy Heat Pipes

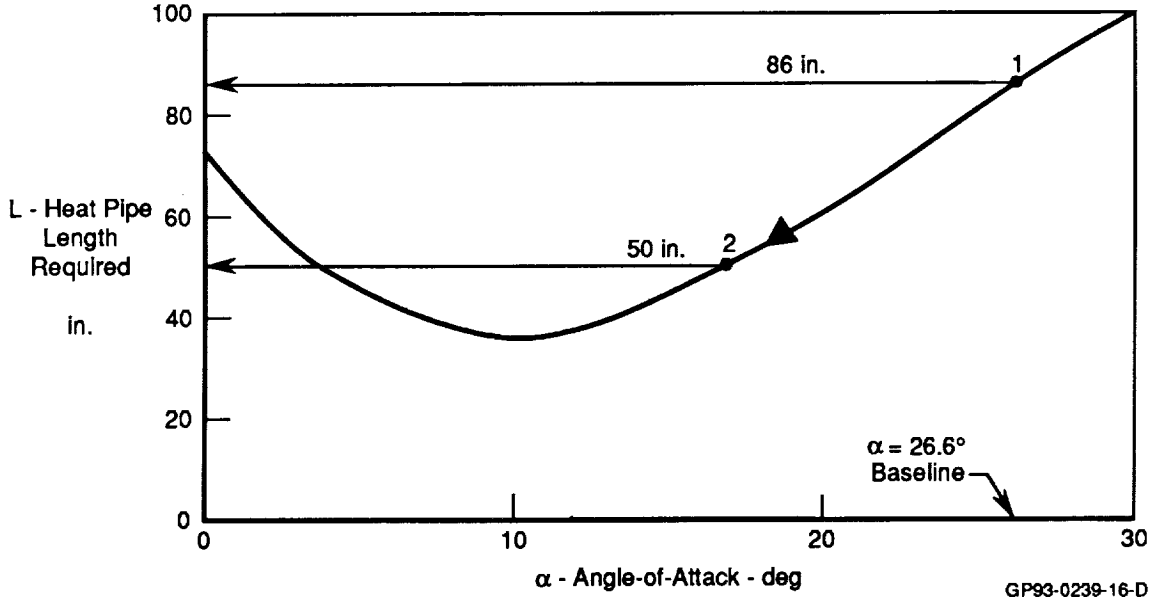

Figure 16. Reducing Angle-of-Attack During Plane Change Could Allow Use of Superalloy Heat Pipes

3.2.2 Aero-Space Plane - Wing leading edge geometries and flight conditions representative of an aero-space plane, as provided by NASA, were used to investigate the feasibility of using heat pipes on this class of vehicles. Aero-space planes have small leading edge radii to minimize drag while operating in a dense part of the atmosphere to provide air to scramjet engines. This can result in severe heating conditions. They also operate at low angles-of-attack and therefore, contrary to re-entry vehicles, produce relatively high temperatures on the top wing surface as well as the bottom. As a result, both radiantly cooled and actively cooled heat pipes were investigated for this application.

A leading edge radius of 0.25 in. with upper and lower surface inclination angles of 3 degrees, was assumed as the base wing design. Operation at 10 degrees angle-of-attack with reference heating rates of 175 and 307 Btu/(ft^2•s) was also assumed representative of bounding airbreathing ascent trajectories.

Radiantly cooled heat pipe lengths and wicking requirements for the less severe reference heating rate are shown in Figure 17 as a function of operating temperature. This shows that it is not feasible to use a radiantly cooled sodium/superalloy heat pipe for this application because of excessive length and wicking requirements at superalloy limit temperatures of 1800°F.

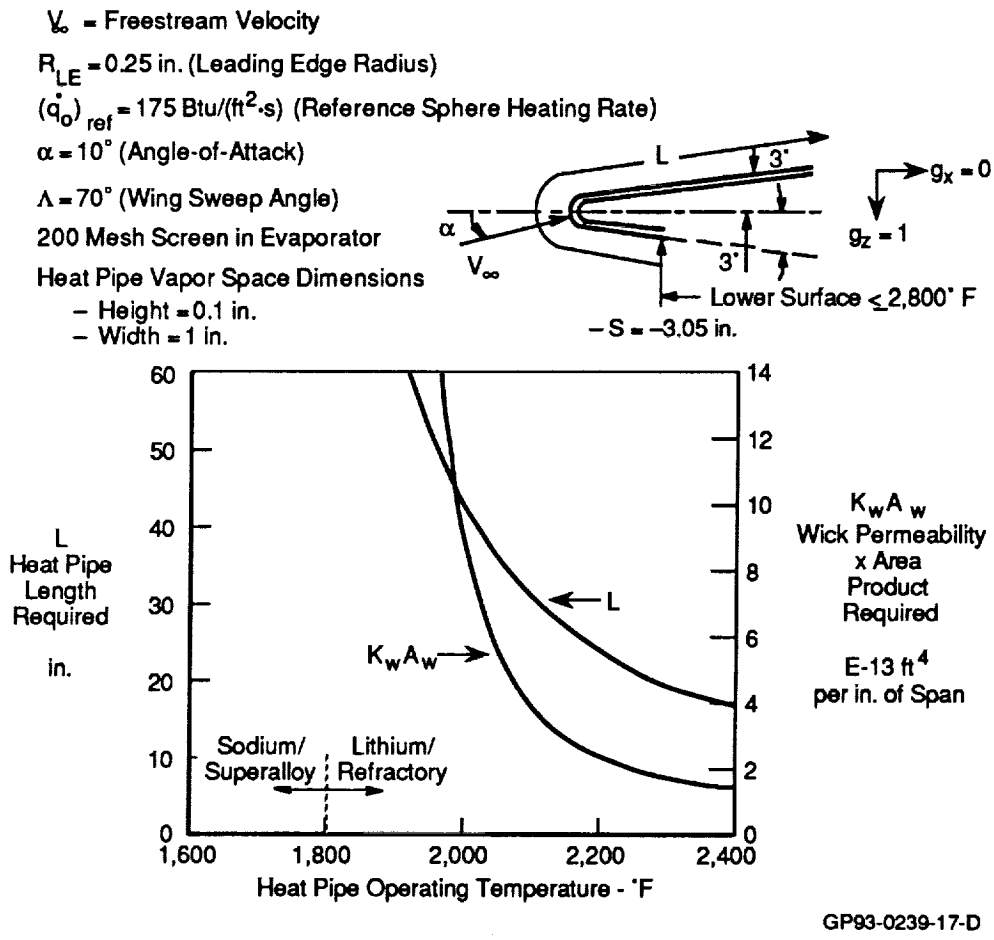

Figure 17. Radiantly Cooled Heat Pipe Design Requirements for Aero-Space Plane

Radiantly cooled lithium/refractory metal heat pipes are, however, feasible for the aero-space plane application. Design requirements at both reference heating conditions are presented in Figure 18. At the higher reference heating rate, a long heat pipe (62 in.) is required while the required heat pipe length at the less severe heating rate is fairly short (16 in.).

$\Lambda = 70°$
$\alpha = 10°$
V_∞ = Freestream Velocity
$\epsilon = 0.8$

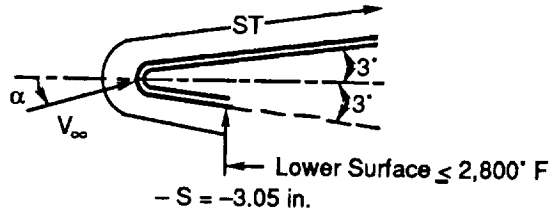

Design Parameters and Limits		$(q_o)_{ref}$ = 307 Btu/(ft²·s) q_{SL} = 517 Btu/(ft²·s) Refractory Heat Pipe	$(q_o)_{ref}$ = 175 Btu/(ft²·s) q_{SL} = 295 Btu/(ft²·s) Refractory Heat Pipe
Heat Pipe Material		Molybdenum	Molybdenum
Working Fluid		Lithium	Lithium
Operating Temperature	(°F)	2,400	2,400
Leading Edge Radius	(in.)	0.25	0.25
Heat Pipe Length	(in.)	62.0	16.4
• –S and +S Lengths	(in.)	(–9.2 and 52.8)	(–3.1 and 13.3)
• Evap and Cond Lengths	(in.)	(9.7 and 52.3)	(3.5 and 12.9)
Axial Heat Transfer	(Btu/sec/in. of Span)	4.53	1.61
Max Radial Heat Flux	Btu/(ft²·s)	490	269
• Boiling Limit[1]	Btu/(ft²·s)	3,271	3,271
Max Axial Heat Flux	Btu/(ft²·s)	7,334	2,603
• Sonic Limit	Btu/(ft²·s)	53,723	53,723
• Entrainment Limit[2]	Btu/(ft²·s)	14,259	14,259
Wick Capillary Pumping Limit[2]	(psf)	116.3	116.3
Net Adverse Gravity Head	(psf)	–7.7	–2.8
• Liquid + Vapor ΔP Limit	(psf)	124	119
Required Minimum Wick[2] Permeability • Area, K_wA_w	(ft⁴/in. of Span)	2.19E–12	1.39E–13
Maximum ΔT Between Fluid and External Surface @ Stagnation Line[3]	(°F)	79	43
Fluid Vapor Pressure	(psia)	13	13
Reference Stagnation Line Equilibrium Temperature for Uncooled Leading Edge	(°F)	5,608	4,813

(1) Based on 3 micron nucleation site radius and 2 layers 200 mesh screen @ wall
(2) Based on 200 mesh screen
(3) Based on 2 layers 200 mesh screen and 0.020 in. wall

GP93-0239-18

Figure 18. Radiantly Cooled Refractory Heat Pipe Design Requirements

Since this conceptual study was performed for aerospace planes in general and not tied to a specific configuration, trade studies were performed to investigate the effect of leading edge radius and gravitational forces on length and wicking requirements for the refractory metal heat pipe. Results are shown in Figures 19 and 20. The reason that the length sensitivity to radius for the lower heating reference heating rate does not parallel the higher reference heating rate (Figure 19) is due to differences in heat pipe starting location. As mentioned in Section 3.1, the heat pipes were assumed to start on the lower wing surface at the point where the radiation equilibrium wall temperature equals 2800°F. For the lower reference heating rate, the starting point occurs close to the stagnation line. Since the change in aeroheating with respect to the distance from the stagnation line is large (near the stagnation line) the starting point location (i.e., distance form stagnation line where 43 Btu/(ft^2•s)) and, therefore, total heat pipe length is relatively insensitive to changes in leading edge radius. However, for the higher reference heating rate, the starting point occurs further aft on the lower surface where the change in aeroheating with respect to the distance from the stagnation line is small. Therefore, the starting piont location and total heat pipe length for the higher reference heating rate is more sensitive to changes in the leading edge radius.

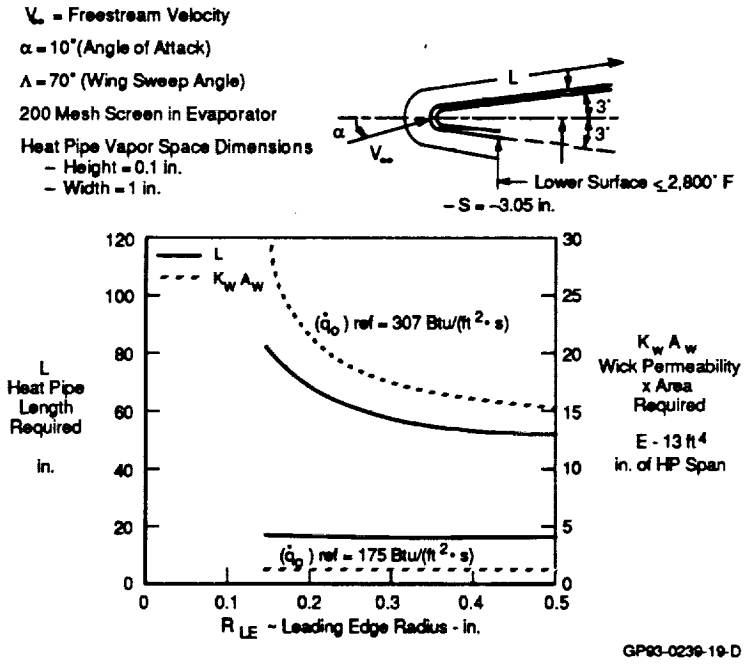

Figure 19. Effect of Leading Edge Radius on Heat Pipe Requirements

As expected, increasing the acceleration (Figure 20) in the direction opposite the liquid sodium flow requires a corresponding decrease in wick pressure loss (i.e., an increase in wick permeability-area product, K_wA_w).

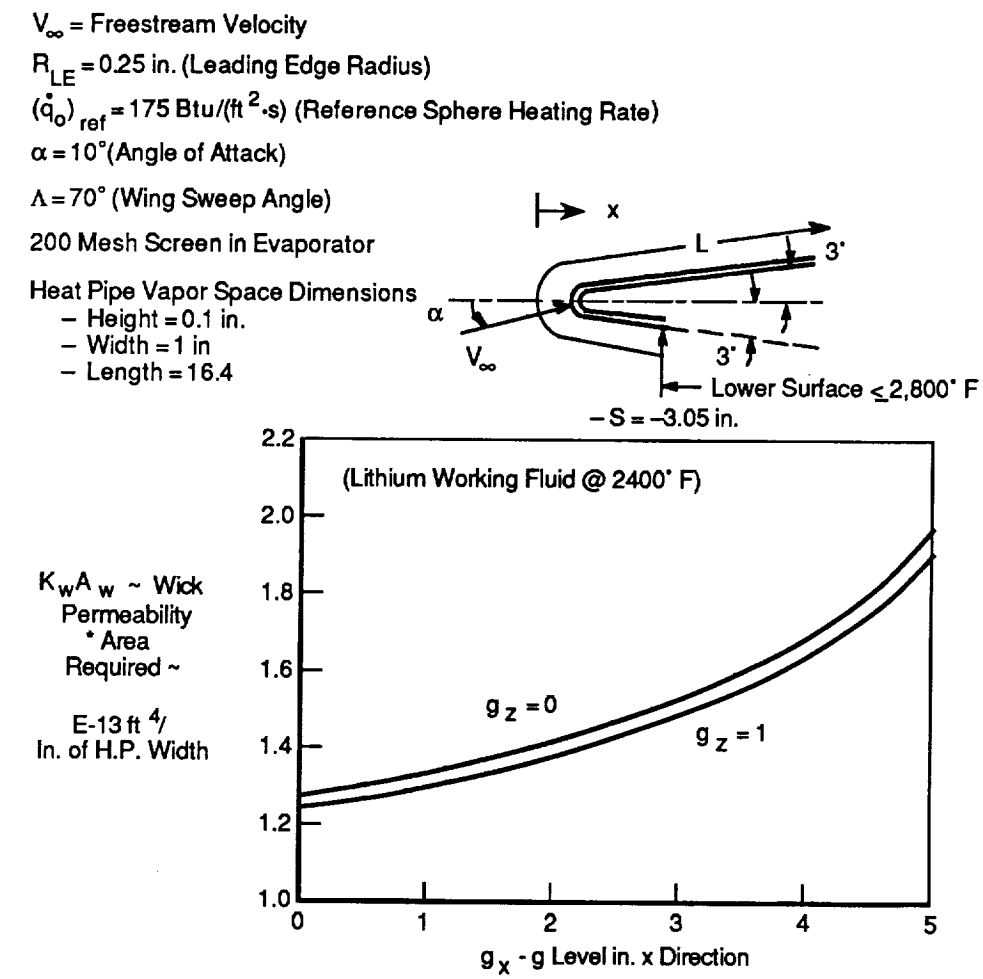

Figure 20. Effect of g Levels on Heat Pipe Wick Permeability Requirements

While radiantly cooled sodium/superalloy heat pipes were shown above to be unfeasible for the aerospace plane application, integrating superalloy heat pipes with an active cooling system would permit their consideration. A hydrogen cooled heat pipe condenser concept, shown in Figure 21, was defined and evaluated. Its design requirements are presented in Figure 22. These results show that a 19 in. sodium/superalloy heat pipe coupled to an active cooling system will reduce leading edge temperatures to 1800°F and result in modest heat pipe length requirements.

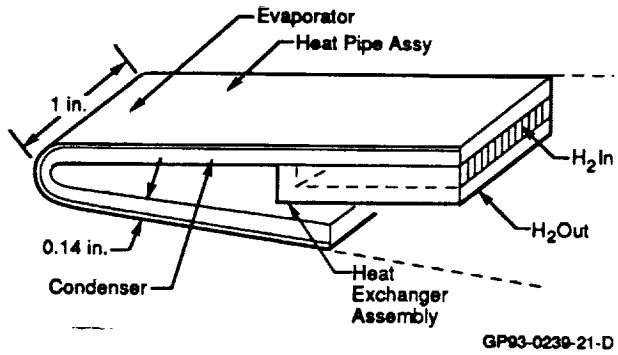

Figure 21. Integration of Superalloy Heat Pipes With Active Cooling System

V_∞ = Freestream Velocity
$\Lambda = 70°, \alpha = 10°$
$\epsilon = 0.8$

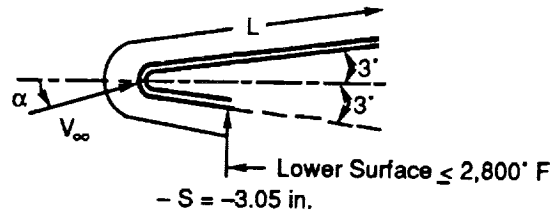

Design Parameters and Limits		$(\dot{q}_o)_{ref}$ = 307 Btu/(ft²·s) q_{SL} = 517 Btu/(ft²·s) Superalloy Heat Pipe	$(\dot{q}_o)_{ref}$ = 175 Btu/(ft²·s) q_{SL} = 295 Btu/(ft²·s) Superalloy Heat Pipe
Heat Pipe Material		Hastelloy X	Hastelloy X
Working Fluid		Sodium	Sodium
Operating Temperature	(°F)	1,800	1,800
Leading Edge Radius	(in.)	0.25	0.25
Heat Pipe Length	(in.)	19.0	7.5
• –S and +S Lengths	(in.)	(–9.2 and 9.8)	(–3.1 and 4.4)
• Evap and Cond Lengths	(in.)	(14.7 and 4.3)	(4.0 and 3.5)
Axial Heat Transfer	(Btu/sec/in. of Span)	5.71	1.98
Max Radial Heat Flux	Btu/(ft²·s)	506	284
• Boiling Limit[1]	Btu/(ft²·s)	537	537
Max Axial Heat Flux	Btu/(ft²·s)	9,243	3,208
• Sonic Limit	Btu/(ft²·s)	83,923	83,923
• Entrainment Limit[2]	Btu/(ft²·s)	9,396	9,396
Wick Capillary Pumping Limit[2]	(psf)	56.5	56.5
Net Adverse Gravity Head	(psf)	–5.5	–3.2
• Liquid + Vapor ΔP Limit	(psf)	51.0	53.3
Required Minimum Wick[2] Permeability • Area, K_wA_w	(ft⁴/in. of Span)	4.96E–12	5.24E–13
Maximum ΔT Between Fluid and External Surface @ Stagnation Line[3]	(°F)	249	140
Fluid Vapor Pressure	(psia)	35	35
Reference Stagnation Line Equilibrium Temperature for Uncooled Leading Edge	(°F)	5,608	4,813

(1) Based on 3 micron nucleation site radius and 2 layers 200 mesh screen @ wall
(2) Based on 200 mesh screen
(3) Based on 2 layers 200 mesh screen and 0.020 in. wall

GP93-0239-22

Figure 22. Aero-Space Plane Actively Cooled Leading Edge Heat Pipe Design Requirements

In summary, for aero-space plane type vehicles, radiant cooled wing leading edge heat pipes only appear promising for heating rates below about 200 BTU/(ft^2•s). Even then, only refractory metal heat pipes result in reasonable lengths. However, integrating heat pipes with active cooling systems appears promising for sharp leading edges where active cooling alone may also be unattractive due to high pressure losses or geometry considerations. However, detailed analysis of these more complex protection concepts was outside the scope of this program.

3.2.3 Advanced Shuttle - The wing leading edge geometry of an advanced shuttle concept is shown in Figure 23. The wing root is characterized by a 4 in. leading edge radius with a 20 degree wing upper/lower surface inclination angle. The wing tip is characterized by a 2 in. leading edge radius with a 12 degree wing upper/lower surface inclination angle.

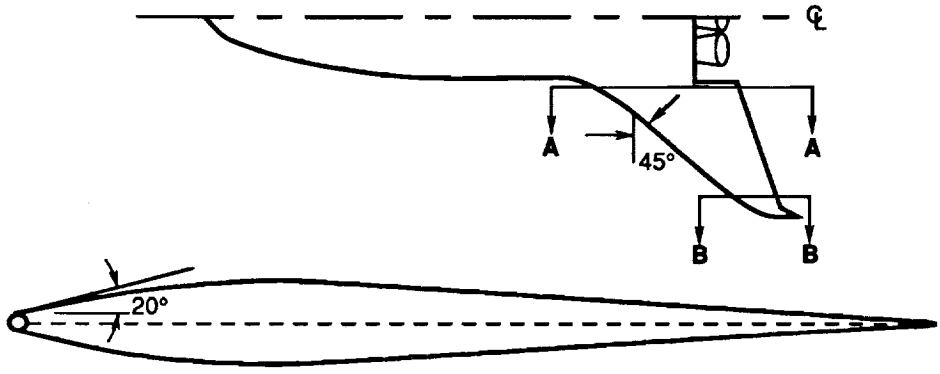

A-A. Wing Root Modeled as 4 in. Leading Edge Radius With 20° Upper/Lower Wing Inclination Angle

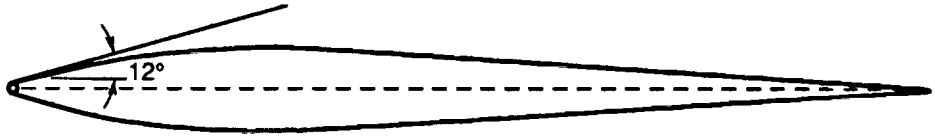

B-B. Wing Tip Modeled as 2 in. Leading Edge Radius With 12° Upper/Lower Wing Inclination Angle

GP93-0239-23-D

Figure 23. Advanced Shuttle Wing Leading Edge Geometry

A typical re-entry trajectory for this vehicle is shown in Figure 24. The reference and stagnation line heating rates shown in Figure 25 were determined using the MINIVER program and the previously defined swept cylinder relationship (Equation 1). The maximum stagnation line heating rate, and therefore the heat pipe design point, occurs about 1400 seconds into the trajectory. Heating rate distributions about the leading edge and on the wing upper surface at the time of peak heating are shown in Figure 26.

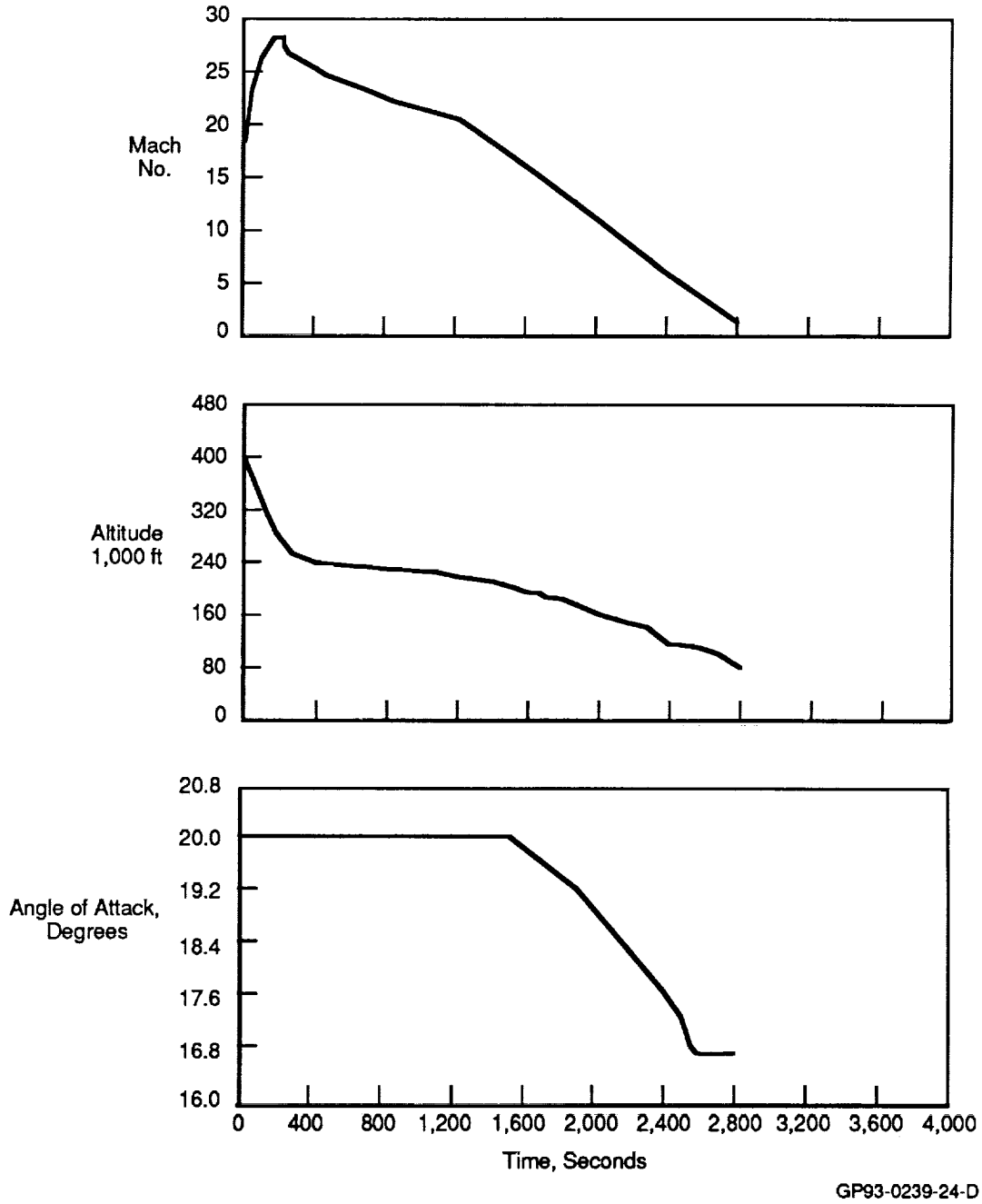

Figure 24. Advanced Shuttle Re-Entry Trajectory

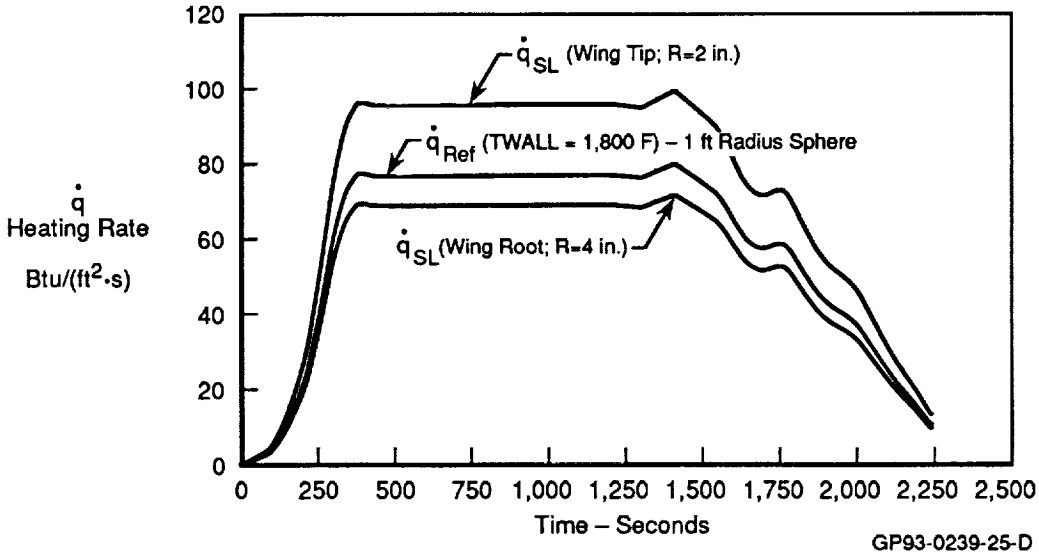

Figure 25. Advanced Shuttle Heating Rates

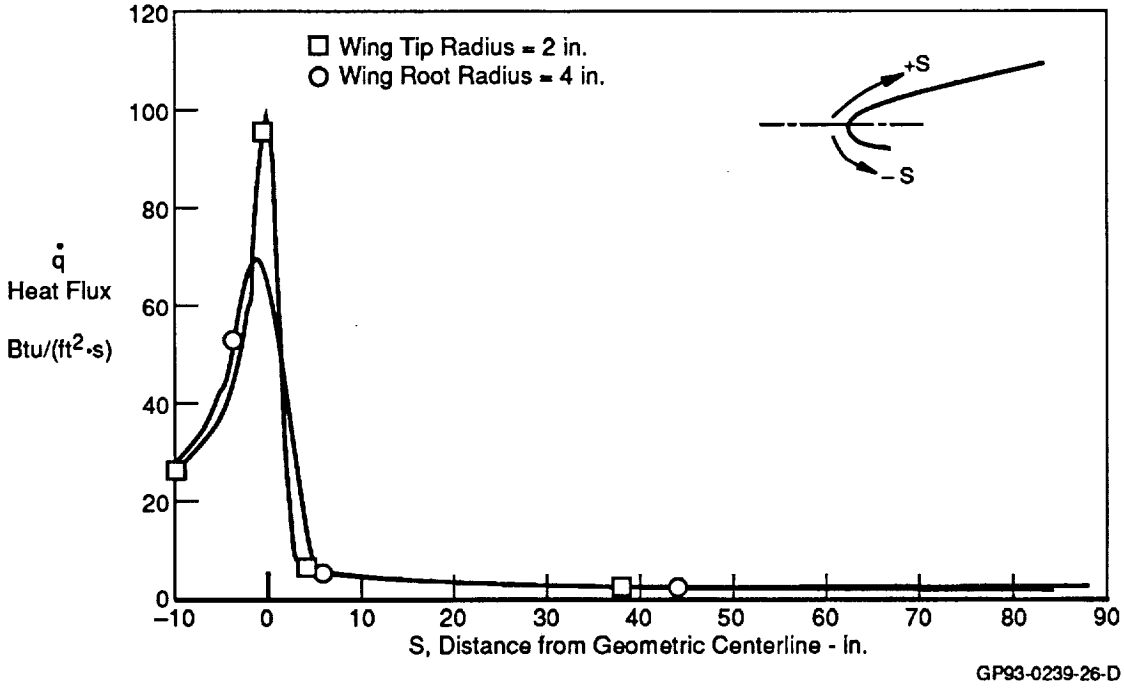

Figure 26. Heating Rate Distribution Around Advanced Shuttle Wing Leading Edge

Heat pipe lengths and wicking requirements (normalized to the capillary radius) at the wing root were determined as a function of operating temperature as shown in Figure 27. At the wing root, the required lengths for a sodium/superalloy and lithium/refractory metal heat pipe are (87.2 and 25.6 inches), respectively. Design requirements for both sodium/superalloy and lithium/refractory metal heat pipes at both the wing root and wing tip are presented in Figure 28. The required lengths at the wing tip for the superalloy and refractory metal heat pipes are 69.4 and 21.7 inches, respectively. These lengths are shorter than at the wing root. However, the wing tip application was used in subsequent analysis because its smaller leading edge radius (2 in. vs. 4 in.) posed more of a design and fabrication challenge.

Either the sodium/superalloy and lithium/refractory metal heat pipes could be integrated into the advanced shuttle wing leading edge.

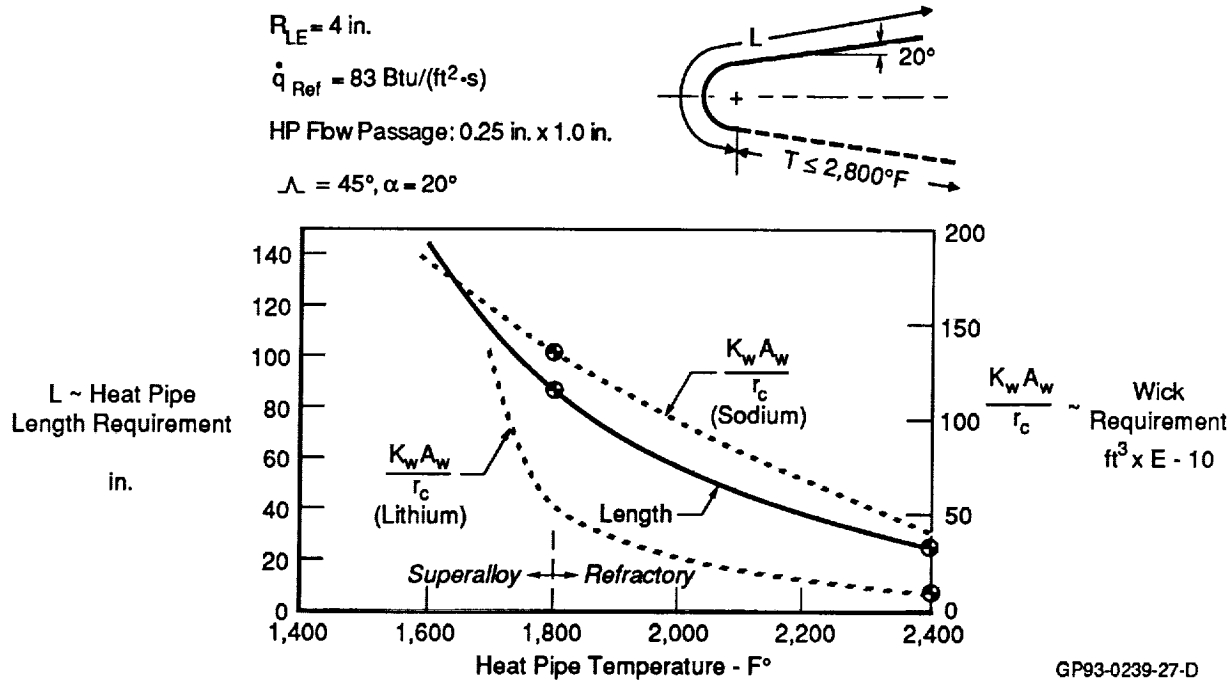

Figure 27. Both Superalloy and Refractory Metal Heat Pipes Feasible for Advanced Shuttle Application

V_∞ = Freestream Velocity
$(\dot{q}_o)_{ref}$ = 78 Btu/(ft^2·s)
Λ = 45° (Sweep Angle)
α = 20° (Angle-of-Attack)
$\dot{q}_{SL}$ = 98 Btu/(ft^2·s) (Wing Tip)
70 Btu/(ft^2·s) (Wing Root)
R = 2 in. $\delta_u = \delta_L$ = 12° (Wing Tip)
4 in. $\delta_u = \delta_L$ = 20° (Wing Root)

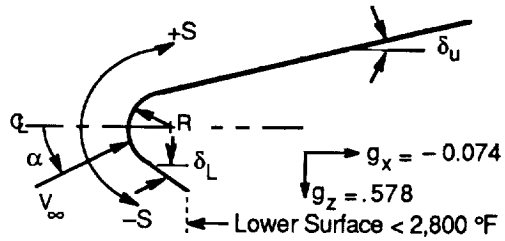

Design Parameters and Limits		Superalloy Heat Pipe		Refractory Heat Pipe	
Heat Pipe Material		Hastelloy X		Molybdenum	
Working Fluid		Sodium		Lithium	
Operating Temperature	(°F)	1,800		2,400	
		Tip	**Root**	**Tip**	**Root**
Leading Edge Radius	(in.)	2	4	2	4
Heat Pipe Length	(in.)	69.4	87.2	21.7	25.6
• −S and +S Lengths	(in.)	(−4.8 and 64.6)	(−6.4 and 80.8)	(−4.8 and 16.9)	(−6.4 and 19.2)
• Evap and Cond Lengths	(in.)	(8.2 and 61.2)	(11.2 and 76.0)	(2.0 and 19.7)	(9.5 and 16.1)
Axial Heat Transfer	(Btu/sec/in. of Span)	2.85	3.20	2.10	2.12
Max Radial Heat Flux	Btu/(ft^2·s)	94	64	79	48
• Boiling Limit[1]	Btu/(ft^2·s)	537	537	3,271	3,271
Max Axial Heat Flux	Btu/(ft^2·s)	1,737	1,956	1,280	1,292
• Sonic Limit	Btu/(ft^2·s)	59,945	59,945	53,723	53,723
• Entrainment Limit[2]	Btu/(ft^2·s)	6,713	6,713	14,259	14,259
Wick Capillary Pumping Limit[2]	(psf)	56.5	56.5	116.3	116.3
Net Adverse Gravity Head	(psf)	−49.0	−87.8	−9.9	−16.6
• Liquid + Vapor ΔP Limit	(psf)	61.5	135.3	89.9	98.4
Required Minimum Wick[2] Permeability • Area, $K_w A_w$	(ft^4/in. of Span)	5.79E−12	3.86E−12	2.29E−13	2.64E−13
Fluid Vapor Pressure	(psia)	35	35	13	13
Reference Stagnation Line[3] Equilibrium Temperature for Uncooled Leading Edge	(°F)	3,607	3,269	3,607	3,269

(1) Based on 3 micron nucleation site radius and 2 layers 200 mesh screen on wall
(2) Based on 200 mesh screen
(3) Based on emissivity = 0.8

GP93-0239-28

Figure 28. Advanced Shuttle Wing Leading Edge Heat Pipe Design Requirements
Superalloy and Refractory Metal Designs

3.3 SELECTION OF DESIGN FOR FABRICATION/TESTING

A summary of the preliminary heat pipe designs for entry research vehicle, aerospace plane, and advanced shuttle applications is shown in Figure 29.

Because the primary objective of this program was to develop a full scale heat pipe for testing, the sodium/superalloy heat pipe was selected for detailed design, analysis, and fabrication. This selection minimized program risk because of our experience in fabricating sodium/superalloy heat pipes (References 3 and 4). Superalloys are more machinable than refractory metals and refractory metals, unlike superalloys, require oxide resistant coatings. In addition, fabricating the lower temperature superalloy heat pipe eased the development of internal instrumentation techniques.

Of the superalloy heat pipe designs, the advanced shuttle application was selected because of NASA's interest in this vehicle and the desire to complement the separate NASP leading edge generic option studies.

	Radius (in.)	Length	
		Superalloy (In.)	Refractory (In.)
ERV	1	86.4	24.3
Aerospace Plane	0.25	Integration With Active Cooling Required	62.0
Advanced Shuttle (Wing Tip)	2	69.4	21.7

GP93-0239-29-D

Figure 29. Summary of Conceptual Designs

4.0 DETAILED HEAT PIPE DESIGN AND ANALYSIS

This section describes the detailed design and analysis of a sodium/superalloy heat pipe sized to isothermalize a 2.0 in. radius, advanced shuttle wing leading edge to 1800°F. Designs for a production-like heat pipe assembly and a non-optimized, readily producible test article are presented. Peak uncooled radiation equilibrium temperatures for this application would be 3500°F. The conceptual design shown in Figure 30, extends from a point on the lower surface where the radiation equilibrium temperature is 2800°F forward around the leading edge radius and aft along the upper surface for a total length of 69.4 in. Aft of these heat pipe terminations, more conventional hot structure designs, using materials such as carbon-carbon on the lower surface and titanium on the upper surface were assumed. The resulting temperature discontinuities between the heat pipe and the adjacent structural systems, that would have to be addressed in the wing structural design, were beyond the scope of this study.

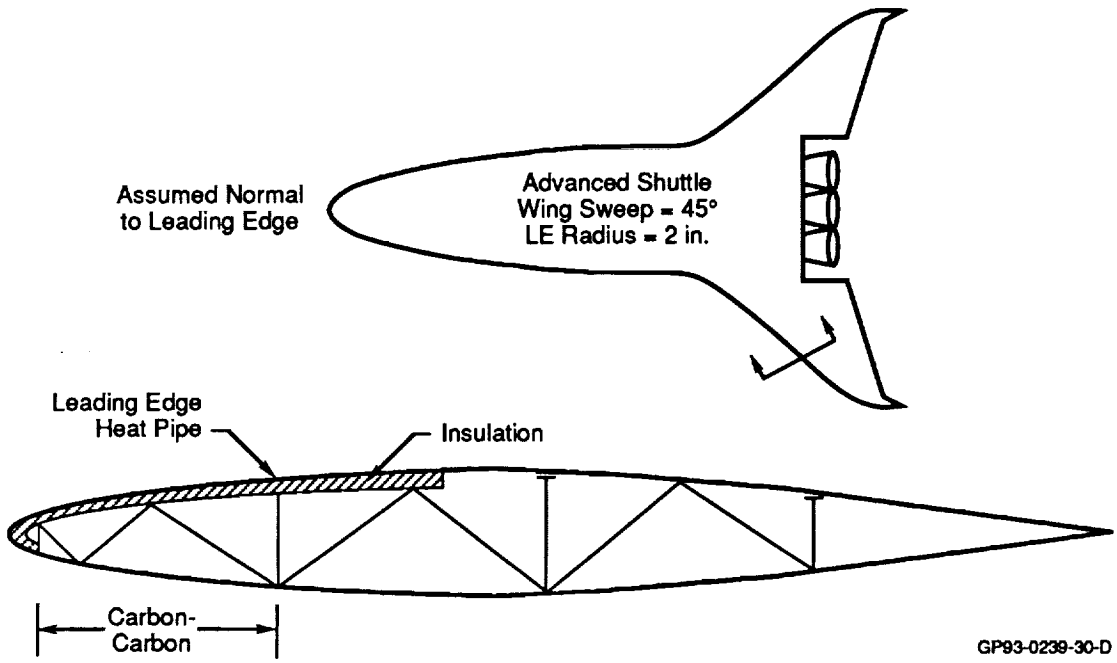

Figure 30. Advanced Shuttle Conceptual Design Selected for Detailed Design, Analysis, and Fabrication

The detailed heat pipe design process consisted of:

- Selecting the case cross-sectional shape
- Selecting the test article material and determining its dimensions
- Selecting a wick configuration and defining its construction

Performance of the heat pipe during normal and off-design conditions (startup and failure) plus an assessment of its design life are discussed in Section 6.0.

4.1 CASE CROSS-SECTION SELECTION

The design and fabrication of a 6 foot long, 2 inch radius, heat pipe provided many challenges. Numerous design cross sections which fall into categories of tubular or corrugated designs, as shown in Figure 31, were addressed. Factors which governed the cross-section selection were:

- Heat Transfer Area Coverage
- Weight
- Adaptability to Failure Protection
- Producibility
- Wick Installation and Inspection

Heat Transfer Area Coverage - Figure 32 shows that the outer mold line (OML) temperature between heat pipes increases significantly as the distance between heat pipes increases. To reduce this temperature rise, this distance should be minimized such that the OML heat transfer area covered by the heat pipes is maximized. Of the tubular designs considered, all except the circular tubes cover approximately the same area. Circular tubes would require a thermally conductive filler material between heat pipes and the OML face sheet to minimize the hot spots. Corrugated designs require additional space between the heat pipes in order to attach the corrugations to the face sheet. To compete with the tubular designs (i.e., same peak OML temperatures), the corrugated design heat pipes must have either thicker walls (for better heat conduction) or increased length (for more condenser surface) to reduce the temperature between pipes.

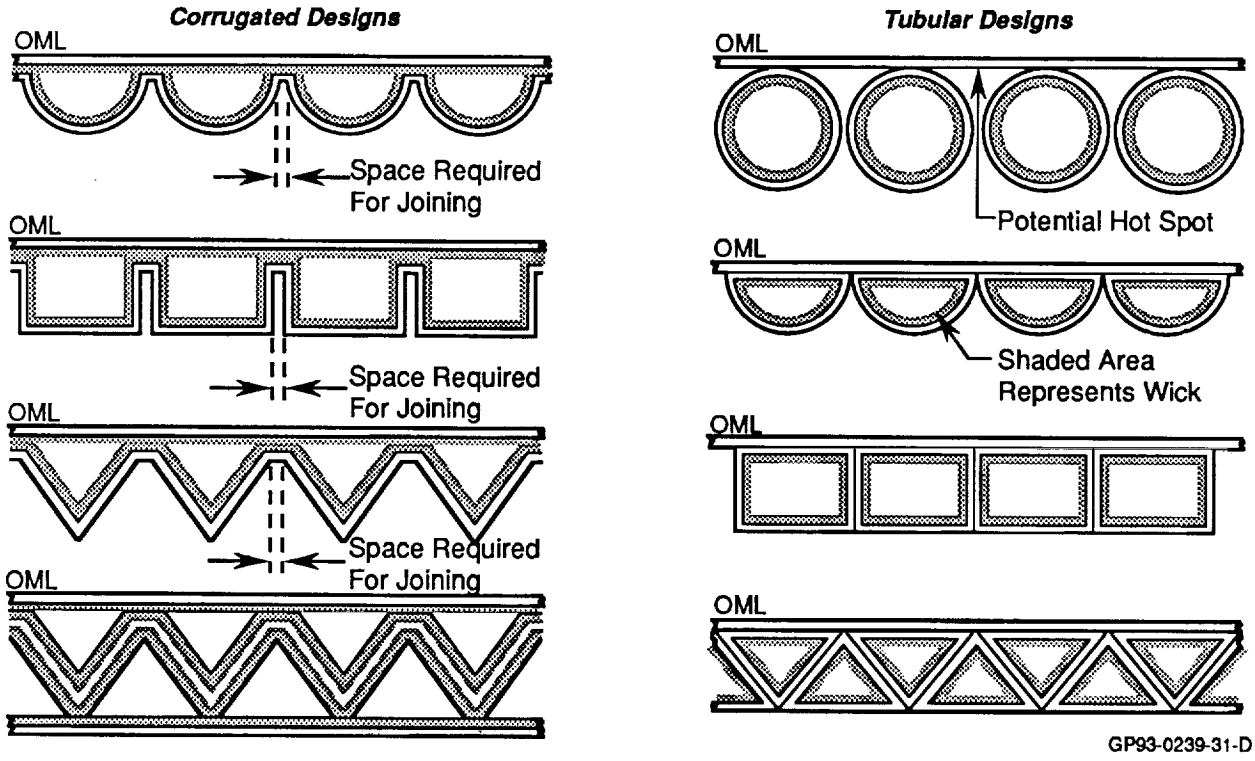

Figure 31. Candidate Case Cross-Section Designs

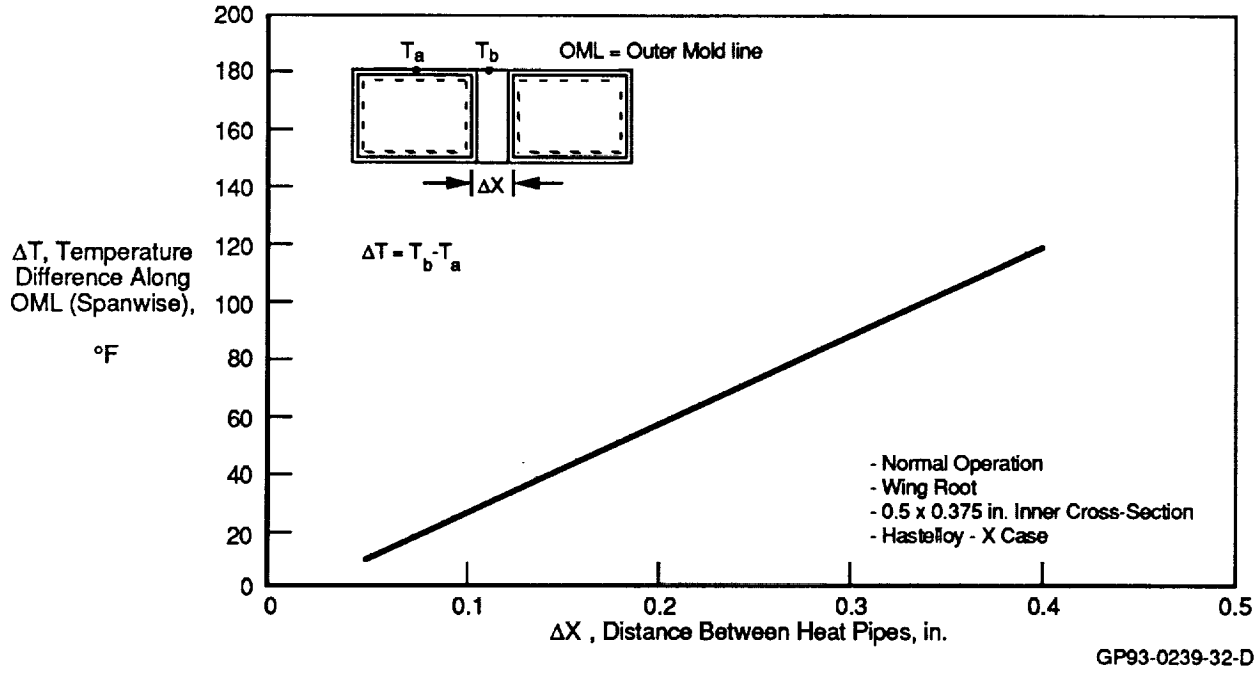

Figure 32. Temperature Distribution Along Outer Mold Line as Function of Heat Pipe Spacing

Weight - A previous study (Reference 11) compared case shapes on the basis of weight. This showed that semi-circular heat pipes designs minimized weight when compared to the other designs. The semi-circular tubes were 17%, 22%, and 15% lighter than circular, triangular, and rectangular heat pipes, respectively. These trends were assumed to be applicable for this study.

Adaptability to Failure Protection - Cases with flat back faces (opposite the OML) are more adaptable to interfacing with active internal failure protection systems than those with curved or discontinuous back faces. Internal transverse heat pipes, high temperature materials, internal radiative cooling, or active cooling systems can be readily interfaced to a flat surface.

The double triangular heat pipe designs (Figure 31) are most tolerant of heat pipe failures because of their redundancy. However, these designs are heavy and are subject to other problems as discussed below.

Producibility - All the heat pipe case designs shown in Figure 31 require four basic process steps: case bending to match the leading edge radius, attachment of the case to a face sheet, wick installation, filling the pipes with working fluid and testing of the assembled heat pipes. Each design type has unique fabrication problems.

The corrugated designs involve complex forming processes to develop the corrugated parts. During the bending process the corrugations must be supported, internally and externally, in order to maintain the cross section. While the tubular designs do not require complex forming processes, internal tube support is still required during the bending process.

Wick Installation and Inspection - A requirement of any heat pipe design is to have intimate contact between the wick and case wall (along the heat transfer surface). It is also highly desirable to have wick continuity all around the case walls in the condenser region. This wick arrangement allows any sodium which condenses on the back face to be wicked back to the front (heated) face where it is subsequently wicked to the evaporator. All the corrugated and tubular designs shown in Figure 31 make wick installation difficult and inspection almost impossible.

Since the one piece tube designs are always closed, wicks would have to be installed from one end of the pipe and then attached to the inner walls. Installing the wick after bending the heat pipe to the leading edge radius would be difficult. Inserting the wick prior to bending the heat pipe would facilitate installation but the risk of the wick being torn from the wall during the bending process is great. In either case, visual inspection of the wick after installation would be nearly impossible.

The corrugated designs require attaching the corrugated parts to a face sheet. If the wick cannot be installed until after this attachment, the problems of wick installation are similar to those of one piece tube designs. Even if some wick sections can be attached to the corrugated part and other sections to the face sheet prior to attachment, continuity of the wick cannot be ensured when the corrugated part and face sheet are assembled.

Cross-Section Selection - Since none of the Figure 31 tubular or corrugated designs readily permit wick installation and inspection, the two-part case design shown in Figure 33 was developed. This design also maximizes heat transfer area coverage and provides a flat back face to make it adaptable to internal failure protection. The Figure 33 configuration represents a design which could be used in a production environment. Significant tooling development would, however, be required to produce both case parts with optimized dimensions.

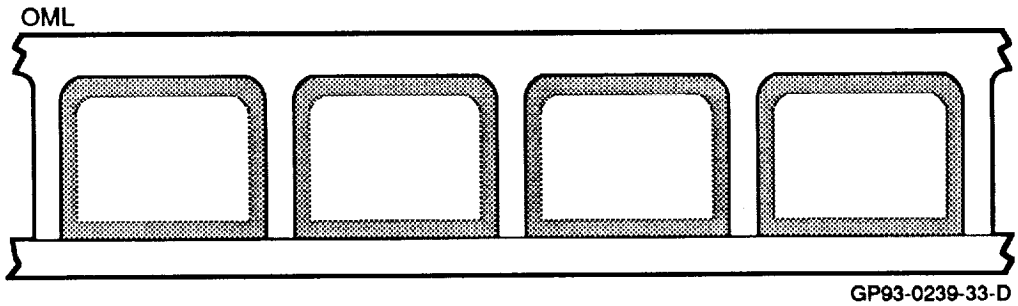

Figure 33. Two Part Rectangular Case Cross-Section Selected

For the purpose of fabricating a representative test article, compromises in this design were made. The resultant design, shown in Figure 34, provides a test article assembly in which two-part heat pipes could be fabricated and verified individually, then brazed to a face sheet. As discussed below, a single two-part heat pipe, shown in Figure 35 representative of the major components of the Figure 34 assembly, was fabricated in this program.

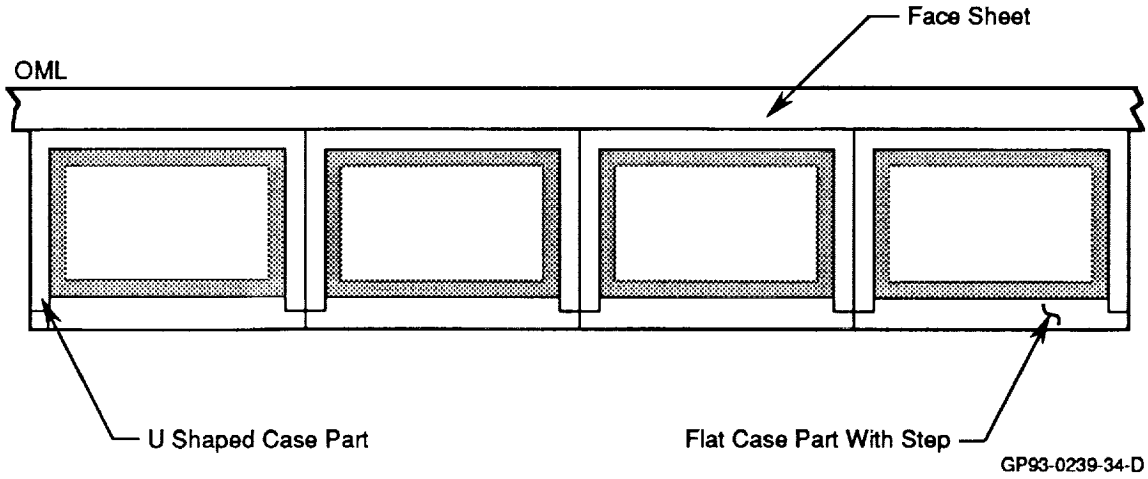

Figure 34. Test Article Case Modified to Facilitate Fabrication

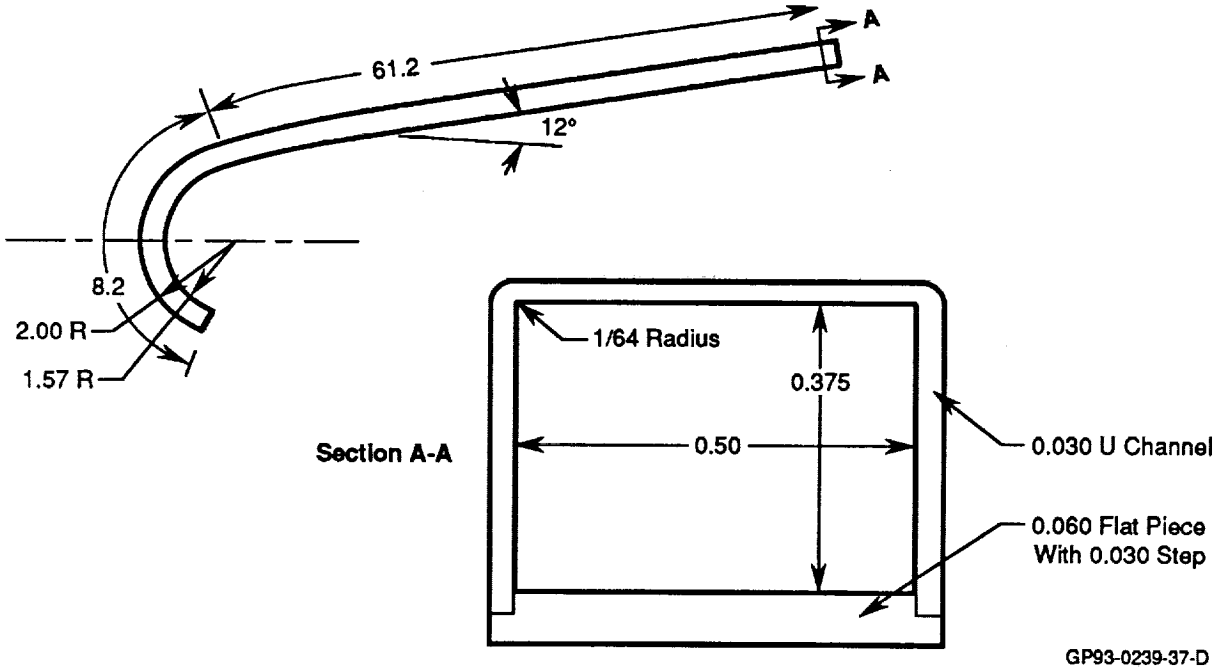

Figure 35. Heat Pipe Test Article Case Design

4.2 CASE MATERIAL SELECTION AND DIMENSIONAL SIZING

While Hastelloy X may not be the best superalloy material for heat pipes in terms of weight (see Section 6.0), it was selected for the test article because of its availability, selection in similar studies (References 3, 4, and 11), and its proven long term compatibility with sodium.

To determine the test article's dimensions (i.e., width and wall thicknesses) a structural analysis was performed. Based on an operating pressure of 35 psia, sodium's saturation pressure at 1800°F, wall thicknesses were calculated as a function of heat pipe width using four criteria; burst, yield, creep rupture, and 5% creep. The results are shown in Figure 36. For a vehicle application with a 150 mission life requirement, the heat pipe would be designed to the 5% creep limit. However for the test article, designing to the yield criteria should be sufficient.

To establish the case width, heat pipe case weights were calculated as a function of case width as shown in Figure 37. To minimize weight, width must be minimized. Prior to fabrication of the test article the minimum producible width, determined to be 0.5 in., was selected. Then, using Figure 36, a 0.030 in. U channel case part thickness was selected as the available Hastelloy X sheet stock which would meet the yield requirements. The flat case part thickness was chosen as 0.060 in. to allow for the step cutout which guards against weld splash. The case height of 0.375 in. was sized to allow room for wick installation. The resulting vapor space easily prevents sonic flow or entrainment of the liquid by the vapor during steady-state operation. The test article case geometry is summarized in Figure 35.

4.3 WICK DESIGN

The wick must be designed such that the heat pipe pressure balance provides a continuous flow of working fluid capable of transferring the design heat loads. The wick provides the pumping power, via capillary forces, but is also responsible for the liquid pressure losses. Wick design is further constrained by the boiling limit which limits the wick thickness in the evaporator region.

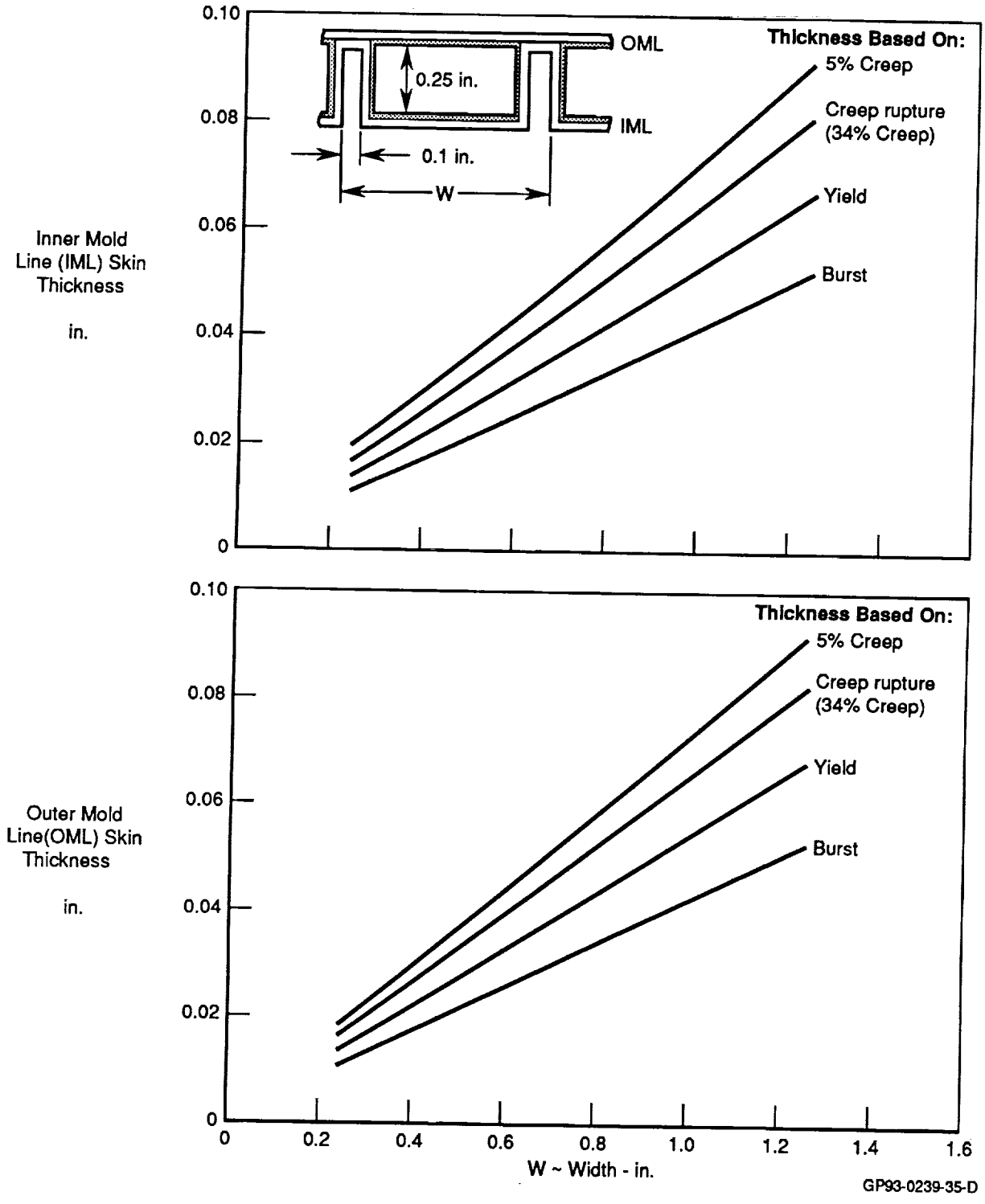

Figure 36. Heat Pipe Case Thickness Requirements

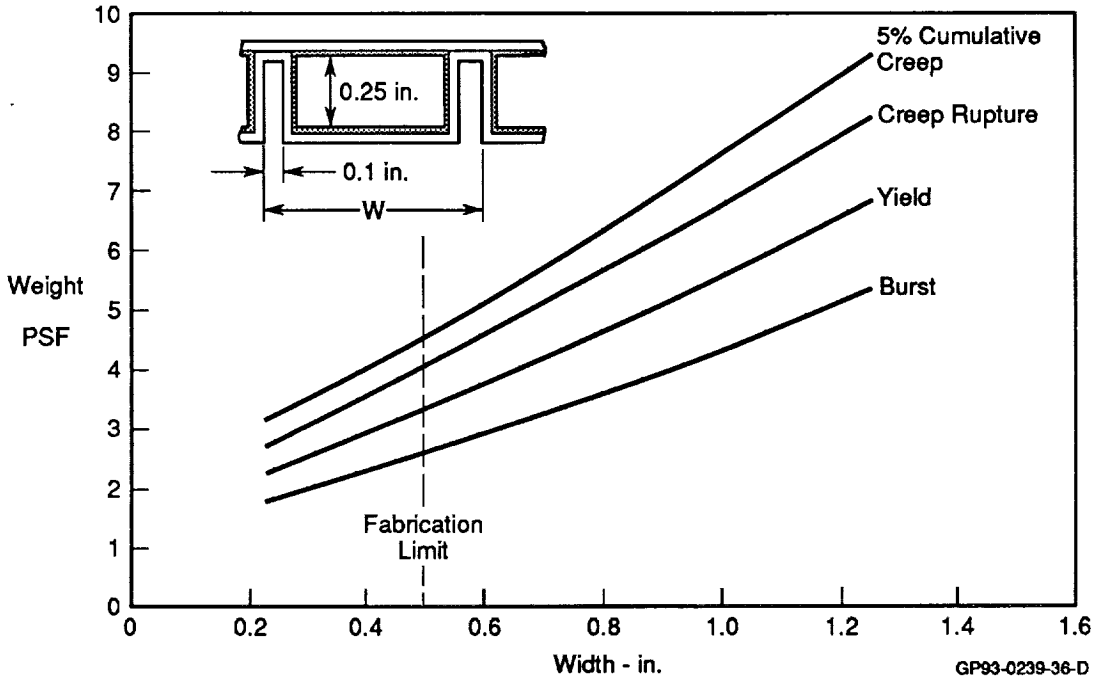

Figure 37. Heat Pipe Case Weight Decreases With Case Width

Wicking requirements established for the test article were an effective capillary radius of 2.57×10^{-4} ft and a permeability area product of 3.27×10^{-12} ft^4. In addition, the wick thickness in the evaporator must be less than 0.786 in.. Wick designs considered for the proposed test article were:

- Isotropic (Simple) Screen Wick
- Isotropic (Simple) Screen Wick with Transport Wick Along Back Face
- Arterial Wicks
- Axial Grooves
- Porous Metal Wick Structure
- Variable Thickness Wick

These designs, shown in Figure 38, have their relative merits as discussed below.

Analysis indicated that an isotropic wick design can not meet the above wicking requirements without exceeding the boiling limits for an 1800°F sodium heat pipe. Various combinations of 50, 100, 200, and 400 mesh screen

were examined but those designs which could provide the required permeability areas product were too thick and exceeded the boiling limit requirement.

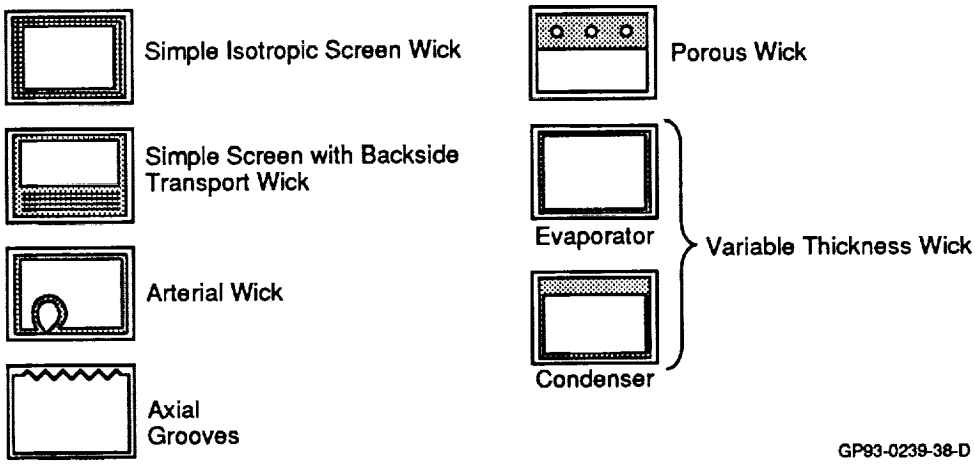

Figure 38. Wick Design Candidates

The isotropic screen wick with a transport wick along the back face can meet the design requirements. Four layers of 50 mesh screen between two layers of 200 mesh screen along the back face will provide the required permeability-area product and a wick consisting of one layer of 100 mesh screen between two layers of 200 mesh screen along the front face (primary heat transfer surface) will not exceed boiling limits. With this design, the sodium condensed in the wick along the front face must be wicked through the side wall wick to the transport wick. Then, the sodium flows longitudinally through the transport wick to the evaporator region where the sodium must be wicked to the front face wick via the side wall wick. Dependence on continuous contact between the case and wick along the side and back walls represent an additional and unnecessary risk for fabrication of the test article as discussed in a later paragraph. Therefore, this design was not pursued further.

An arterial wick design with arteries on the back surface can meet the design requirements but also must rely on sodium transfer between the front and back faces as discussed above. In addition, ensuring the integrity of the artery over a heat pipe of this length would be difficult.

Axial groove designs can theoretically meet the wicking requirements. However, the resultant groove depth requirements of at least 0.033 in. would necessitate substantial case thickness and weight penalties since the desired test article case thickness is 0.030 in. without grooves.

Porous metal wick designs also require the addition of arteries to meet the permeability-area product requirement. In addition, the porous wick structure's ability to withstand large thermal gradients during startup was questioned.

The variable thickness wick design provides a wick of varying thickness along the front face (heat transfer surface). In the long condenser section, layers of coarse (permeable) wick are used to minimize wick pressure losses. In the evaporator section fewer layers of screen are used to minimize the wick thickness and preclude boiling within the wick. This design is attractive because good wick-to-wall contact is required only on the heat transfer surface of the heat pipe. However, fine mesh screen can be provided around the three remaining surfaces in the condenser region. This acts only as a scavenger wick to transport small amounts of sodium which may condense on the back face to the primary wick.

Wick Design Selection - The variable thickness wick design chosen for the Sodium/Hastelloy X heat pipe test article is shown in Figure 39. In the evaporator, 2 layers of 50 mesh screen are sandwiched between 2 layers of 200 mesh screen while the condenser has 8 layers of 50 mesh screen between 2 layers of 200 mesh screen. The 200 mesh screen continues around the side walls of the U channel and in the condenser section 200 mesh screen attached to the flat case part is spot welded to the side wall wick. Combinations of 50 mesh and 200 mesh screen were selected because 50 mesh screen is very permeable (low pressure loss) and the 200 mesh screen has small capillary radii (high pumping power). The specific condenser and evaporator designs were established using the wick characteristics shown in Figure 6. Stainless steel was chosen as the wick material because of its compatibility with sodium and Hastelloy X and its availability in screen form. The indicated wick design leaves room for 0.116 in^2 of vapor space in the condenser and 0.153 in^2 in the evaporator, which is sufficient (more than

three times) to prevent exceeding the sonic and entrainment limits during normal operation.

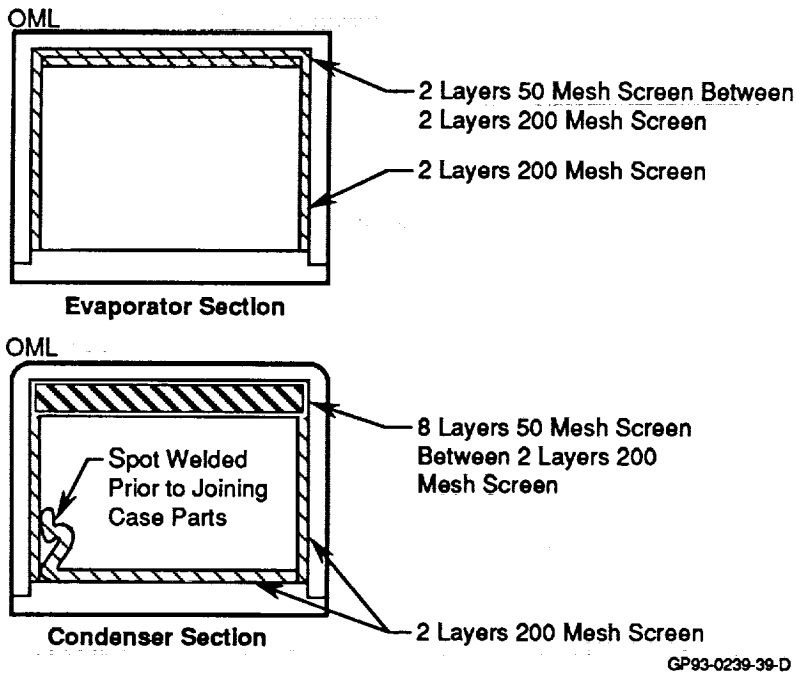

Figure 39. Heat Pipe Test Article Wick Design

5.0 MANUFACTURING DEVELOPMENT AND FABRICATION

A major objective of this program was to advance the heat pipe fabrication technology. By fabricating a full scale sodium/Hastelloy X heat pipe, while addressing the issues of production requirements and test article instrumentation needs, numerous new and improved fabrication processes evolved.

5.1 MANUFACTURING TECHNIQUES

Manufacturing techniques for forming the case, fabricating and installing the wick, and sealing the case were developed and demonstrated.

Case Forming - The heat pipe test article case design, shown in Figure 37, consists of two parts: a 0.030 in. thick "U" shaped channel and 0.060 in. thick flat strip with a 0.030 in. step milled in its edges. During the manufacturing development phase, case parts were limited to 40 in. lengths, for compatibility with existing facilities. This length was adequate for developing the required case forming processes.

Simple, cold working methods were successfully employed to shape and bend the parts from Hastelloy X sheet stock. The U channel was formed with a 1/64 in. radius using 72 in. long brake machine. Both case parts were bent to their leading edge radius - 2.0 in. for the U channel and 1.57 in. for the flat strip - using the hardened steel tooling shown in Figure 40. Hastelloy X's high ductility enabled the bend to be completed without discernible crimping.

Case Sealing - It was originally planned to weld the U channel and flat plate case parts after wick installation by simply clamping the parts together. That technique did not prove satisfactory. Therefore, tooling to house both case parts during welding had to be developed. A resulting weld sample, obtained using this tooling, is shown in Figure 41. Visual observation indicated there was no weld splash and that welding would not degrade the wick sintered to the inner case wall. A case sample, without wick, was welded and successfully pressure tested to 1500 psi without failure (see Figure 42).

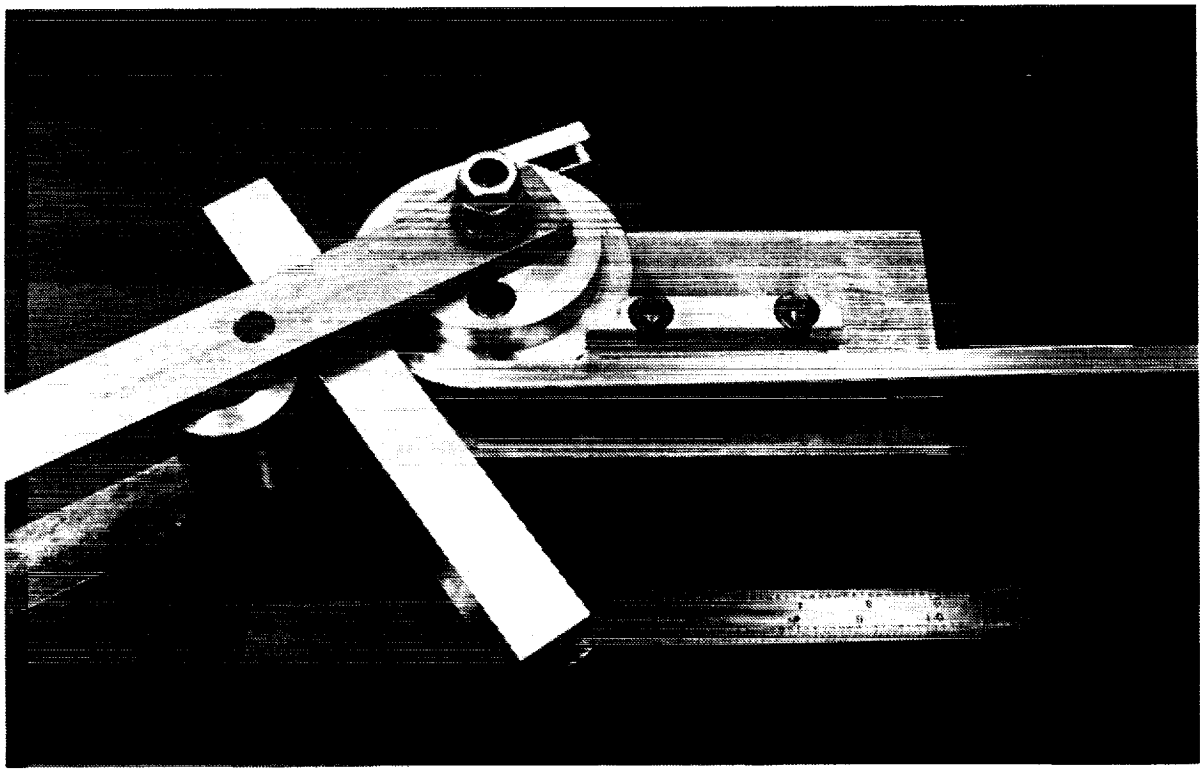

GP93-0239-40

Figure 40. Case Forming Tool

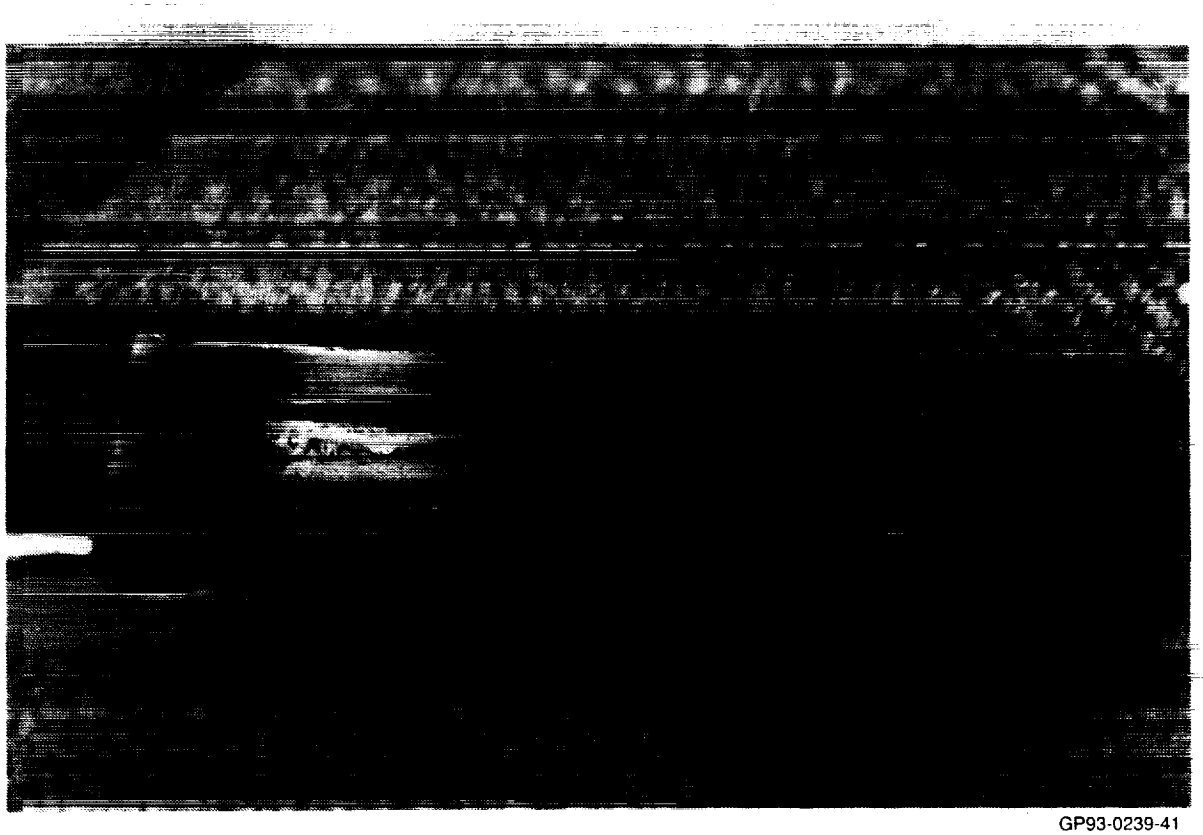

GP93-0239-41

Figure 41. Heat Pipe Case Welding Development Weld Sample

GP93-0239-42

Figure 42. Heat Pipe Case Sample Assembled for Pressure Testing

Wick Assembly Fabrication and Installation - The required wicking characteristics established for the test article were as follows:

Evaporator, $KA_w = 8.11 \times 10^{-13}$ ft^4
Condenser, $KA_w = 3.59 \times 10^{-12}$ ft^4
Capillary Radius, $r_c = 2.57 \times 10^{-4}$ ft

These values were determined using the analytical methods discussed in 3.1. However, the only way to verify assembled wick performance is through experimental measurements. As part of our manufacturing development efforts, wick samples were fabricated to measure resultant wick characteristics. This effort required more time and resources than anticipated because of difficulties in achieving the desired wick performance characteristics.

Initially, short wick-case sandwich sections (6 layers of 50 mesh screen between 2 layers of 200 mesh screen between 2 Hastelloy X sheets) were fabricated (assembled and diffusion bonded) in a vacuum furnace (10^{-4} Torr).

The purpose of these samples was to determine the conditions required to provide good bonding between the stainless steel screen and the Hastelloy X sheet. The best diffusion bonding (sintering) conditions were 2275°F for 1 hr with a 2 psi clamping pressure. While good bonding was achieved (i.e., significant force was required to tear the screen away from the case), micrographs of the wick structure showed an unwanted oxide layer between the screen and the Hastelloy X sheet.

Therefore, a method of removing the oxide layer from Hastelloy X sheet was developed. The screen and sheet samples were first degreased; then cleaned in an alkaline solution; then pickled in hydrochloric acid;,then pickled in a hydrofluoric and nitric acid mixture; then rinsed in tap water, followed by rinsings in de-ionized water and isopropyl alcohol; and finally force dried with clean filtered air.

Additional wick samples were fabricated with various numbers of coarse mesh screen sandwiched between fine mesh screen (0, 2, 4, 5, 6, and 8 layers of 50 mesh screen between 2 layers of 200 mesh screen) to determine wick permeability-area products. These samples were tested to measure their permeability-area products as shown in Figure 43. The mass flow rate of water flowing through the wick sample for a know elevation head was measured and the permeability-area product was computed as follows:

$$K_w A_w = \frac{\dot{m}\mu L}{\rho_L \Delta P} \qquad (13)$$

Results of these permeability tests are shown in Figure 44. Unfortunately, all measured values were less than the predicted required values. This was attributed to the fact that design values are based on loosely wrapped screen but the sintering process results in compression of the wick structure. Compression results from the blending of individual screen wires as the molecules diffuse. This was evidenced by the post-sintering thickness of the 8 layer sample being equal to the pre-sintering thickness of 6 layer samples.

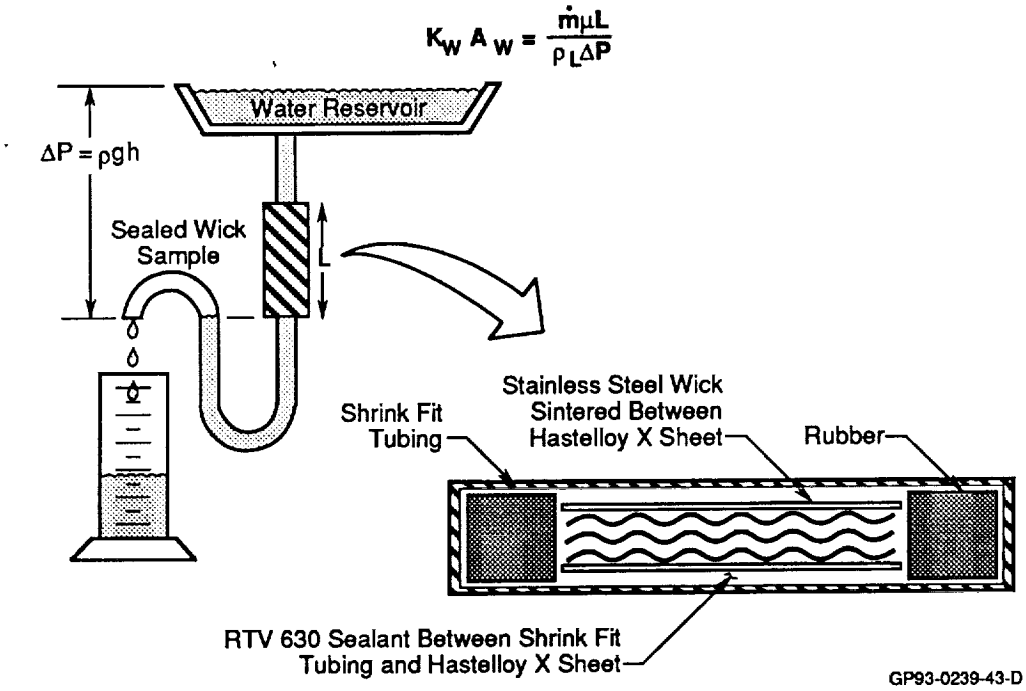

Figure 43. Wick Permeability-Area Products Determined by Testing

Number of 50 Mesh Screens Between 200 Mesh Screen	Thickness (in.)	Permeability (ft^2)	Permeability * Area (ft^4)
2	0.032	2.66×10^{-9}	3.28×10^{-13}
	0.035	2.16×10^{-9}	2.63×10^{-13}
	0.031	2.86×10^{-9}	3.08×10^{-13}
4	0.060	3.65×10^{-9}	7.60×10^{-13}
	0.054	3.75×10^{-9}	7.02×10^{-13}
	0.059	1.32×10^{-9}	2.71×10^{-13}
6*	0.078	2.77×10^{-9}	7.48×10^{-13}
	0.079	2.67×10^{-9}	7.35×10^{-13}
	0.086	3.70×10^{-9}	1.11×10^{-13}
	0.080	2.29×10^{-9}	6.36×10^{-13}
8	0.113	2.91×10^{-9}	1.49×10^{-12}
	0.113	3.50×10^{-9}	1.81×10^{-12}
	0.123	4.27×10^{-9}	1.83×10^{-12}
	0.126	4.77×10^{-9}	2.09×10^{-12}
	0.125	4.95×10^{-9}	2.16×10^{-12}
Required	—	8.57×10^{-9}	3.71×10^{-12}

*Predicted number of 50 mesh screens for design

GP93-0239-44-T

Figure 44. Wick Permeability – Area Product Results for Wick Samples

An alternate, innovative fabrication process which provided larger permeability-area products and a relatively easy method of installing the wick into the U channel case part was then developed. The tooling for this operation is shown in Figure 45. First, the wick assembly buildup is laid into the case. Then a titanium tube is inserted inside the wick assembly. The titanium tube is ultimately used to force the wick against the three sides of the U channel. The purpose of the zirconia cloth and tantalum sheet is to separate the titanium tube and stainless steel wick. Should the titanium and stainless steel come in contact during the sintering, an undesirable eutectic (molten metal) will be formed.

The tooling is put in an oven and heated to 1650°F for 30 minutes. At this temperature, the titanium tube is superplastic. Then the tube is pressurized to 125 psig, which expands the tube into the channel shape. The applied pressure is then reduced to 0.5 psig and the temperature further raised to 2075°F and maintained for 6 hours to facilitate diffusion bonding of the stainless steel wick to the Hastelloy X case.

This technique was initially demonstrated on an 8-inch-long straight U channel section with the condenser wick design (8 layers 50 mesh between 2 layers 200 mesh screen). A photograph of the resultant deformed titanium tube is shown in Figure 46. Visual inspection of the sample indicated good bonding was achieved. To complete the wick structure, two layers of 200 mesh screen were sintered to the flat case part with an overhang of wick which was spot welded to the side wall wick of the U channel as shown in Figure 47.

After demonstrating the wick installation in a straight case part, the evaporator wick (2 layers of 50 mesh between 2 layers of 200 mesh screen) was successfully sintered into a case sample bent to the leading edge radius (Figure 48). Evaporator and condenser wick permeability-area products were determined using test data from these samples developed using the superplastic titanium tube technique. While the condenser wick value compared very favorable to its design value (3.47×10^{-12} ft^4 - measured vs. 3.59×10^{-12} ft^4 - design), the evaporator wick value was significantly lower than its design value (3.01×10^{-13} ft^4 vs. 8.11×10^{-13} ft^4).

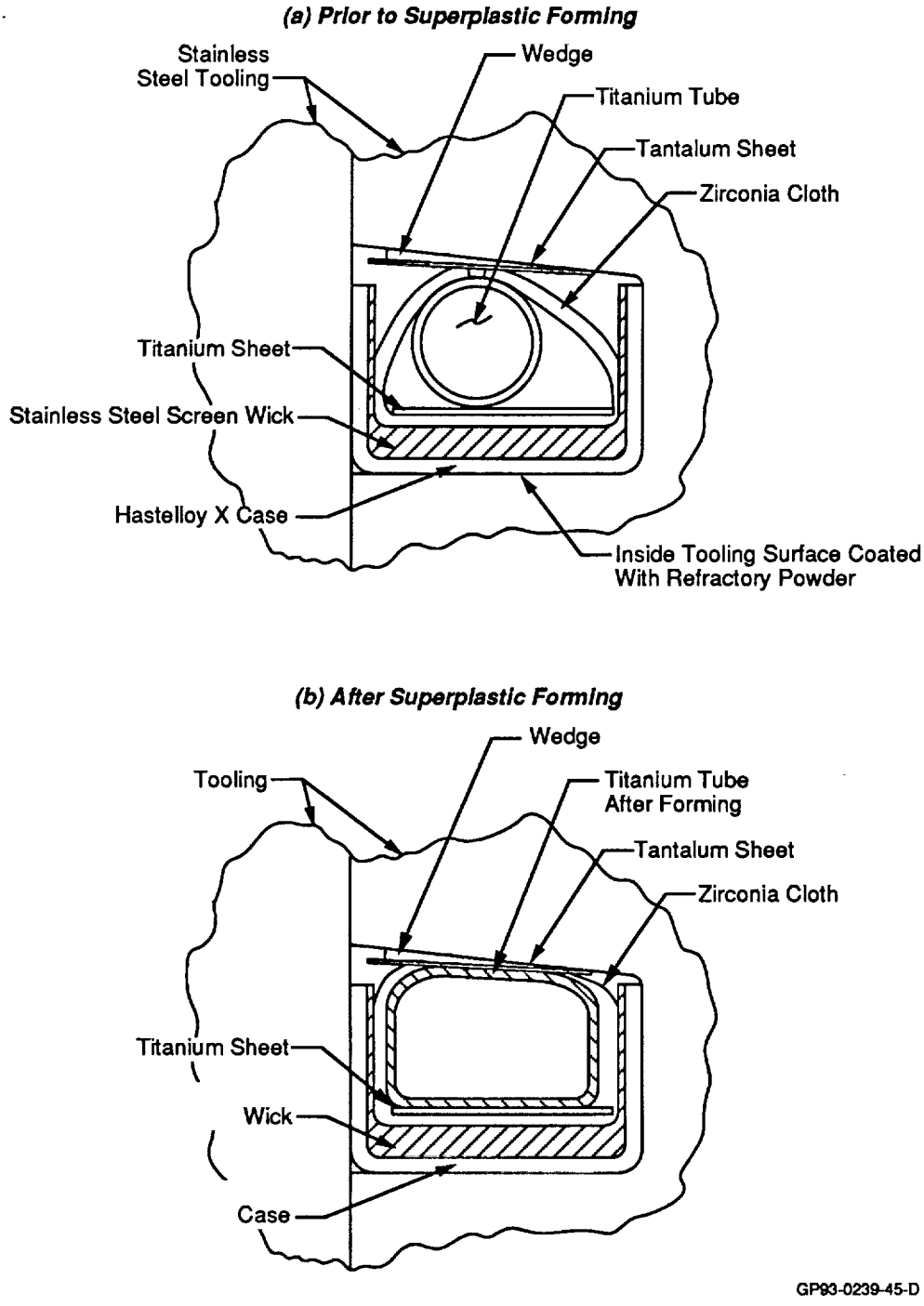

Figure 45. Tooling for Diffusion Bonding Wick to Heat Pipe Case

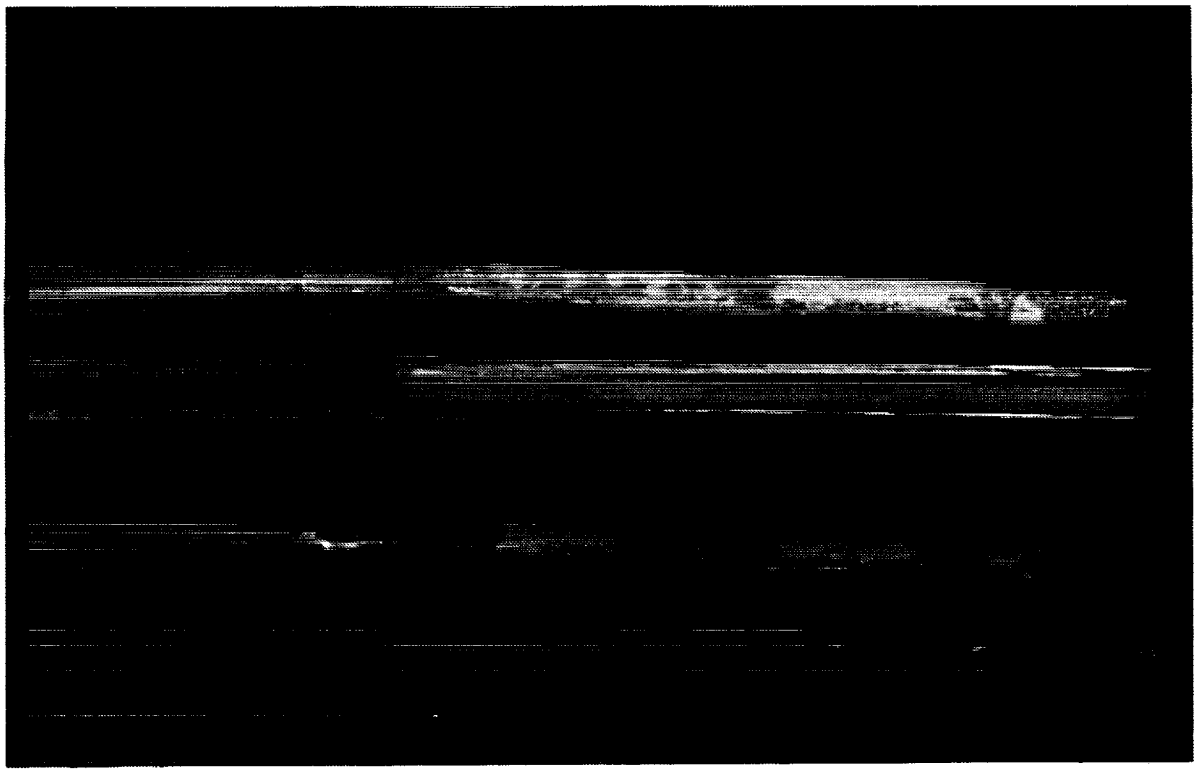

GP93-0239-46

Figure 46. Superplastic Shaping of Titanium Tube Successfully Bonds Wick Assembly to Case

GP93-0239-47

Figure 47. Heat Pipe Wick Installation Development – Hinged Wick Attachment

GP93-0239-48

Figure 48. Heat Pipe Wick Installation Development – Leading Edge Section

To compensate for the higher than design fluid resistance (i.e., lower K_wA_w) in the evaporator, its pumping power was increased (approximately doubled) by substituting 400 mesh screen for the 200 mesh screen. While the 400 mesh screen does not significantly alter the K_wA_w of the evaporator and condenser wick, it reduces the capillary radius r_c by a factor of two. The new wick design consists of 2 layers of 50 mesh screen sandwiched between 400 mesh screen in the evaporator section and 8 layers of 50 mesh screen sandwiched between 400 mesh screen in the condenser section.

To verify the capillary radius of the new wick design, wick samples of 400 mesh screen were tested. The test samples, two layers of 400 mesh screen diffusion bonded between Hastelloy X sheets, are shown in Figure 49. The test apparatus shown in Figure 50 was used. The procedure is to flow air through the wick into the water, and to decrease the air pressure until the flow through the wick is observed to cease. The pressure at this time is recorded, and from this pressure the capillary radius was calculated to be 1.51×10^{-4} ft. The predicted value was 2.57×10^{-4} ft. Since pumping power is inversely proportional to the capillary radius, the 400 mesh screen should be sufficient to provide the design working fluid flow.

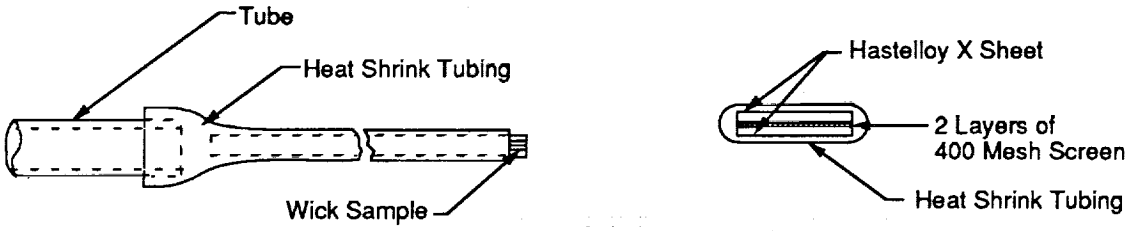

In Plane Wick Test Sample

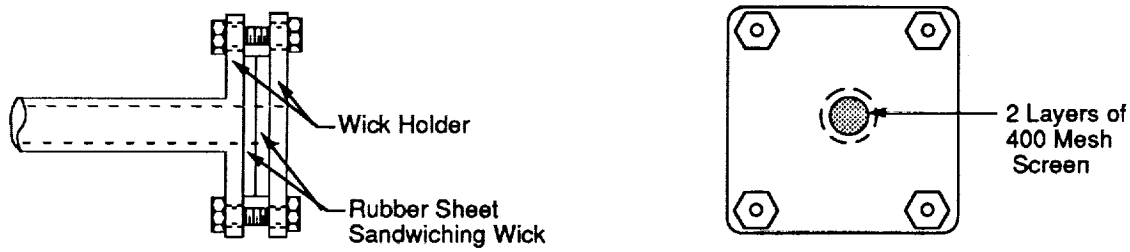

Normal To Plane Wick Test Sample

GP93-0239-49-D

Figure 49. Wick Test Samples for Capillary Radius Measurement

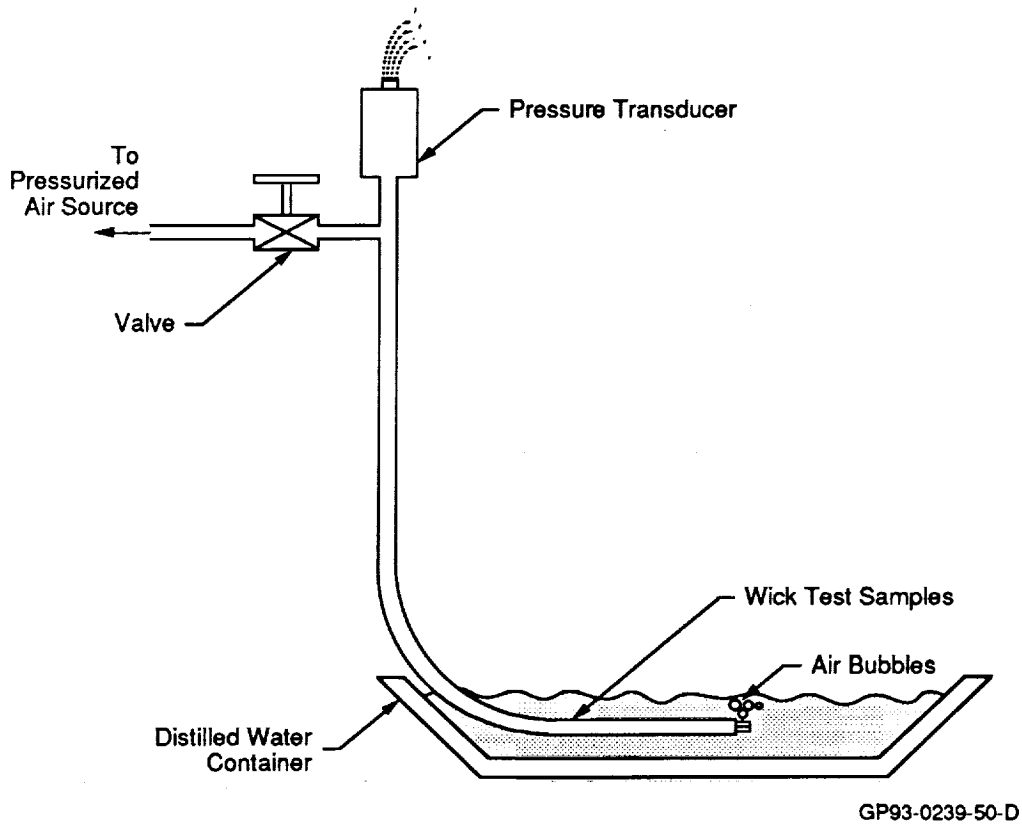

GP93-0239-50-D

Figure 50. Test Setup for Wick Capillary Radius Measurement

5.2 FULL SCALE FABRICATION

Three, full scale (69.4 in. long) U channel and flat plate case parts were fabricated and bent to the 2 in. leading edge radius using the techniques described in 5.1. The wick was cut and set inside the case. The wick/case assemblies were then heated and pressurized to diffusion bond the wick to the case as described in 5.1. One of the assemblies is shown before and after bonding in Figures 51-54. The first case/wick assembly, which experienced some wick tearing, was cut up for inspection. With the exception of a few minor tears, wick bonding and continuity was very good.

Due to oven availability and the heat pipe length, diffusion bonding was conducted at the Progressive Steel Treating Company in Rockford, Illinois. Their facility satisfied the size, temperature (2100°F), pressure (vacuum), and titanium tube pressurization (125 psig) requirements.

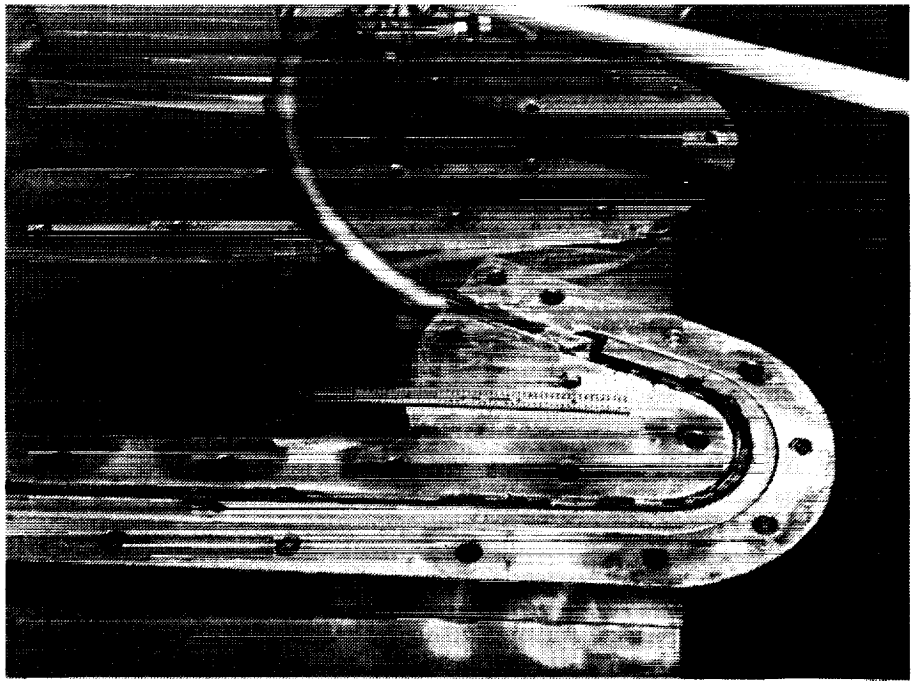

GP93-0239-51

Figure 51. Wick/Case Installation Using Titanium Tube to Hold Wick Against Case

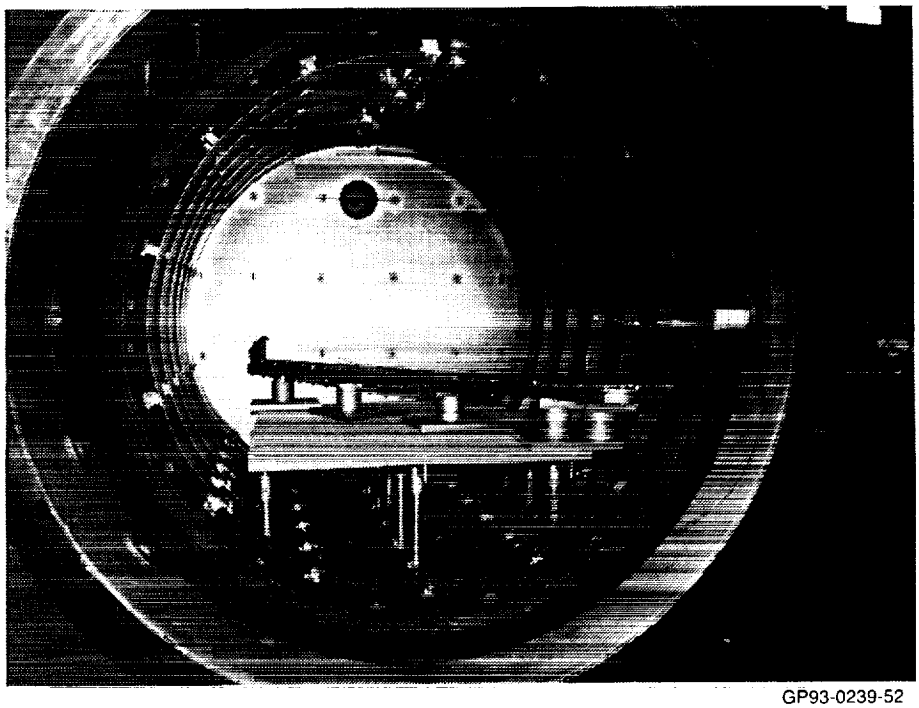

GP93-0239-52

Figure 52. Wick/Case Installation Diffusion Bonding Furnace

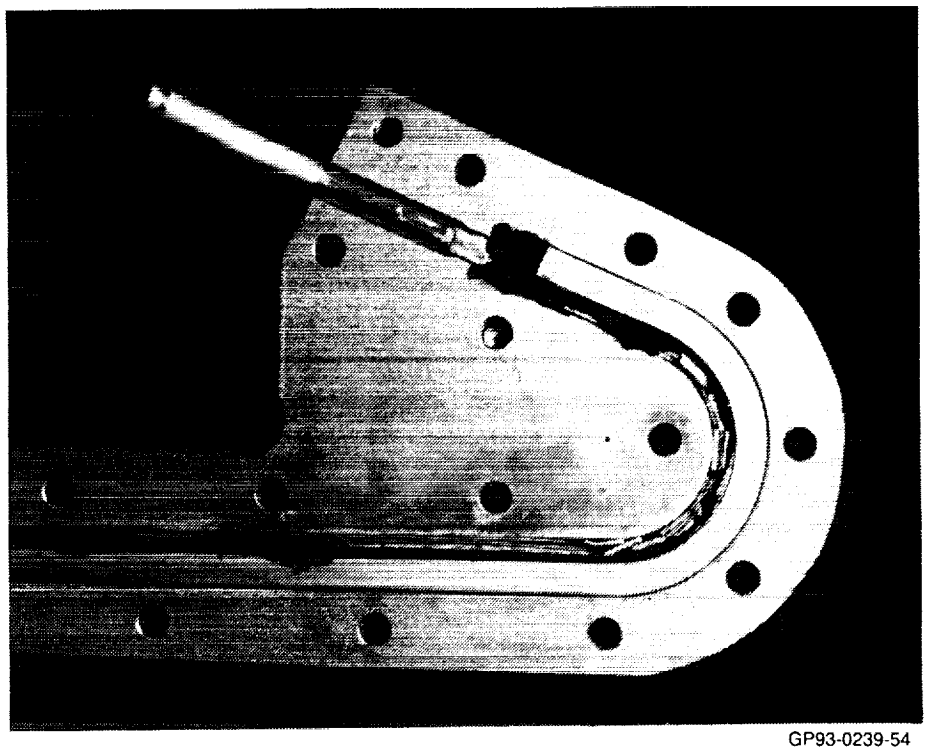

GP93-0239-54

Figure 53. Post Wick Sintering – Leading Edge Section

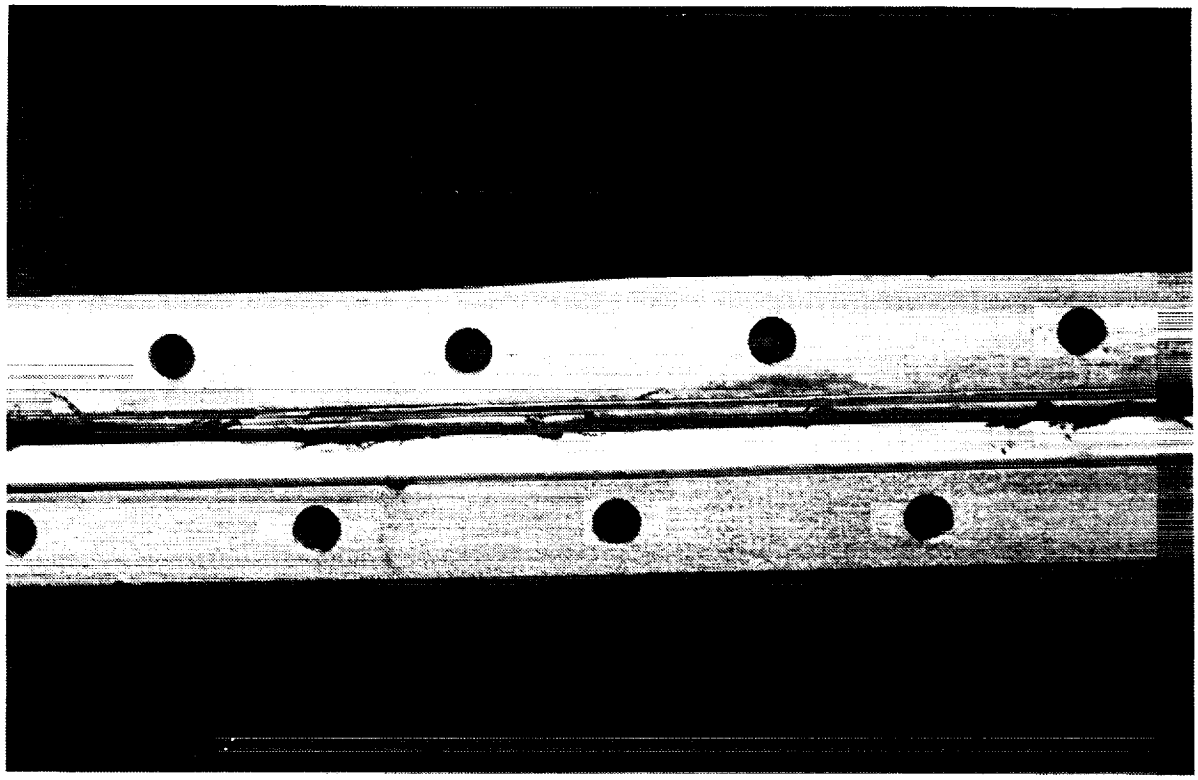

GP93-0239-53

Figure 54. Post Wick Sintering – Straight Section

The two remaining cases were cleaned to remove residual zirconia fibers. Zirconia was used in the diffusion bonding process to separate the stainless steel wick and titanium tube, in order to prevent the formation of a eutectic. The flat plate wick was spot welded to the U channel case part and then the case was welded closed. After the test article was internally instrumented (see Section 5.3) and tested using water (see Section 5.4), it was pressure tested to 341 psig (no yield at proof pressure). Then the heat pipe was evacuated and filled with 3.4 in^3 of sodium to saturate the wick and fill the pressure sensor tubing.

5.3 INSTRUMENTATION

To validate heat pipe analytical techniques, test data are required for comparison purposes. Previous test efforts (References 1-4) have relied on external temperature measurements during steady-state and transient operation. To gather data for comparison with sophisticated computer codes (e.g., Reference 5), the heat pipe was internally instrumented as shown in Figure 55 to measure heat pipe vapor pressures and temperatures during startup.

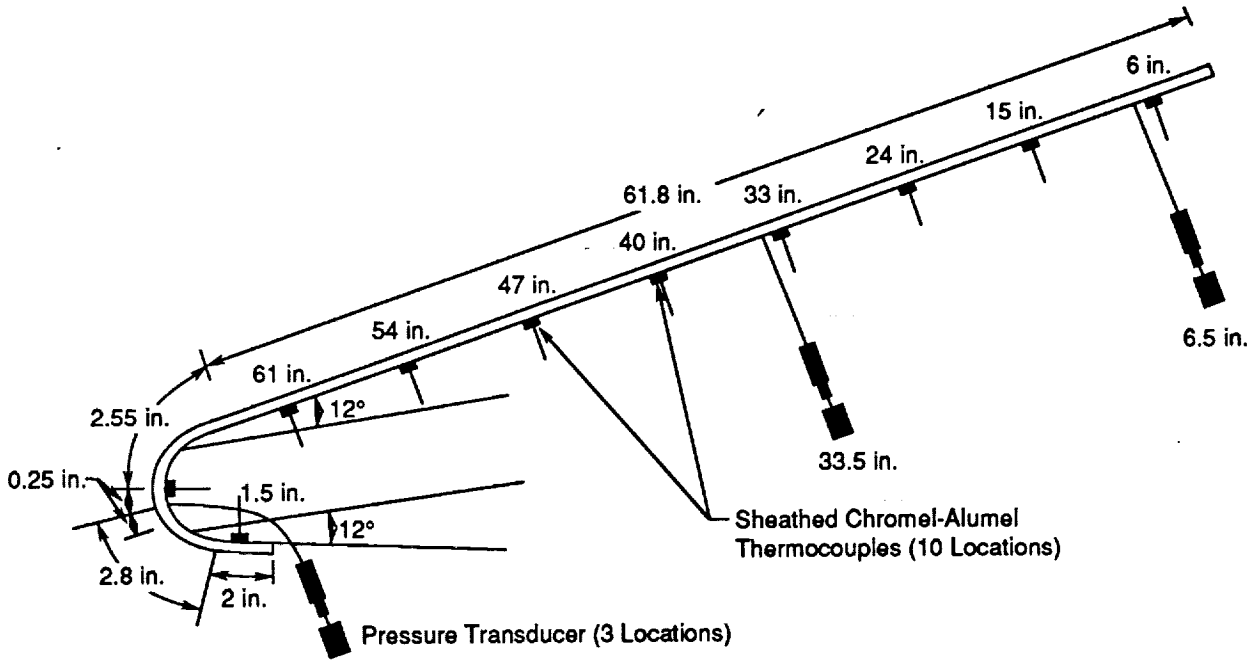

Figure 55. Heat Pipe Internal Instrumentation Locations

The internally instrumented, full scale heat pipe is shown in Figure 56. The techniques developed for these measurements, developed under MCAIR Independent Research and Development (IRAD), are discussed below.

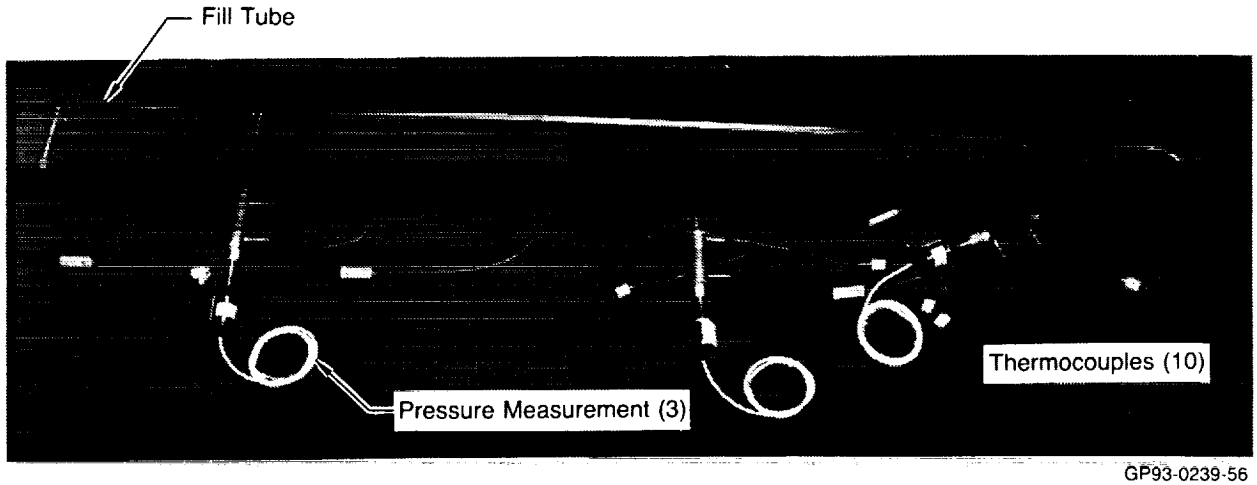

Figure 56. Full Scale Instrumented Heat Pipe

Ten 0.040 inch diameter, Inconel sheathed Chromel-Alumel thermocouples were installed in the heat pipe as shown in Figure 57. Because of their small diameter, these thermocouples are very brittle and several had to be replaced during and after installation.

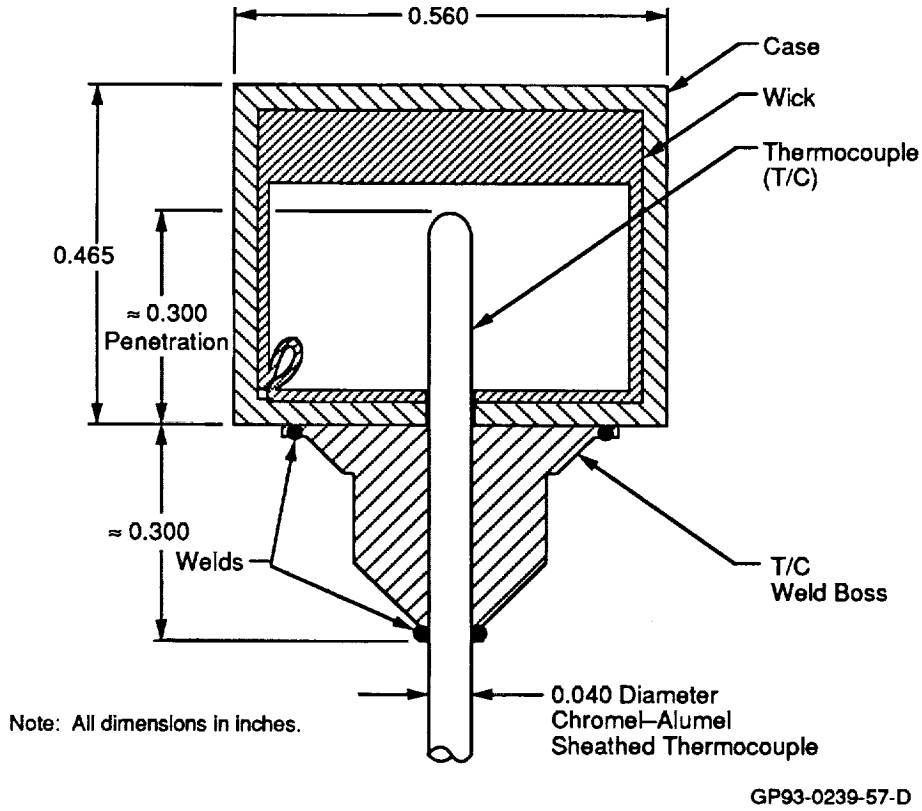

Figure 57. Internal Temperature Measurement Thermocouple Installation

The time constant for the sodium vapor thermocouple was calculated to assess its capability to measure accurate temperatures during heat pipe startup. Due to the low vapor velocities during startup and low vapor thermal conductivity, the time constant is approximately 30 seconds at 900°F and 10 seconds at 1800°F. There appears to be very little room for improvement as the thermocouple heat capacity is very small to begin with. Therefore, vapor pressure and external thermocouple measurements must be used in conjunction with the internal temperature measurements to quantify the heat pipe startup behavior.

A system for measuring the sodium vapor pressure has been conceptually designed as shown in Figure 58. Due to the extreme temperature conditions within the heat pipe (i.e., 1800°F), the system was designed to locally reduce the sodium temperature to a value acceptable for pressure transducers (less than 350°F). A tube connects the transducer to the heat pipe. The insulation, heater, and cooling system were designed to maintain 300°F liquid sodium at the transducer. Before startup, heaters keep the sodium in the pressure tap liquid at 300°F while the heat pipe is at room temperature. During steady-state operation, the cooling system cools the sodium from 1800°F at the heat pipe/tube interface to 300°F at the tube/transducer interface.

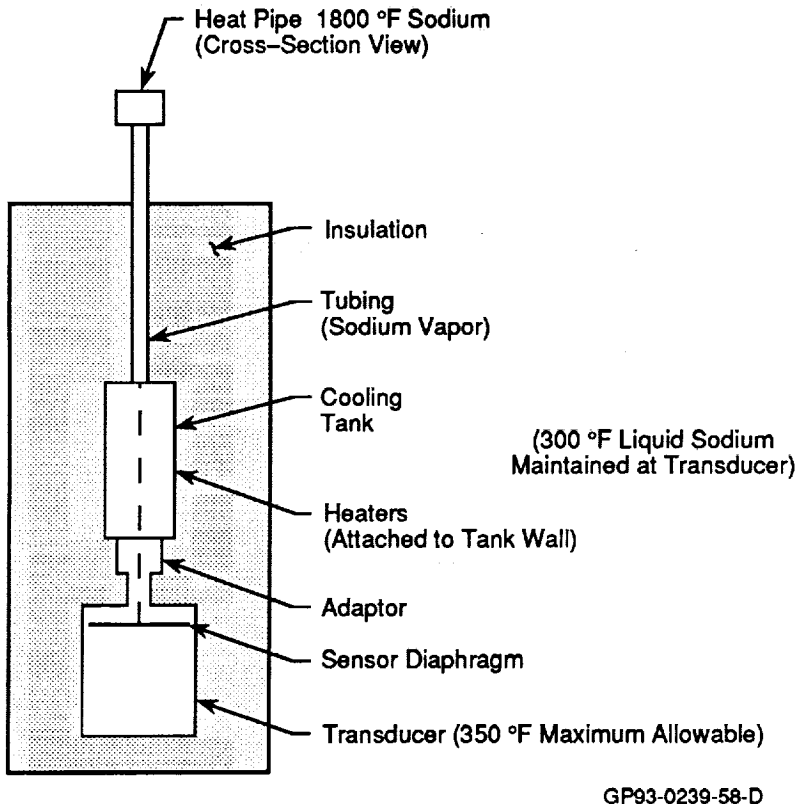

Figure 58. Internal Pressure Measurement System

The sensor is a modified Model 401, High Temperature Pressure Transducer made by Precise Sensors. This sensor is sodium compatible, has a maximum temperature of 350°F, and measures 0-50 psig. The modifications made to the sensor are the enhancement of the temperature compensation range and the addition of the adaptor to the sensor pressure port. This sensor is a strain gage with a stainless steel diaphragm and all welded construction.

Accuracy during startup will be better at higher temperatures than at lower temperatures because of low sodium vapor pressure (e.g., vapor pressure = .081 psia at 940°F). At higher temperatures the sodium vapor pressure (35 psia at 1800°F) is well within the sensor's capability (50 psig).

The heat pipe has been externally instrumented with fifteen Type K thermocouples as shown in Figure 59. In the evaporator region, six thermocouples are spaced approximately every 1.5 in. while in the condenser region nine thermocouples have been attached to the case. Of these, five thermocouples have been densely located (within 1.0 in) in the condenser 46.5 in. from the end of the heat pipe to mark the passage of the continuum front and define case temperature gradients during startup (see Section 6.2 for a discussion of heat pipe startup).

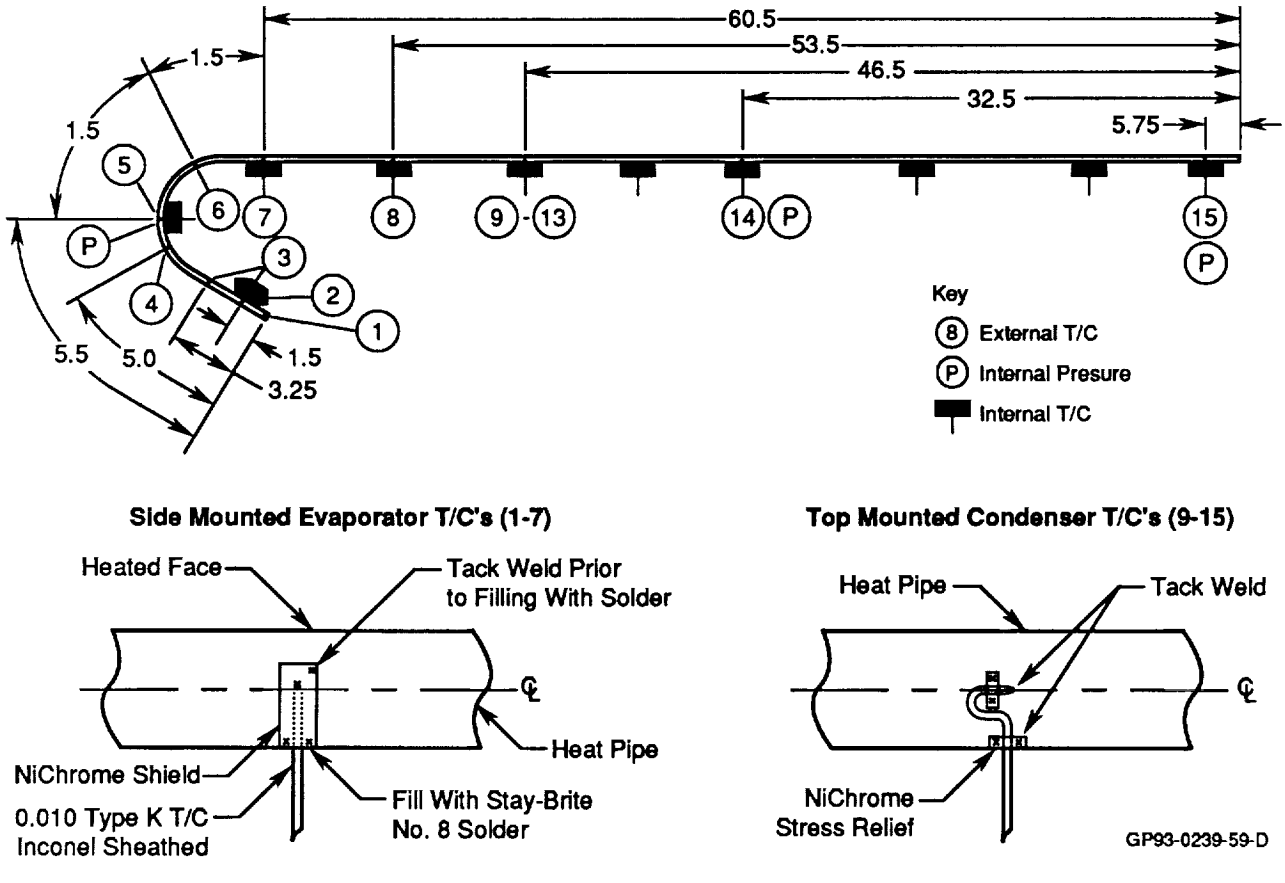

Figure 59. External Thermocouple Locations

5.4 INSTALLED WICK PERFORMANCE

As a complement to this contract we developed, under MCAIR IRAD, a technique to determine heat pipe wick performance characteristics at low temperatures prior to operation with sodium at high temperatures. Testing at low temperature with water as the working fluid allows the wick characteristics to be determined while minimizing the risk of heat pipe failure due to high heat fluxes at high temperatures.

Initial operation of a heat pipe filled with a liquid metal at design power can be risky. "As installed" heat pipe characteristics, specifically wick permeability and pore size, can differ significantly from design values and even experimental values from sub-scale test specimens. If wick dryout occurs during operation due to either insufficient permeability or capillary pressure, the heat pipe temperatures will increase very rapidly (500°F/sec for a sodium-filled heat pipe) and could result in case failure.

To minimize this risk, permeability and capillary pressure values obtained from water-testing can be used to determine heat pipe performance when operating with liquid metals. The wick characteristics (permeability and capillary pore size of the test article) were determined using the following equation:

$$\dot{Q} = \frac{\rho\lambda}{\mu}\left(\frac{2\sigma}{r_c} - \frac{\rho g h}{g_c}\right)/\left(\frac{L}{K_w A_w}\right) \qquad (14)$$

Maximum heat transfer capacities were determined as a function of tilt and are as shown in Figure 60. As expected from the equation, the maximum heat transfer rate varies linearly with the tilt. Deviation of the data points from the curve is due to the time-based thermocouple behavior. It should be noted that non-condensible gases were present in the heat pipe during testing which may have adversely affected the results. The wick pore size and permeability were determined by equating the linear relationship from this figure with the preceding equation (using water properties).

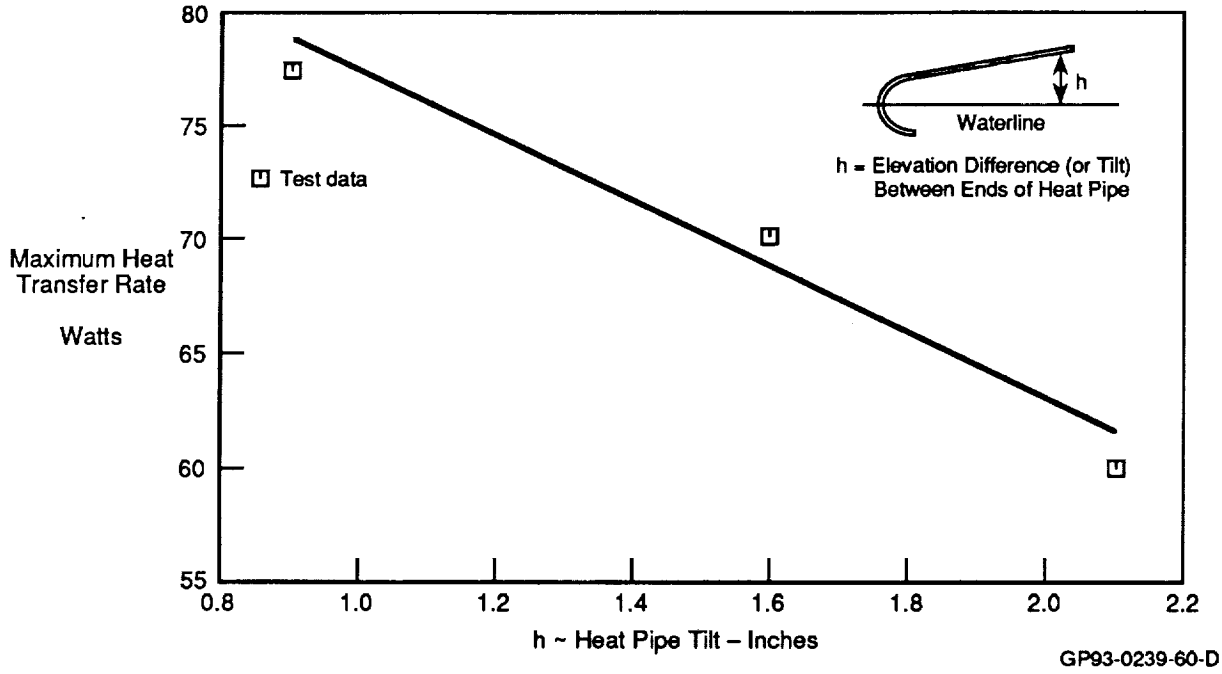

Figure 60. Maximum Heat Transfer Capability of the Water Filled Wing Leading Edge Heat Pipe

The maximum heat transfer capacity of the heat pipe filled with sodium was determined by substituting properties of sodium into the preceding equation (14). The "as installed", component test, and design values of wick pore size, permeability and the resulting heat transfer capacity are presented in Figure 61. Some non-condensable gases were present during the water tests and have been accounted for as a reduction in heat pipe length. The heat pipe performance prediction technique developed suggests that the fabricated test article has approximately the same heat transfer capability as the design heat pipe (1.61 Btu/s vs. 1.42 Btu/s).

	Wick Permeability Area Product, kA (ft^4)	Wick Pore Size (ft)	Maximum Heat Pipe Heat Transfer Rate (BTU/sec) Based on Wick Characteristics
Design[1]	1.85×10^{-12}	1.35×10^{-4}	1.42
From Component Tests	3.11×10^{-12}	1.50×10^{-4}	—
From Completed Heat Pipe Tests[2]	2.55×10^{-12}[3]	4.00×10^{-4}	1.61
	1.61×10^{-12}[4]	2.76×10^{-4}	1.21

(1) Assumes Condenser section: 61.2 in. long 8 layers 50 mesh + 2 layers 400 mesh
Evaporator section: 8.2 in. long 2 layers 50 mesh + 2 layers 400 mesh
(2) Assumes Heat pipe length = 45.6 in. (discounting non-condensable length)
(3) Uses fit of 3 data points
(4) Uses 1st 2 data points

GP93-0239-61-T

Figure 61. Wick Performance Based on Test Data

6.0 HEAT PIPE PERFORMANCE

In this section, heat pipe thermal and structural performance during steady state design and startup conditions is analyzed. A fatigue analysis to assess the flight mission life was conducted. Also, the impact of heat pipe failure was evaluated and the relative performance of alternate heat pipe designs was assessed.

6.1 STEADY STATE (NORMAL) PERFORMANCE OF SELECTED HEAT PIPE DESIGN

A steady state thermal stress analysis was conducted. To integrate the heat pipe into the wing leading edge, stresses due to the restraint of thermal growth and air loads must be considered. Since details of the advanced shuttle wing structure design and airload information were not available, integration was assessed parametrically as a function of the number of external wing leading supports.

Steady state thermal stresses were calculated by superimposing unrestrained thermal stresses due to the through-the-thickness temperature distribution with those required to hold the heat pipe to the mold line configuration.

Unrestrained thermal stresses were calculated for both the test article and production geometries using the steady-state temperature gradients at the stagnation line (see Figure 62). For the design heat flux, the test article configuration experiences a higher thermal gradient across the face skin due to the thicker material buildup. During the initial steady state operation (1800°F), high thermal stresses occur (see Figure 63). These high thermal stresses result in creep rates in excess of 1% per hour. The resulting creep will relieve the stress during high temperature operation, but will result in residual stresses upon cool down. These residual stresses are small and will not cause failure but have the potential of limiting heat pipe operational life and adversely affecting supportability due to attachment preload.

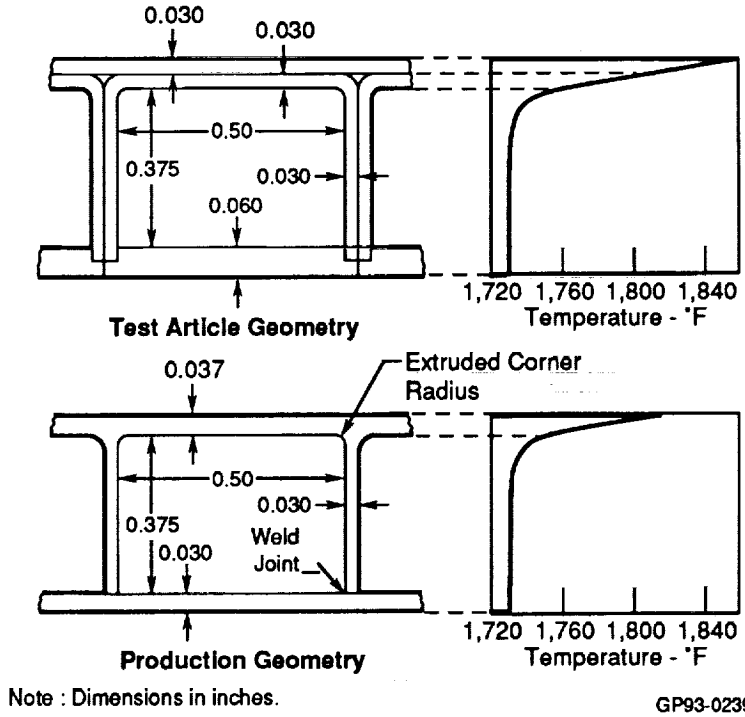

Figure 62. Steady-State Stagnation Line Temperature Distribution

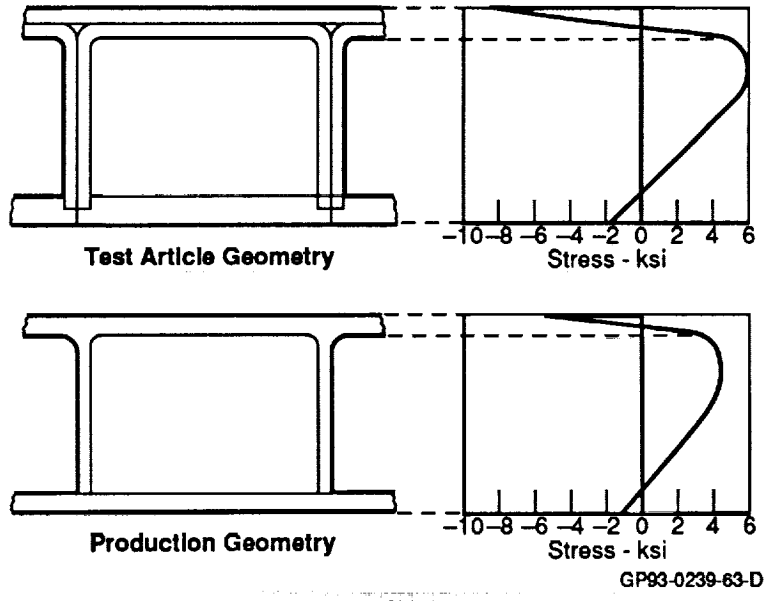

Figure 63. Unrestrained Thermal Stresses Due to Through-the-Thickness Temperature Gradient

Heat pipe stress distributions during steady state operation due to restraint to the mold line configuration were determined parametrically as a function of the number of supports. A NASTRAN finite element model of a heat pipe (production design) was developed. Support reactions were normal to the mold line, allowing thermal growth tangential to the mold line. The attachment interfaces were assumed to remain at the theoretical mold line. Figure 64 shows the temperature profile used in the analysis. Typical results are shown in Figure 65.

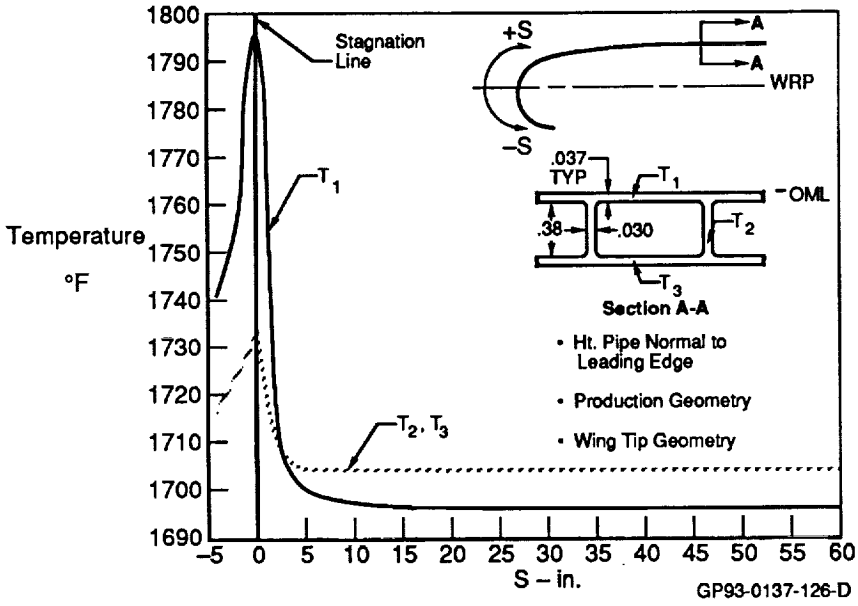

Figure 64. Steady State Temperature Distribution (Axial)

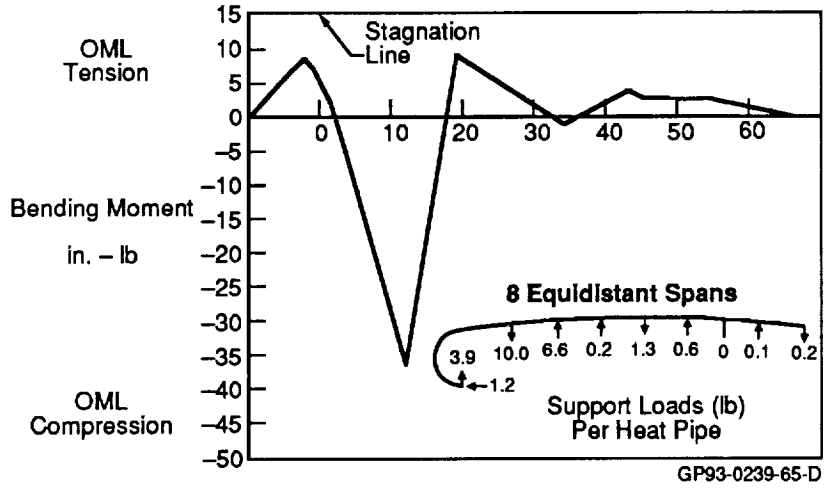

Figure 65. Internal Moments Due to Restraint of Thermal Growth

Two critical heat pipe locations were identified for detailed analysis: the stagnation line and the first support located on the top surface of the wing, approximately 20 in. from the wing centerline. The bending moments at these two locations are shown in Figure 66 as a function of number of supports. The stagnation line location is subject to positive bending moments (OML in tension) and the forward support is subject to negative bending moments (OML in compression). The stress state of the heat pipe is determined by superimposing the stresses due to the support reactions with the unrestrained thermal stresses as shown in Figure 67. The maximum net tensile and compressive stresses at these two locations are shown in Figure 68 as a function of the number of supports. At the stagnation line, the unrestrained thermal stresses dominate; superimposing the stresses due to the restraint only increases the stresses by about 10%. However, at the forward support, the unrestrained thermal stresses are low due to the small temperature gradients, so the restraint stresses dominate. Stress levels associated with yield and a creep rate of 0.1%/hr are shown for reference purposes.

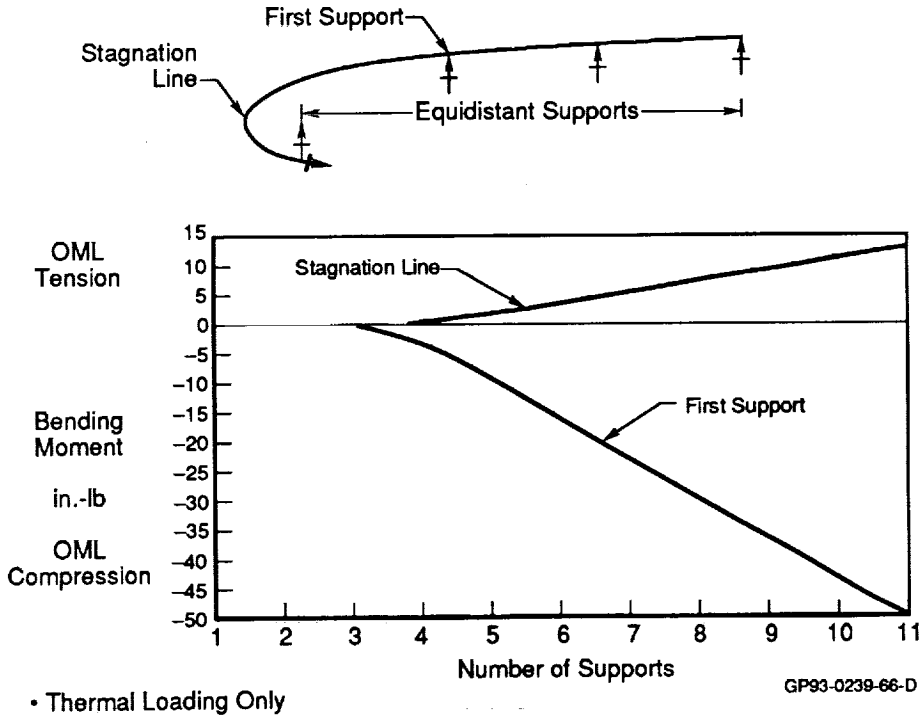

Figure 66. Loading Increases With Supports

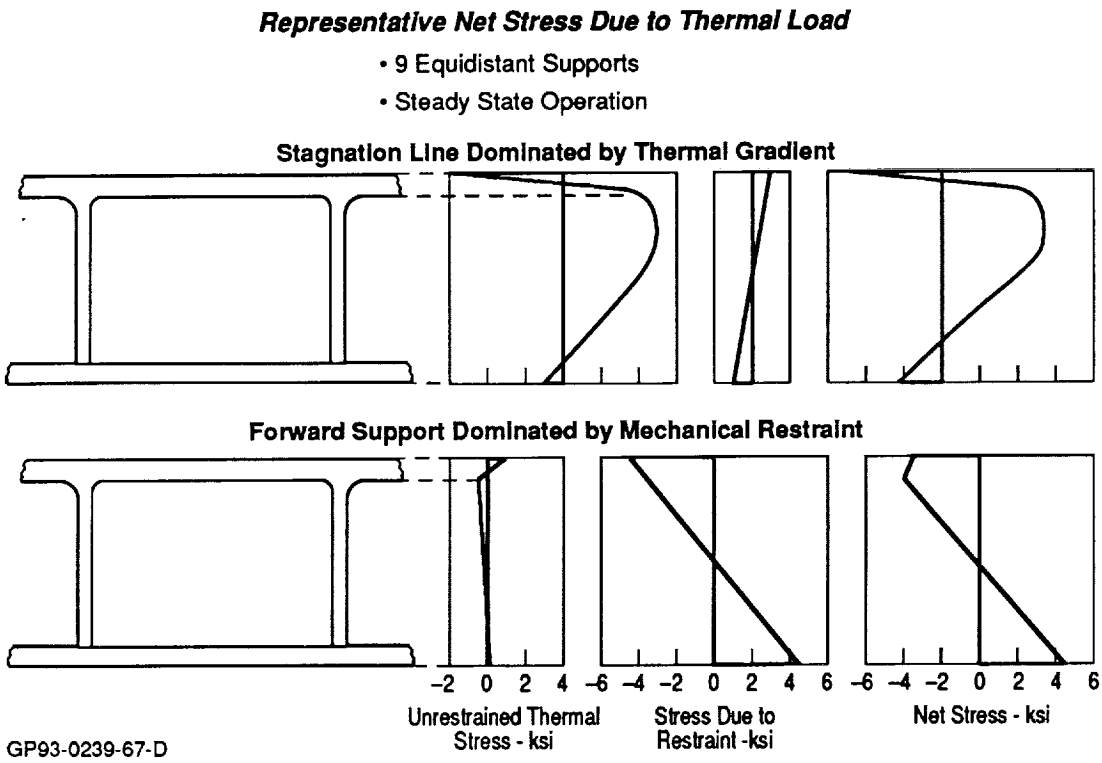

Figure 67. Typical Leading Edge Heat Pipe Stress Distribution

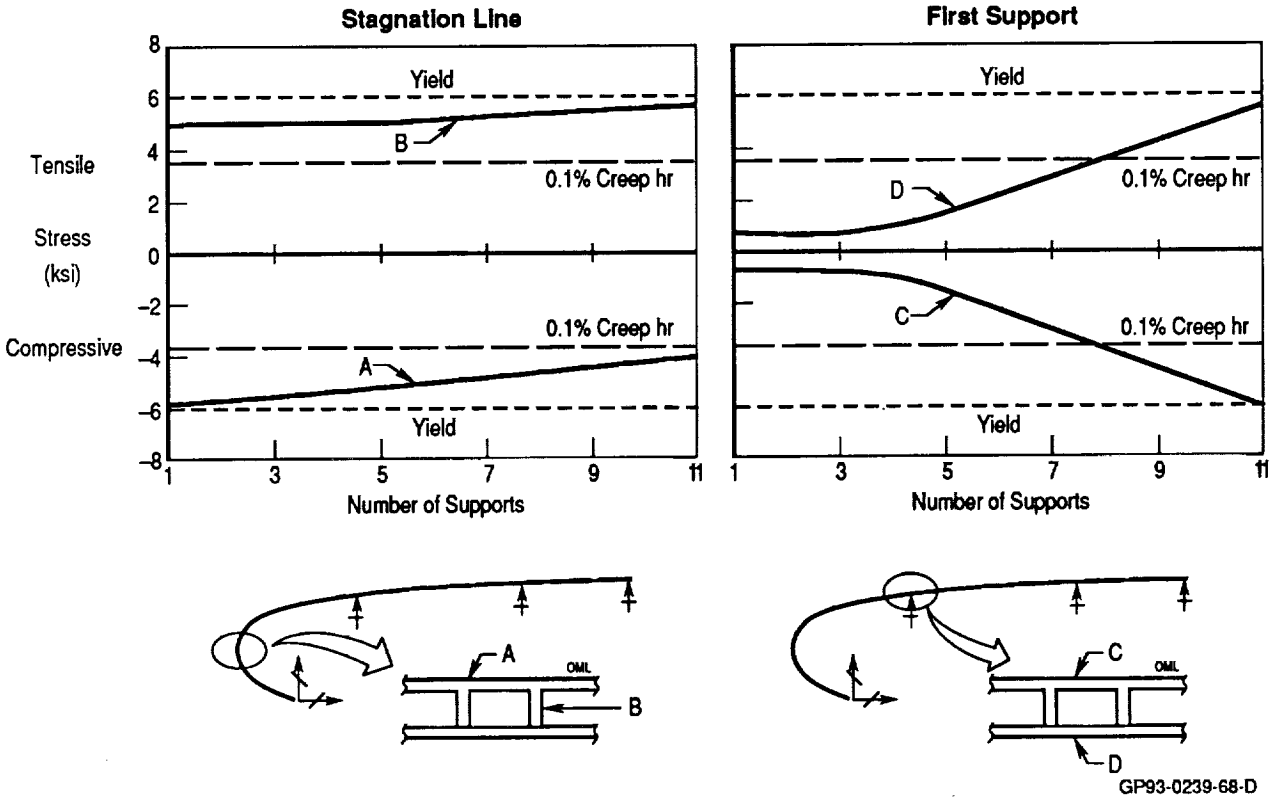

Figure 68. Net Steady-State Thermal Stresses Due to Through-the-Thickness Thermal Gradient and Longitudinal Restraint of Thermal Growth

Based on experience, it was assumed that the integrated heat pipe design will require about 8 restraints (8.5 in. between supports). This configuration would creep at the rate of 0.1%/hour at both the stagnation line and forward support, resulting in residual stresses and attachment pre-load upon cool-down. These residual stresses are small and will not cause failure but have the potential of limiting heat pipe life. As a result, a fatigue analysis has been performed (Section 6.3). Furthermore, available Section Strength to carry external air loads is greatly diminished.

6.2 STARTUP PERFORMANCE OF SELECTED HEAT PIPE DESIGN

At 8 supports thermally induced stresses alone utilize 77% of the yield strength, leaving only 23% of the section strength to carry limit air loads (Figure 68). Prior to atmospheric re-entry, the sodium will be frozen within the leading edge heat pipe wick structure since sodium melts at 208°F, and wing temperatures will be much less than that in space. As the vehicle re-enters the atmosphere (typically 400,000 ft), frictional heating will begin and the sodium will melt. Initially, the vapor density in the heat pipe is so low that molecular flow conditions prevail and axial heat transport is negligible (Reference 1). The sodium will begin to operate locally about the stagnation region once the sodium vapor density increases to a point where continuum flow can occur. As the heat pipe case and wick temperatures increase due to aeroheating and conduction, the continuum flow region expands and the continuum "front" moves down the heat pipe (see Figure 69). During this time, as the heat pipe "starts up", the axial heat transfer is limited by the sonic flow velocity of the working fluid vapor. If surface heating rate increases too rapidly, heat pipe temperatures may overshoot the design temperature and result in heat pipe failure. In addition, large thermal gradients will occur at the continuum front during startup. This will result in high, localized thermal stresses.

A three dimensional, finite difference heat transfer model was developed (Figure 70) to determine the transient heat pipe temperatures. Nodes representing the heat pipe case, wick, and vapor were used. Forty-seven axial segments, with finer resolution in the stagnation region were used. The stagnation line heating shown in Figure 25 was imposed and local heating rates were calculated using the methods described in Section 3.0. Axial and radial conduction between case nodes and wick nodes were modeled. Large

boiling and condensing heat transfer coefficient values were used at the wick/fluid interfaces. The vapor space consisted of two regions: (1) a continuum flow region where the vapor temperature exceeds the continuum temperature, and (2) a molecular flow region where the vapor temperature is below the continuum temperature. The continuum transition temperature used was 830°F for a vapor channel hydraulic diameter of .3 in. (.4812 in. x .2246 in. cross section) (see Figure 71).

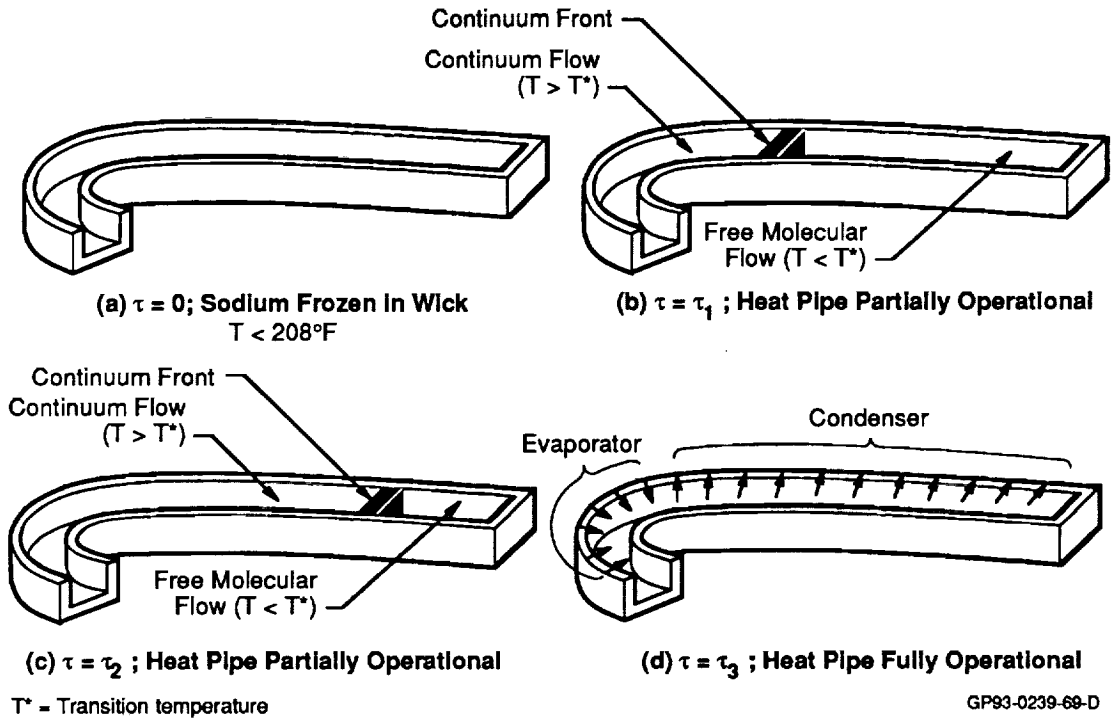

Figure 69. Heat Pipe Startup Modes

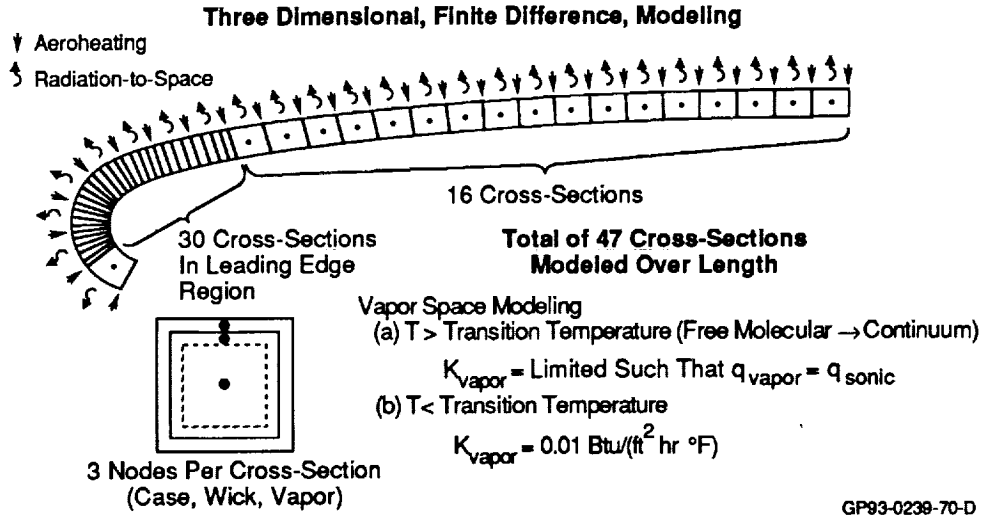

Figure 70. Heat Pipe Startup Heat Transfer Model

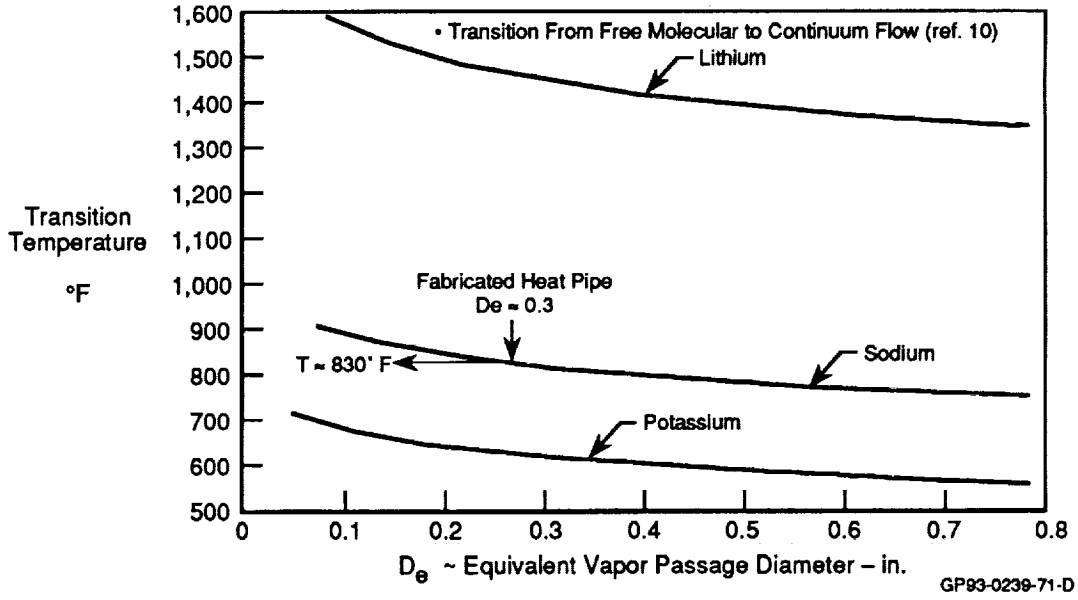

Figure 71. Heat Pipe Transition Temperature Established

In the continuum region, maximum required axial heat transfer rates were calculated and compared to the sonic limited axial heat transfer rates. When the required axial heat transfer rate exceeded the sonic limit, the thermal conductivity was limited to a value which would cause the axial heat transfer rate to equal the sonic limited heat transfer rate. When the required axial heat transfer rate was calculated to be less than the sonic limit, a very high thermal conductivity value was used such that the vapor nodes in the continuum region would be isothermal. The molecular flow region is modeled by vapor nodes with very small thermal conductivity.

The resulting temperature histories of selected nodes are shown in Figure 72. The area around the stagnation line heats up quickly and these vapor nodes transition from molecular flow to continuum flow. During the first 200 to 210 seconds, the axial heat transfer was limited by sonic flow. After this time, use of the large conductivity value kept the vapor temperature constant in the continuum region.

The oscillatory temperature behavior (250-500 seconds) was caused by the model structure and is not physically representative. As the vapor node at the continuum front heated up above the continuum temperature, it became part of the continuum region and the vapor temperature suddenly dropped. This was because the continuum region which was at one uniform temperature was effectively averaged (due to the high conductivity) with the lower temperature node at the continuum front. Additional heating causes the vapor temperature to increase until another node becomes part of the continuum region. During this time (250-500 seconds) the vapor temperature was actually decreasing even though the heat flux increased or remained constant. This was because additional heat storage capability became available and was used as the continuum front traveled down the heat pipe. Finally, the entire vapor space was above the continuum temperature (500 seconds) and the heat pipe heated up to steady state values. The heat flux peaked at 1425 seconds (see Figure 26) and then decreased. As shown in Figure 72, the heat pipe temperatures followed this trend. Note that, at no time during the startup, were temperatures predicted greater than the design temperature.

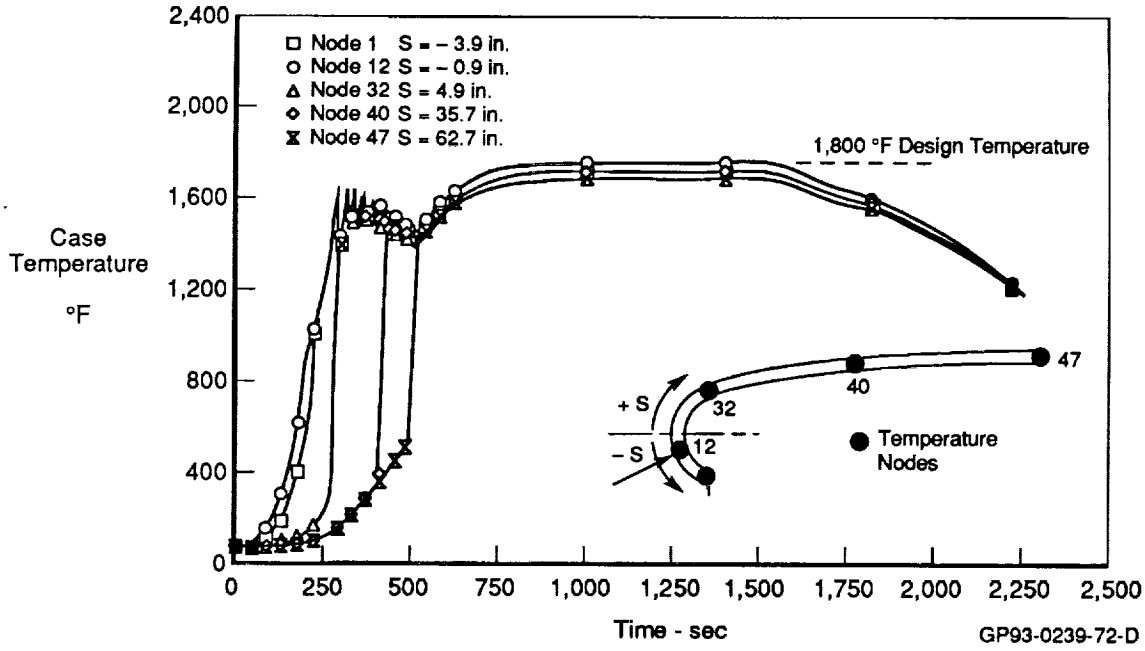

Figure 72. No Overshoot of Design Temperature Predicted During Startup

Thermal stresses during startup were determined using this transient temperature response. Axial temperature distributions during startup are shown in Figure 73. The temperature distribution at 260 seconds was identified as the most severe due to the near peak temperature (1550°F) and the severe thermal gradient (1000°F/in.).

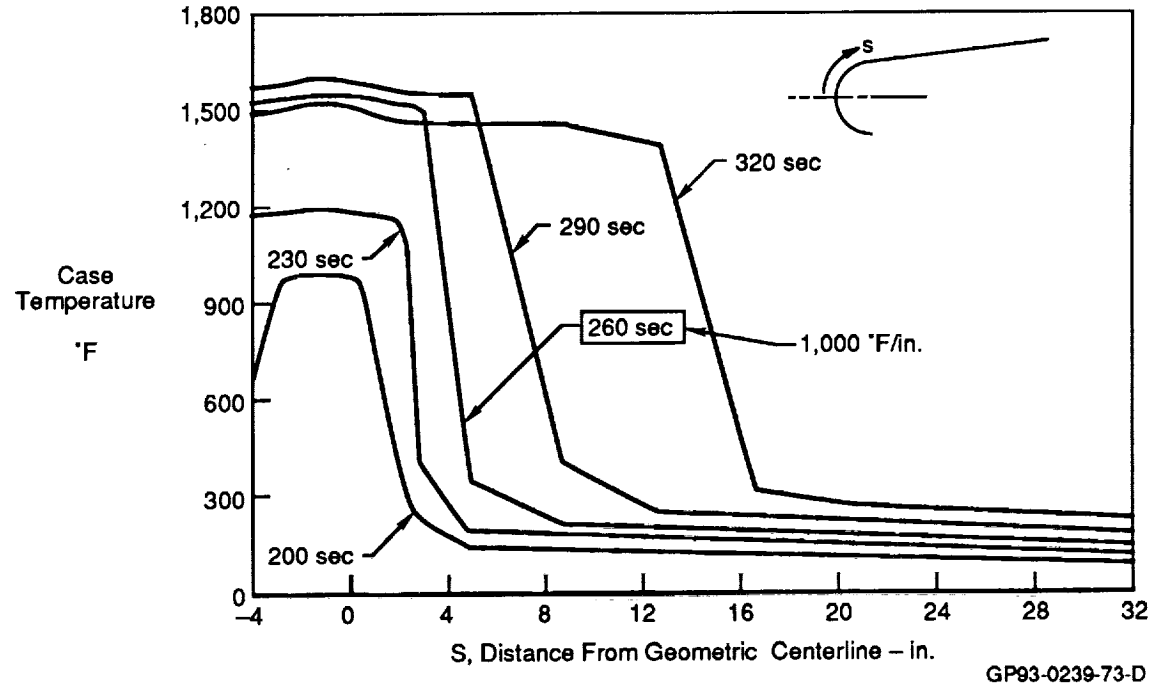

Figure 73. Heat Pipe Experiences Large Axial Temperature Gradients During Startup

The very high thermal gradient in the clockwise direction produces high spanwise stresses. In lieu of a complex three dimensional finite element solution, the spanwise stresses were assessed by the method from Theory of Elasticity by Timoshenko and Goodier (Reference 12) which assumes that plane sections remain plane. This implies that the entire heat pipe length of 69.4 in. is effective in resisting the spanwise thermal expansion at the leading edge. Although conservative, it was felt that this would give an upper bound to the thermal stresses. In an effort to set a lower bound on the thermal stresses, a 5.0 in. section of heat pipe, centered about the steep thermal gradient, was isolated from the remainder of the structure. This accounted for shear lap and free edge effects which would limit the effectiveness of much of the heat pipe material in resisting the thermal growth.

Stress results are shown in Figure 74. The shape and relative magnitude of the stress distribution correlate well with each other. In either case, thermal stresses are well in excess of the yield strength (22 ksi) of Hastelloy-X at 1500°F. Thus it can be concluded that the heat pipe would suffer plastic deformation during the startup transient. A three dimensional finite element model would provide quantitatively better results, but is not expected to affect this conclusion.

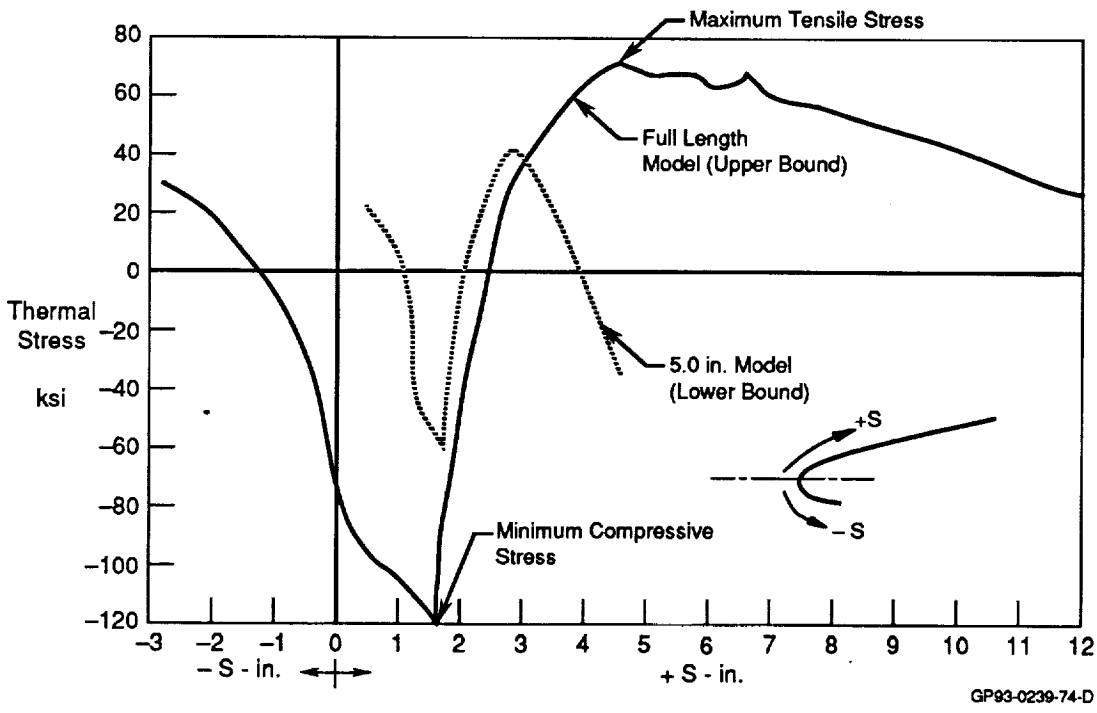

Figure 74. Heat Pipe Thermal Stresses During Startup

During re-entry, the current heat pipe design will suffer compressive yield, in the spanwise direction. This will limit the usable life of the heat pipe assembly and could result in loss of adequate sealing at the expansion joints.

The thermal stress analysis results indicate that thermal stresses during steady state and transient operations are significant design considerations. Thermal stresses during steady state operation at the first support could be reduced by decreasing the number of supports. However, this will tend to increase the bending moment due to air loads. A trade between these effects cannot be made until air loads have been defined. Steady state thermal stresses at the stagnation line, and those during start-up, are primarily a function of the trajectory. These could be reduced by reshaping the vehicle trajectory. In addition a more rigorous transient temperature solution, using Dr. Colwell's heat pipe computer code (Reference 5), may predict less severe thermal gradients and thus the thermal stresses may be less severe.

6.3 FATIGUE ANALYSIS

The fatigue life of the heat pipe was predicted at several locations for the production design. The critical areas were identified as the following high stress regions:

a. The extruded corner radius.
b. The weld joint.
c. The area of maximum through-the-thickness thermal stress at the stagnation line.
d. The area of maximum compressive thermal stress (spanwise) near the leading edge.

Baseline fatigue data for Hastelloy X (Reference 13) is reproduced here as Figure 75. An estimate of the strain versus fatigue life curve at 1800°F was obtained by linear extrapolation of the available data at 1000 and 1600°F.

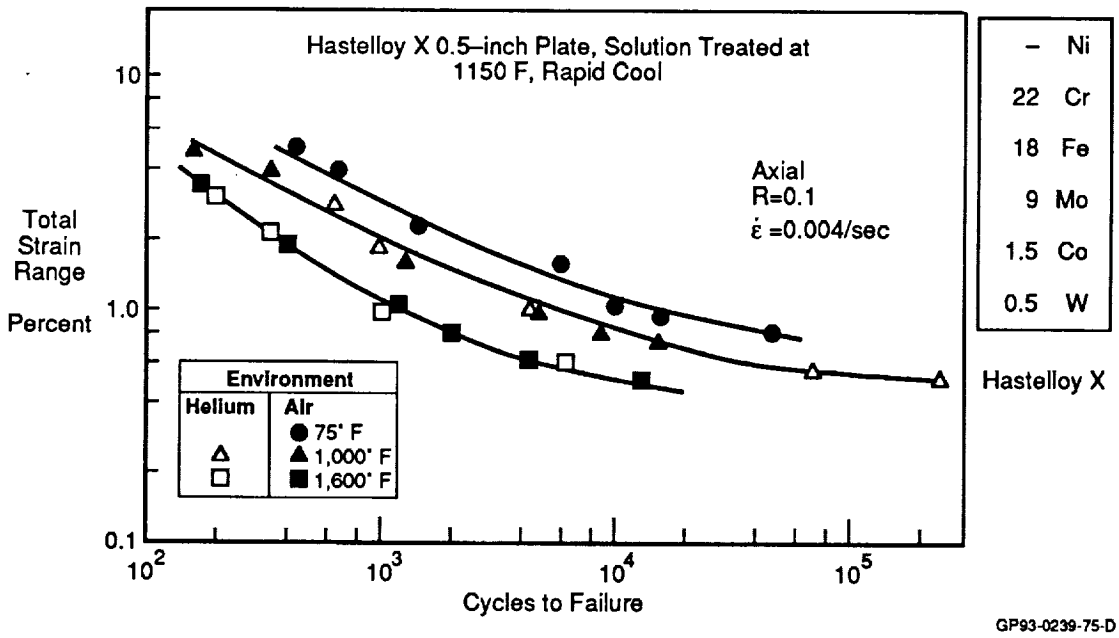

Figure 75. Hastelloy X Fatigue Life Data

Effective Strain Computation - The strain versus life information in Figure 75 is based on tests conducted at a minimum to maximum load ratio of -1 (i.e. R=-1). In order to use this figure in the analysis of other R-ratio cases, the data can be adapted into an effective strain parameter which compensates for different ratios of load. This effective strain is formulated as

$$\varepsilon_{eff} = \sqrt{\frac{f_{max}\Delta\varepsilon}{2E}} \qquad (15)$$

Effective strain is graphed versus the number of cycles to failure in Figure 76.

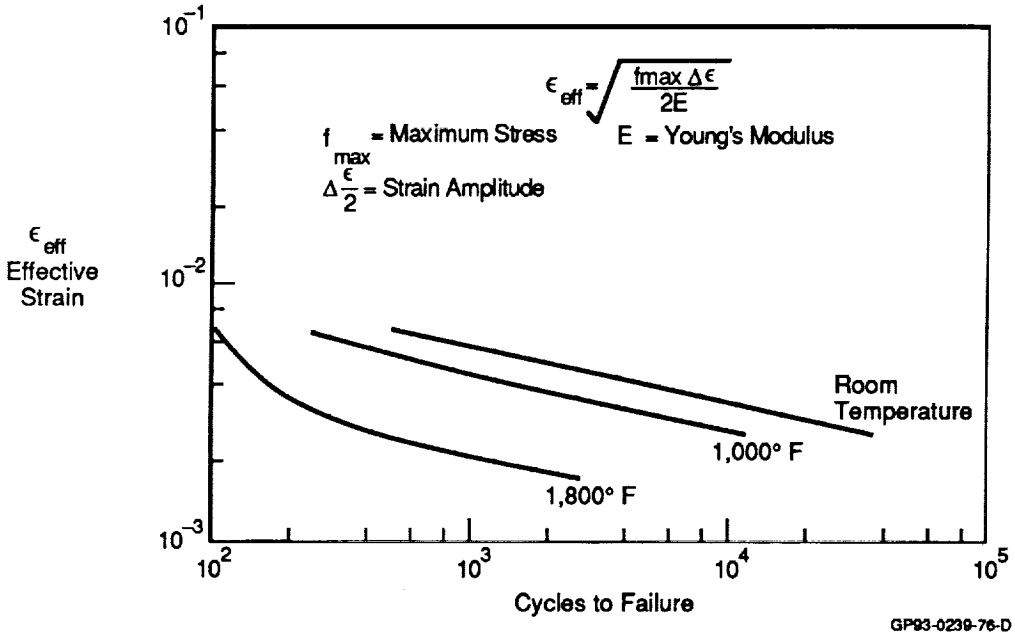

Figure 76. Effective Strain vs. Life of Hastelloy X

Extruded Corner Radius and Weld Joint - NASTRAN finite element analyses at these two locations were used to obtain the stresses caused by normal operating pressures. Stresses were computed for various corner radii and web taper widths as shown in Figure 77. The highest stress at the corner was 4.5 ksi for a radius of 0.013 inches. The corresponding effective strain of 0.0003 in./in. gives a fatigue life greater than 10^5 cycles (or flights) at 1800°F (see Figure 76). Since a comparable life was obtained at the weld joint, these two locations do not represent critical fatigue locations.

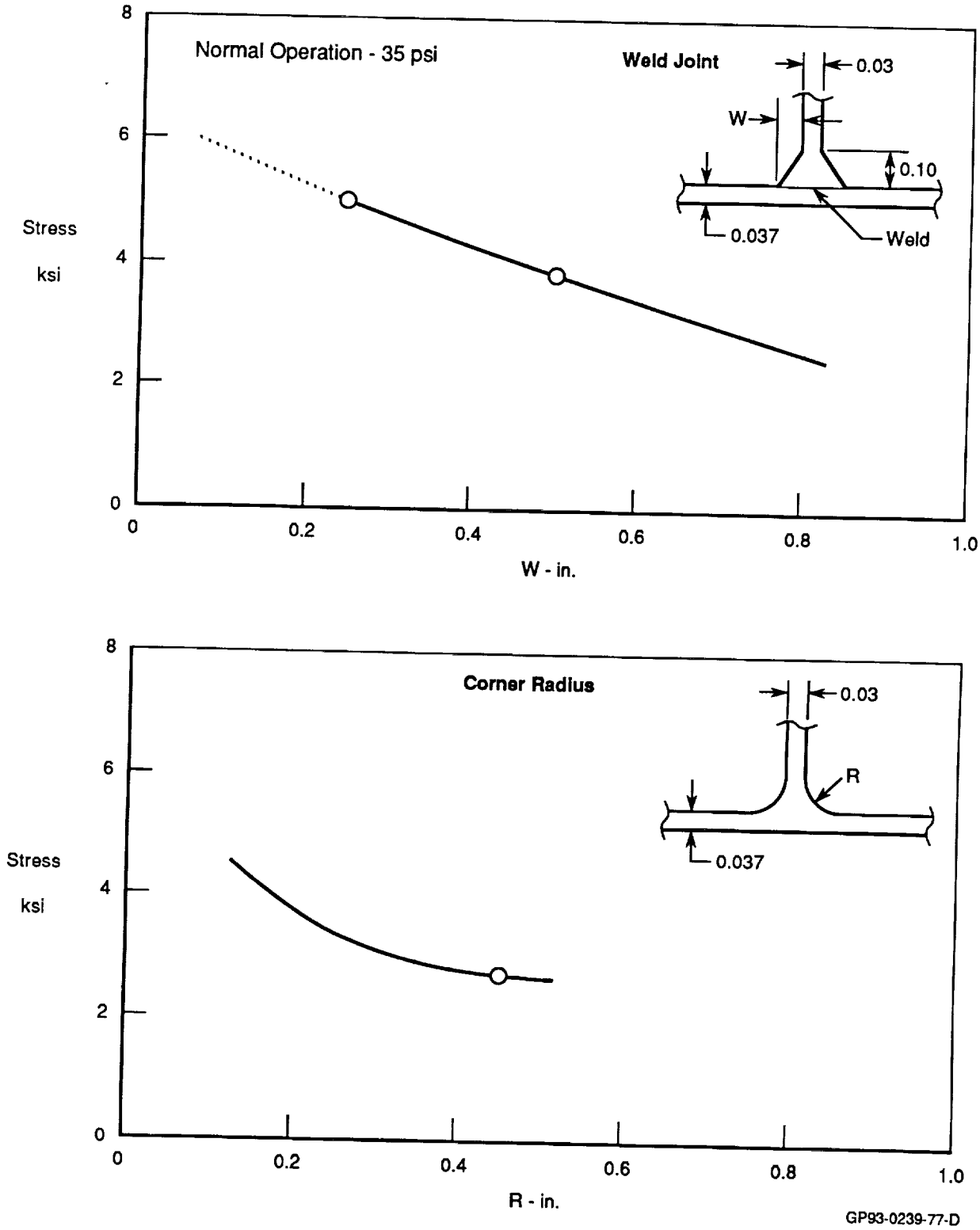

Figure 77. Maximum Stresses at the Weld Joint and Corner Radius (Production Geometry)

Through-the-Thickness Thermal Stresses at the Stagnation Line - The superposition of through-the-thickness thermal stress and stresses due to restraints results in a maximum tensile stress of 5.2 ksi for 7 supports (Figure 68). The effective strain of 0.0003 in./in. results in a life in excess of 10^5 cycles to failure at 1800°F.

A wick on the inner surface of the heat pipe will create areas of stress concentrations at the attachment points. A stress concentration factor equal to 2 gives an effective strain of 0.0006 in./in. The predicted fatigue life still exceeds 10^5 flights, and therefore, is not critical.

Area of Maximum Compressive Stress - The startup thermal stresses were calculated previously and are shown in Figure 74. The two critical areas are at S=1.6 inches (maximum "elastic" compressive stress) and at S=4.5 inches (maximum "elastic" tensile stress). At 260 seconds into the re-entry the latter location temperature is 300°F; much lower than the 1800°F near S=1.6 inches. High compressive strains at S=1.6 in. result in residual tensile stresses upon cooling. Because of this, the S=1.6 in. location was identified as the most critical.

Figure 74 also presents the distribution of stresses using a 5.0 inch segment model. Since the magnitudes of the stresses were lower (resulting in longer fatigue lives), this case was not analyzed in detail.

The first phase of the analysis required a model of the stress versus strain history during the thermal cycle. When the temperature range is low enough, the material does not yield during the cycle, and the thermal stresses and strains return to zero at the original temperature. If the thermal stresses increase past yield, the material is left with residual stresses. This is the case presented herein, since the compressive "elastic" stress of -120 ksi at S=1.6 is beyond the yield stress at 1800°F.

The model developed to describe the stress-strain history during the initial cycle is outlined in Figure 78. An element of length, L, experiences an increase from an initial temperature, T_1, to a higher temperature, T_2. The component is assumed to be constrained by the boundary so that it

maintains a constant length. The various steps in the initial thermal cycle are:

(1) An initial temperature T_1 and element length, L.

(2) The amount of free expansion due to a temperature increase to T_2 is computed.

(3) The compressive thermal stress required to maintain the original length, L, is computed. The magnitude of this stress causes yielding of the material.

(4) The thermal contraction due to a temperature drop to the original T_1 is determined.

(5) The compressive thermal stress vanishes with lower temperatures.

(6) A residual tensile stress results when the specimen is constrained to the original length, L. This stress may cause yielding in tension.

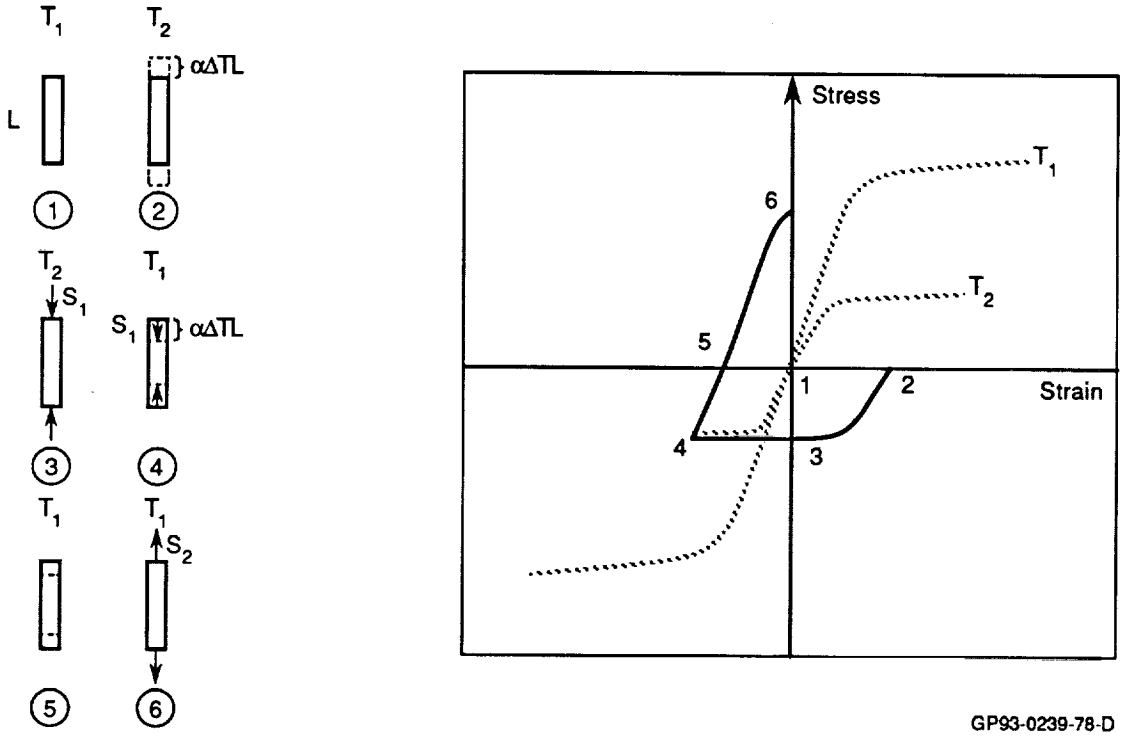

Figure 78. Initial Thermal Cycle Stress-Strain Model

Subsequent thermal cycles are described by the model in Figure 79. As the temperature increases to T_2 after step (6), expansion of the element is prevented by compressive thermal stresses. Therefore, the total stress acting on the element is given by the superposition of residual and thermal stresses. The change in total stress as the temperature increases to T_2 is modeled in steps (7) to (9).

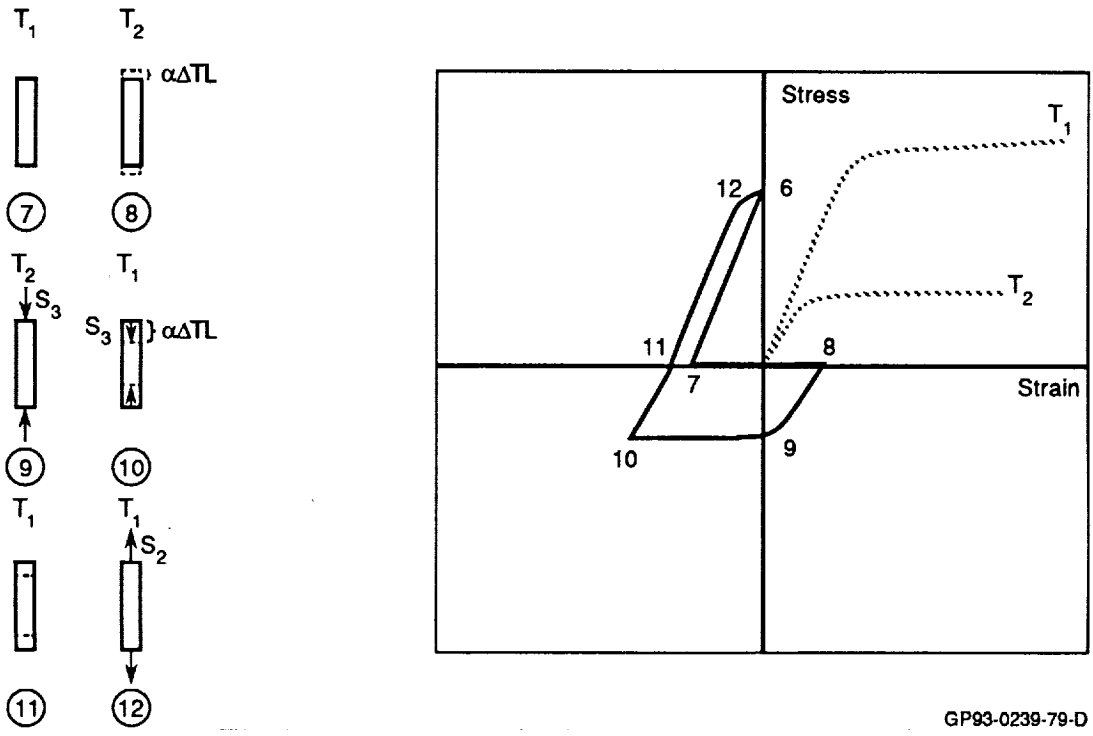

Figure 79. Subsequent Thermal Cycle Stress-Stain Model

(7) The total stress vanishes as compressive thermal stresses increase with temperature.

(8) The amount of expansion due to a temperature increase to T_2 is calculated.

(9) A compressive thermal stress required to maintain the original length, L, is calculated.

(10) The thermal contraction due to a temperature drop to the original T_1 is determined.

(11) The compressive thermal stress vanishes with lower temperature.

(12) A residual tensile stress required to maintain the original length, L, is calculated.

This model shows the interaction that occurs when cycling from one stress-strain curve at one temperature to another at a different temperature. Some of the steps in the cyclic model may be rearranged as long as the end state is the same.

The fatigue damage which occurs during the cycle was assumed to be caused by applied external loads such as thermal or residual stresses only. In order to determine the strain amplitude caused by the external loads alone, the strains due to thermal expansion were ignored in Figure 80. This figure presents the stress-strain cycle expected to occur during each flight. This above model is applicable to any generic metal exposed to extreme thermal cycling.

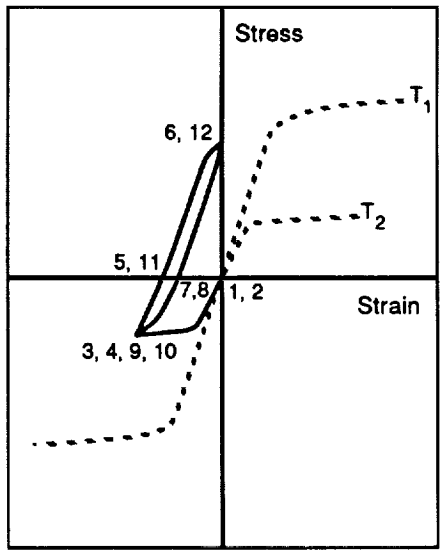

GP93-0239-80-D

Figure 80. Strain Amplitude Caused by External Loads Only

In the case of Hastelloy X the stress-strain history is described in Figure 81. The cycle is defined by the elastic stress of -120 ksi of Figure 74, which results in a strain range $\Delta\varepsilon$ of 0.0076 in./in. and a maximum stress f_{max} of 53 ksi. The material suffers fatigue damage as the temperature varies from 75° to 1800° and back to 75°. The two limits in predicted fatigue life are obtained by assuming that all fatigue damage occurs at either room temperature or at 1800°. The latter assumption results in a very conservative lower bound life of 200 flights. On the other extreme, life at room temperature is 34,000 flights. These values of fatigue life were obtained by calculating effective strain with equation (1) and referring to the curves in Figure 76 at the appropriate temperature. The "real" life falls between these two limits since damage occurs during constantly changing temperature.

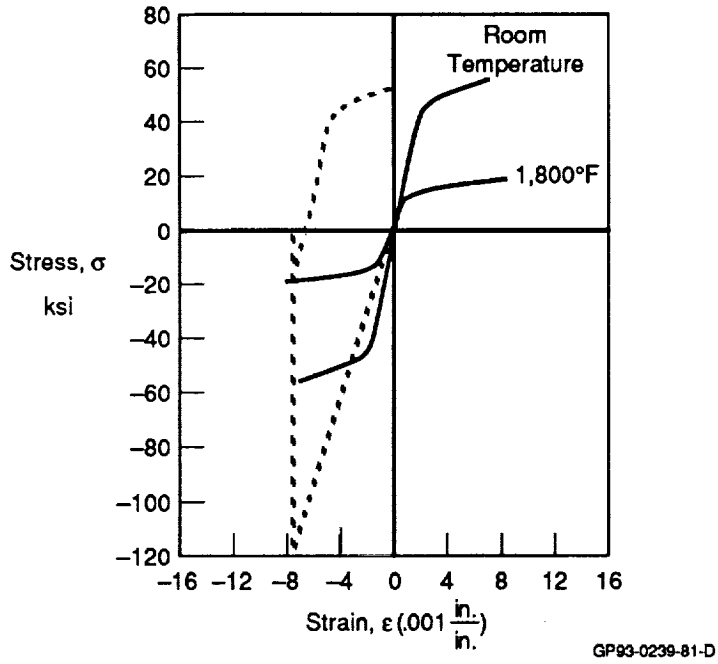

Figure 81. Hastelloy X Stress-Strain History

In order to study the effect of the wick, two stress concentration factors equal to 1.5 and 2.0 were included in the analysis. These K_ts cover the range of stress concentrations expected to be caused by the wick. A Neuber analysis was used to find the stresses and strains caused by the stress concentrations. The resulting stress-strain histories are shown in Figures 82 and 83. Predictions of fatigue life (without scatter factors) for

the various stress concentration factors are summarized in Figure 84. It is evident that stress concentration factors cause a dramatic decrease in fatigue life.

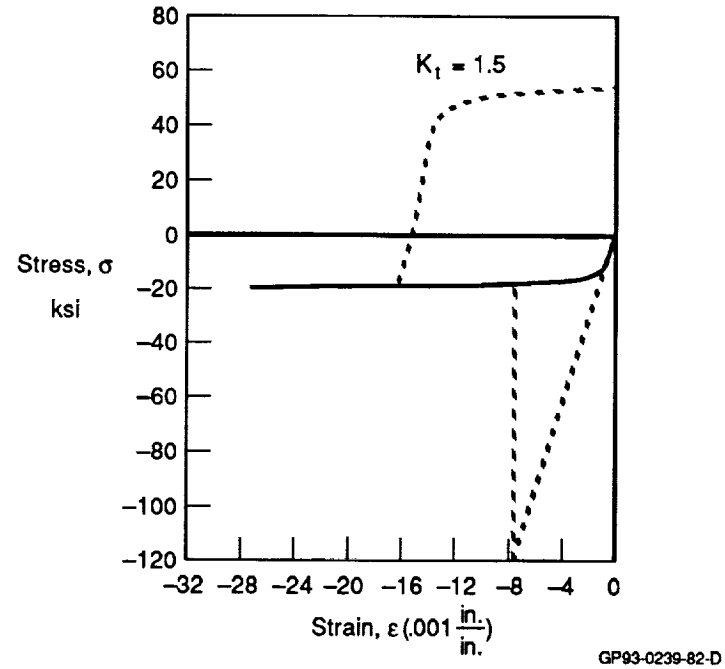

Figure 82. Heat Pipe Stress-Strain History (K_T = 1.5)

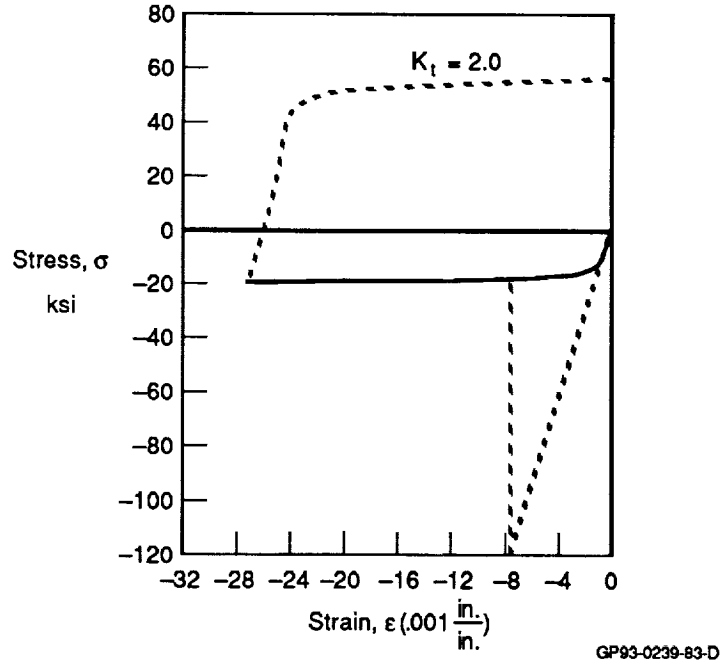

Figure 83. Heat Pipe Stress-Strain History (K_T = 2.0)

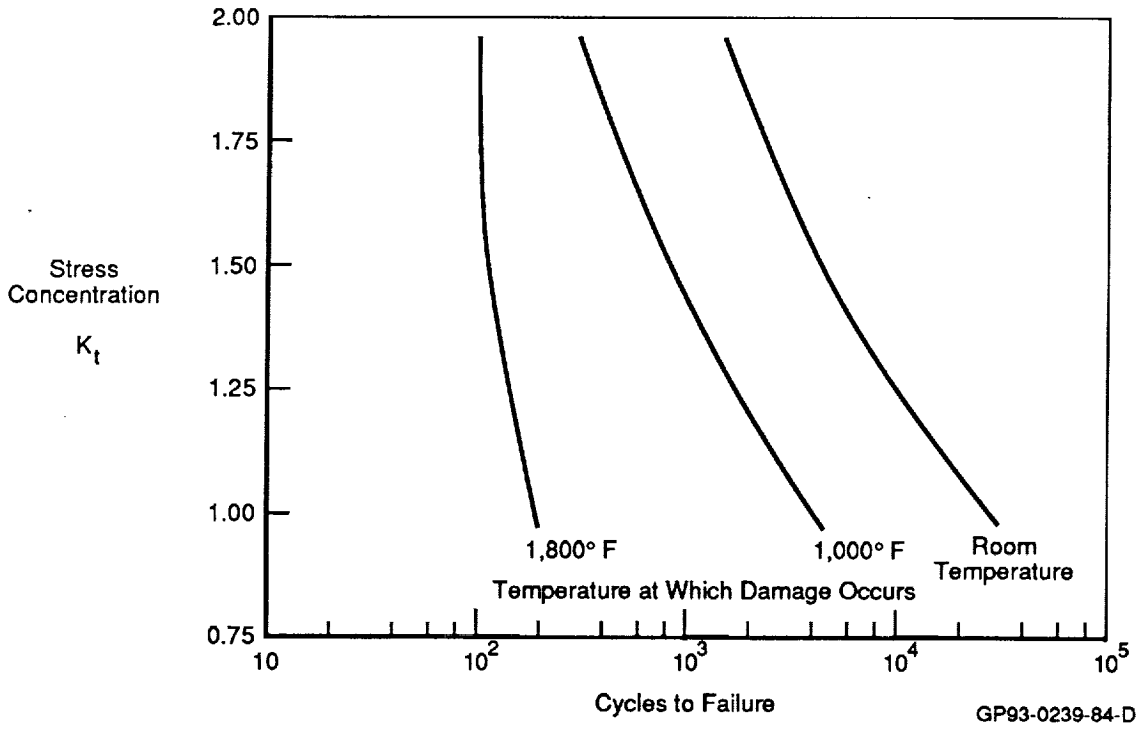

Figure 84. Heat Pipe Fatigue Life vs. Stress Concentration Factor

Fatigue Anaysis Conclusions

The critical fatigue area was determined to be the region of maximum compressive thermal stresses at S=1.6 inches from the leading edge (Figure 74). At this location, high residual tension occurs as a result of the thermal cycle. The predicted fatigue life under extreme conditions could be as low as 100 flights. In addition, there can be other complications due to the interactions between the wick and the heat pipe. This includes stress concentration factors and differences in thermal expansion.

The other locations studied (extruded corner, weld joint, etc.) do not present fatigue problems. Predicted fatigue lives were longer than 10^5 flights at these areas.

The analysis was preliminary and was limited by the available data on Hastelloy X. A more complete analysis should involve a gradual transition from room temperature to 1800°F in a series of steps. The fatigue damage due to the incremental steps should be calculated and added to give the total damage expected during each cycle. This requires more strain versus fatigue life data at different temperatures.

The computations completed and reported herein ignore the effect of creep since they assume that fatigue damage is caused by the residual thermal stresses during each flight. The interaction between fatigue cycles and creep must be evaluated and, if present, incorporated into future analysis.

6.4 HEAT PIPE FAILURE ANALYSIS

The test article assembly (Figure 34) consists of wall-to-wall heat pipes brazed to each other and a 0.030 inch face sheet and oriented normal to the swept wing. A basic objective of heat pipe design was to prevent catastrophic failure should a heat pipe fail. Failure protection analyses were categorized in two groups: (1) prevent burn through of the failed heat pipe external wall, and (2) allow burn through of failed heat pipe external wall but prevent burn through of internal wall and adjacent heat pipes. These failure modes are illustrated in Figure 85 for the sodium/Hastelloy X configuration. The corresponding three and one-half heat pipe heat transfer models used are shown in Figures 86 and 87. Twenty of these sections were modeled over the heat pipe length.

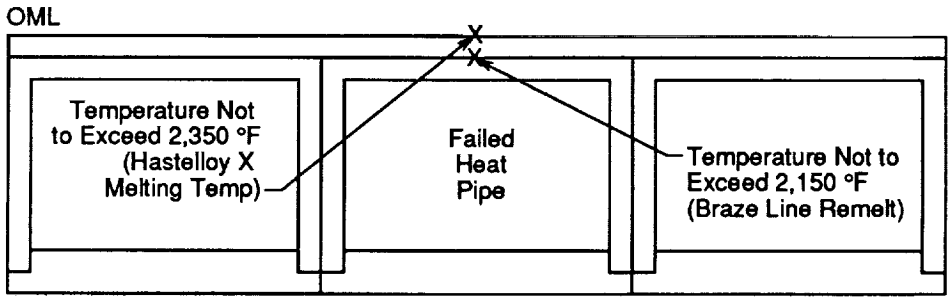

(a) Prevent External Wall Burn Through

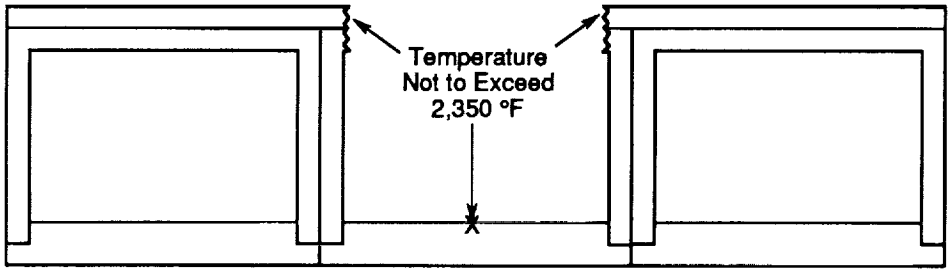

(b) Allow External Wall Burn Through But Prevent Additional Wall Burn Throughs

GP93-0239-85-D

Figure 85. Failure Analysis Modes

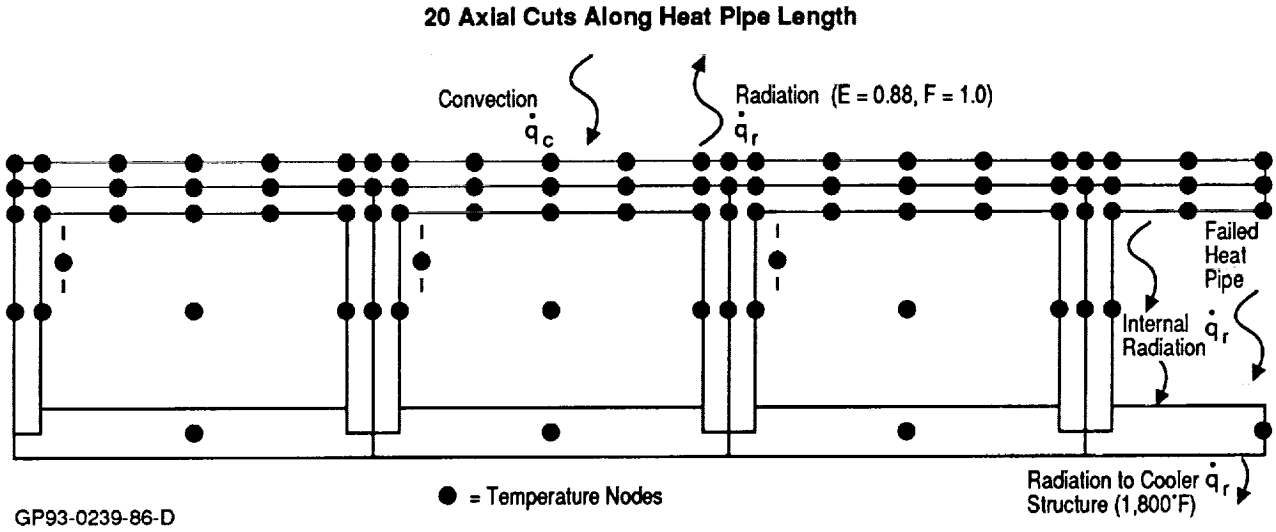

Figure 86. Heat Transfer Model of Failed Heat Pipe (No Burn Through)

C-2

(a) Burn Through Section ~ Used for 3 Sections: $-2.0 \leq S \leq 0.4$

Modifications :
- External Nodes Deleted
- Convection Increased in Cavity
- Radiation to Sky Reduced in Cavity
  (Parallel Resistance Added for Transverse Heat Pipes)

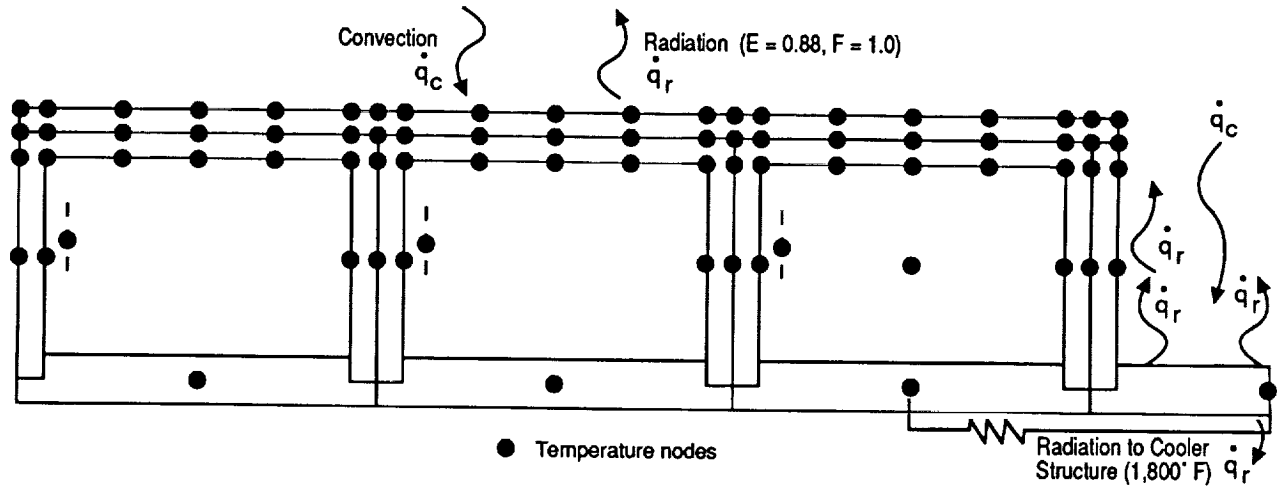

(b) Non Burn Through Section - Used for 17 Sections:
$-4.8 < -2.0$
$0.4 < S < 64.6$ } T_{OML} Below 2350° F

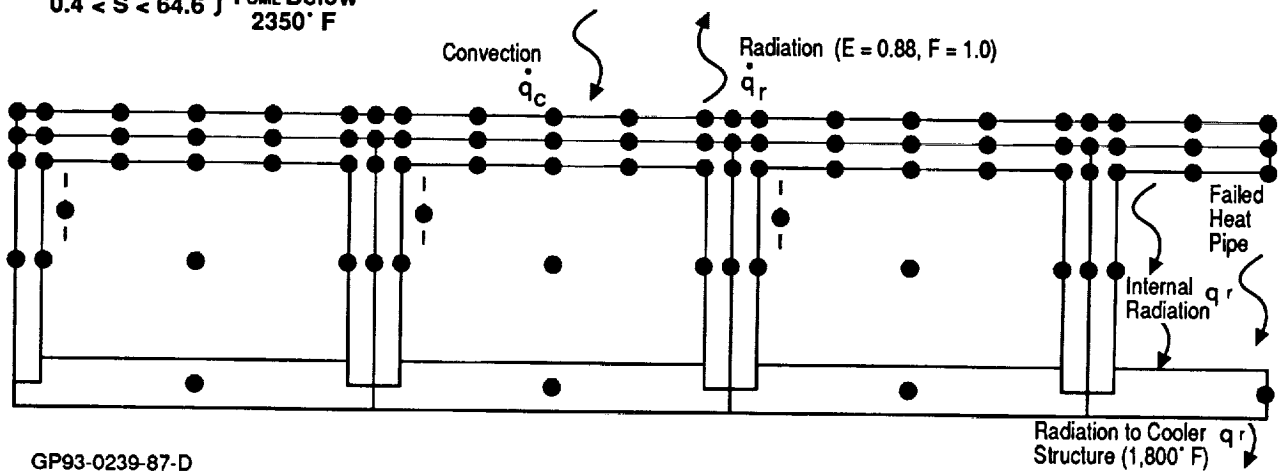

GP93-0239-87-D

Figure 87. Heat Transfer Model of Failed Heat Pipe (Burn Through)

Failure analysis results (Figure 88) showed that for the 0.5 inch wide heat pipes the outer moldline temperature exceeds the Hastelloy X melting temperature (2350°F) and the adjoining heat pipe's face sheet/case braze line remelt temperature (nominally 2050°F) would be exceeded. The 0.5 in. width was selected based on "conservative" producibility limits in order to successfully fabricate the test article within program constraints. Based upon experience gained in fabrication of the test article, narrower heat pipes may be producible. As shown in Figure 89, heat pipe width's less than 0.375 in. are necessary to prevent melting of a failed heat pipe outer moldline.

Additional variations in test article geometry (length, face sheet thickness, and face sheet thermal conductivity) were investigated for prevention of burn through. Figure 90 shows that significant increases in length, while reducing the vapor temperature, do not significantly decrease the maximum external wall temperature of the failed heat pipe. Therefore, increasing heat pipe length is not a feasible method of preventing burn through.

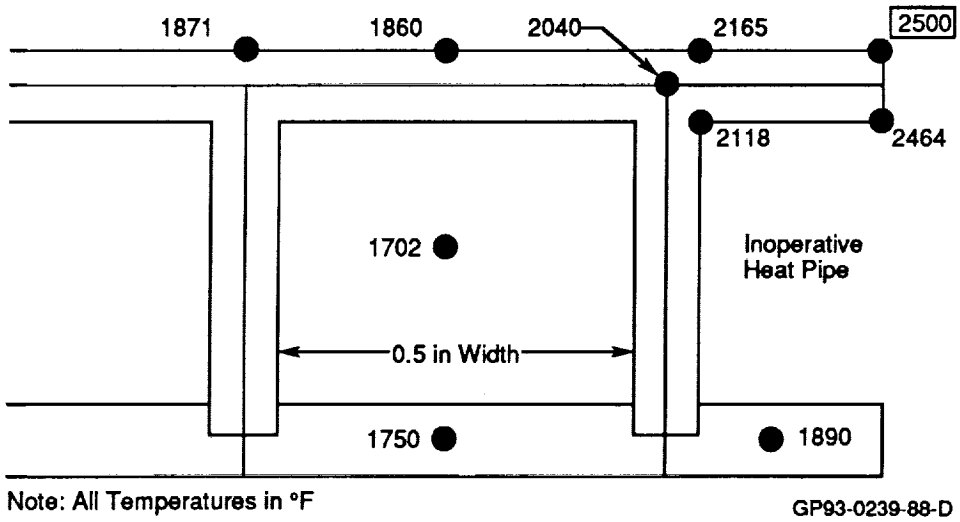

Figure 88. Burn Through of Inoperative Heat Pipe Predicted for Test Article Design

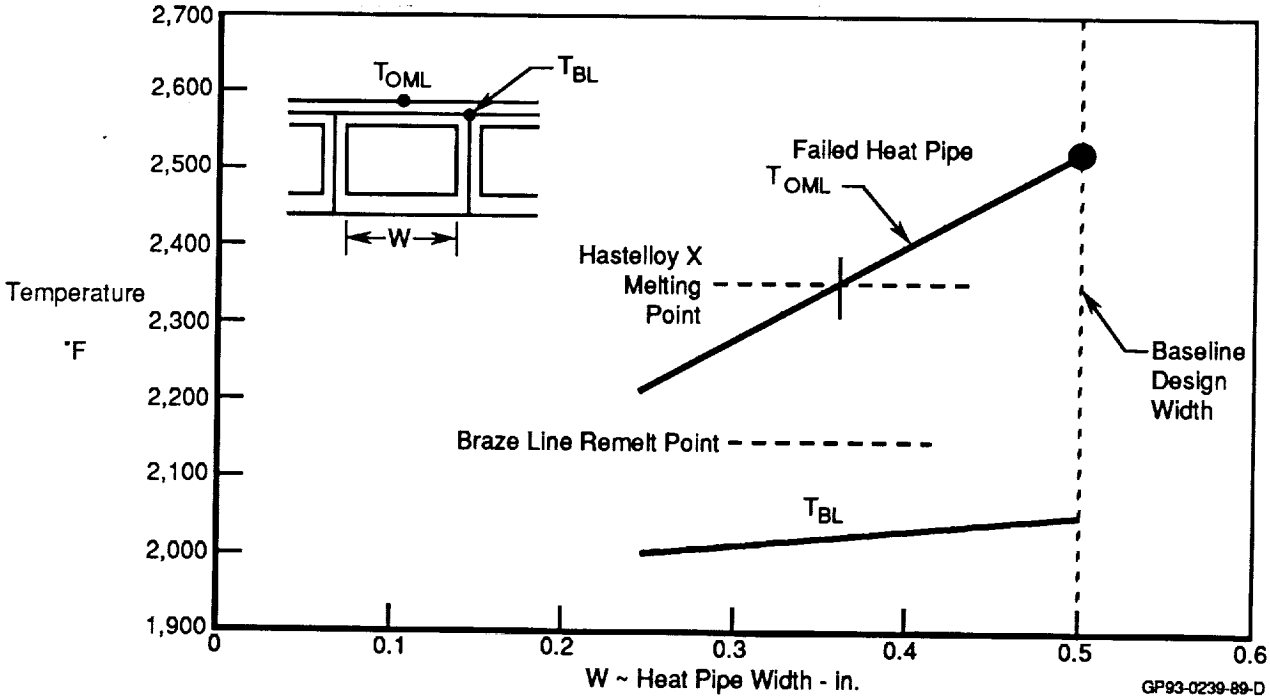

Figure 89. Small Heat Pipe Widths Necessary to Prevent Burn Through

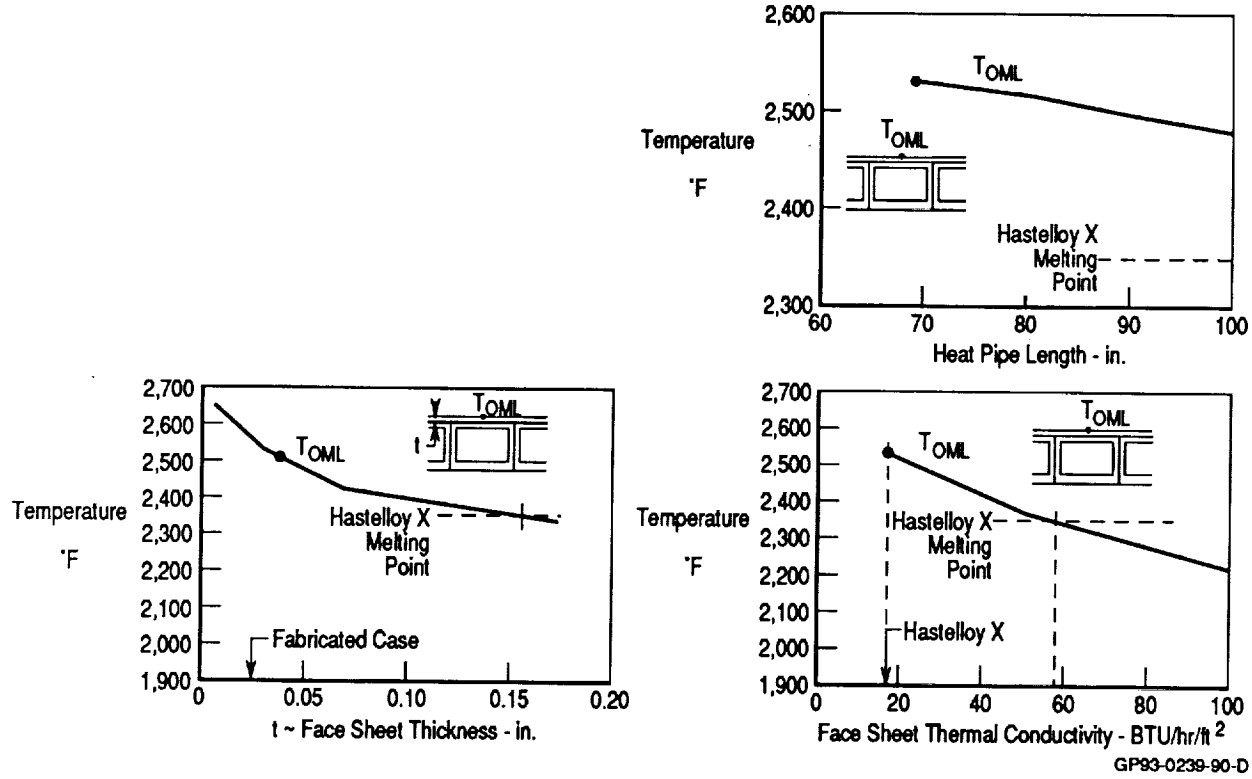

Figure 90. Additional Design Changes to Prevent Burn Through Require Significant Penalties

Increasing the face sheet thickness of the current design can reduce the failed heat pipe temperatures (Figure 90). However, the thickness must be increased by a factor in excess of five times to maintain the outer moldline temperature below the braze alloy melt temperature. This represents a significant weight penalty.

Figure 90 also confirms that increasing the face sheet thermal conductivity reduces the failed heat pipe temperatures. However, the use of a non-superalloy face sheet material would be required to significantly reduce temperatures. This can result in other problems (e.g., thermal expansion mismatch) that would require investigation.

An alternative method to increase the effective face sheet thermal conductivity would be the use of stagnation region externally mounted transverse heat pipes in the stagnation region (see Figure 91). These transverse heat pipes eliminate temperature gradients in the transverse or spanwise direction. The use of external transverse heat pipes may also allow the longitudinal heat pipe geometry to be modified. "D" shaped tubes with a wider spacing between tubes may be possible and could result in a significant weight savings.

The impact of allowing external wall burn through was also investigated. Analyses were conducted with and without internally mounted transverse heat pipes. The effects of increased external convection in the cavity was predicted using relationships for stagnation heating on a cylinder, assuming its radius equal to the inner wall radius. Additional convective heating due to the cavity was not modeled. A hemi-cylinder distribution multiplier was used to account for heating away from the stagnation line. Radiation view factors were calculated between the inner walls and the sky to account for radiation heat transfer. A parallel resistance through the transverse heat pipe was calculated (assuming a similar heat pipe design) and the resulting effective conductivity was added to the model.

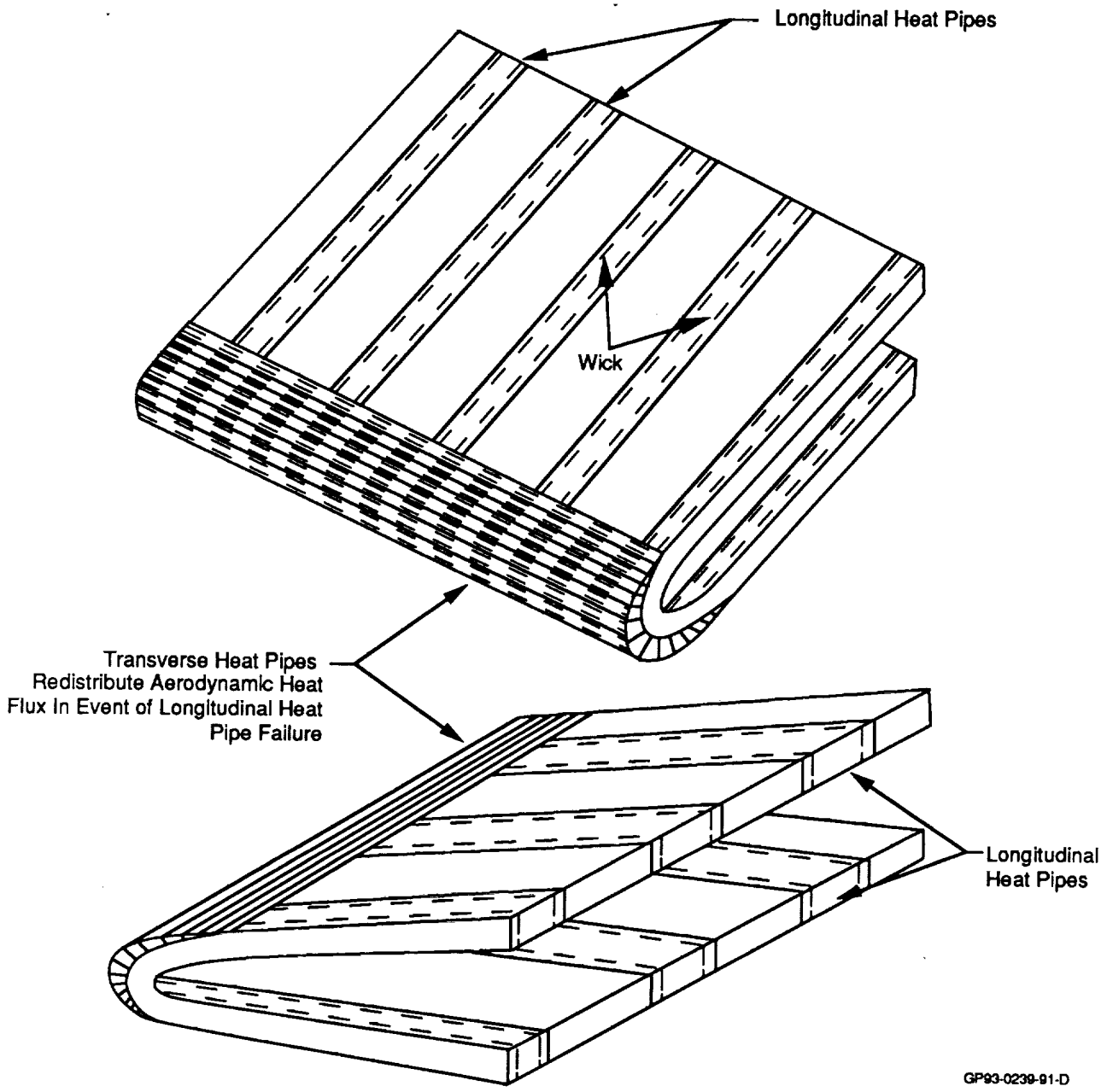

Figure 91. External Transverse Heat Pipes Provide Failure Protection

Resulting temperature distributions without transverse heat pipes, are shown in Figure 92. As expected, the inner wall temperature will also exceed the Hastelloy X melting temperature and catastrophic failure would result. If internal transverse heat pipes are used (Figure 93), inner wall temperatures would remain below the melting temperature, preventing the original failure from propagating. Use of internal transverse heat pipes, unlike those mounted externally, does not eliminate the steady-state spanwise temperature gradients.

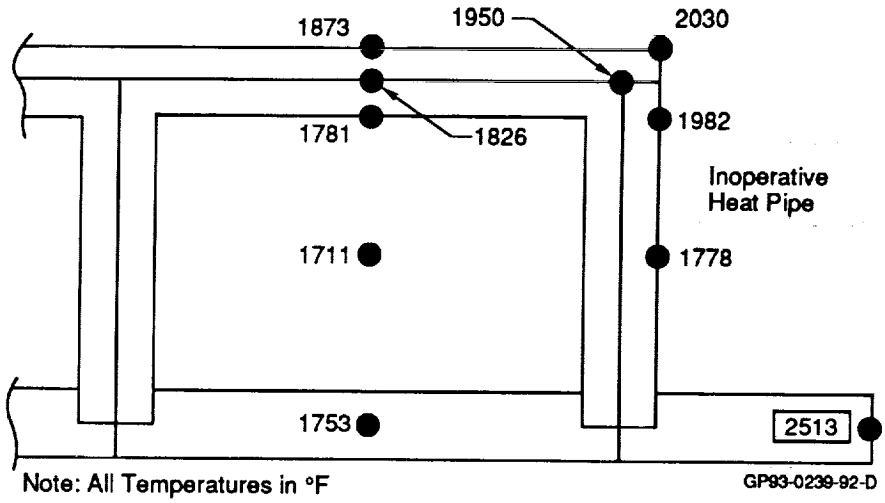

Figure 92. Allowing Burn Through Results in Melting of Inner Wall

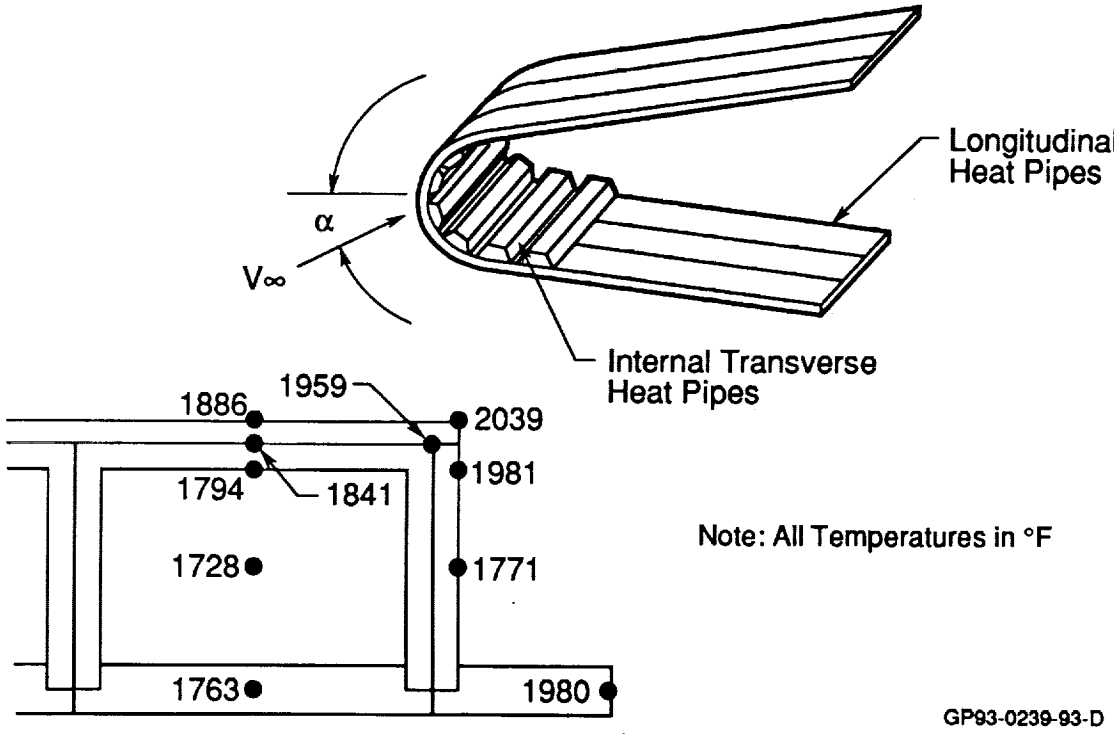

Figure 93. Internal Transverse Heat Pipes Provide Failure Protection

6.5 ALTERNATE MATERIALS ASSESSMENT

Hastelloy X was chosen for the test article because of its availability, selection in previous studies, and its proven long term compatibility with sodium. The effect of substituting another superalloy and even use of a lithium/refractory metal (molybdenum) heat pipe is discussed in this section.

Alternate Superalloys - Use of a different superalloy would have a minimal effect from a heat transfer point of view. Since superalloys have similar useful temperature ranges and thermal conductivities, the heat pipe length and temperature distribution during normal, transient, and failure operation would be similar. The greatest impact of a different superalloy is on weight.

Precipitation hardened grades are not suitable for this particular application where the heat pipe must sustain 1800°F for 75 hours. In this environment microstructural changes occur, which degrade the mechanical properties. These include the breakdown of primary carbides, agglomeration of the primary strengthening phases, and formation of embrittling phases. Therefore, precipitation hardened grades would be suitable only if the temperature, or time at temperature, was decreased.

Alloys such as Alloy 188, Inconel 617, and Inconel 625, are more suitable for this application. Trade studies comparing relative weights for these superalloys and tube geometries were performed for an 1800°F sodium/superalloy heat pipe. Wall thicknesses and weights were calculated using Hastelloy X, Alloy 188, Inconel 617, and Inconel 625 for a 0.5 in. rectangular tube and a 0.75 in. diameter rectangular D-tube. This D-tube dimension provides a vapor space area similar to the rectangular tube.

A minimum gage of 0.015 inch was used in the study. Our experience has shown this to be a fabrication and handling limitation due to the low room temperature yield strength of these materials. This gage met the design requirements for the "D" tube inner skin for all conditions studied.

Four design conditions were evaluated:

(1) No failure at Burst Pressure (twice normal operating)

(2) No yield at Normal Operating Pressure

(3) No creep rupture failure during 150 flights

(4) 5% creep deformation in 150 flights

The weight results are shown in Figure 94. The results show how weight comparisons and thus tube shape and material selection depend on the design criteria. For short life applications an Alloy 188 heat pipe would result in the lightest weight. As life requirements increase, the improved creep performance of Inconel 617 yields a reduced weight heat pipe.

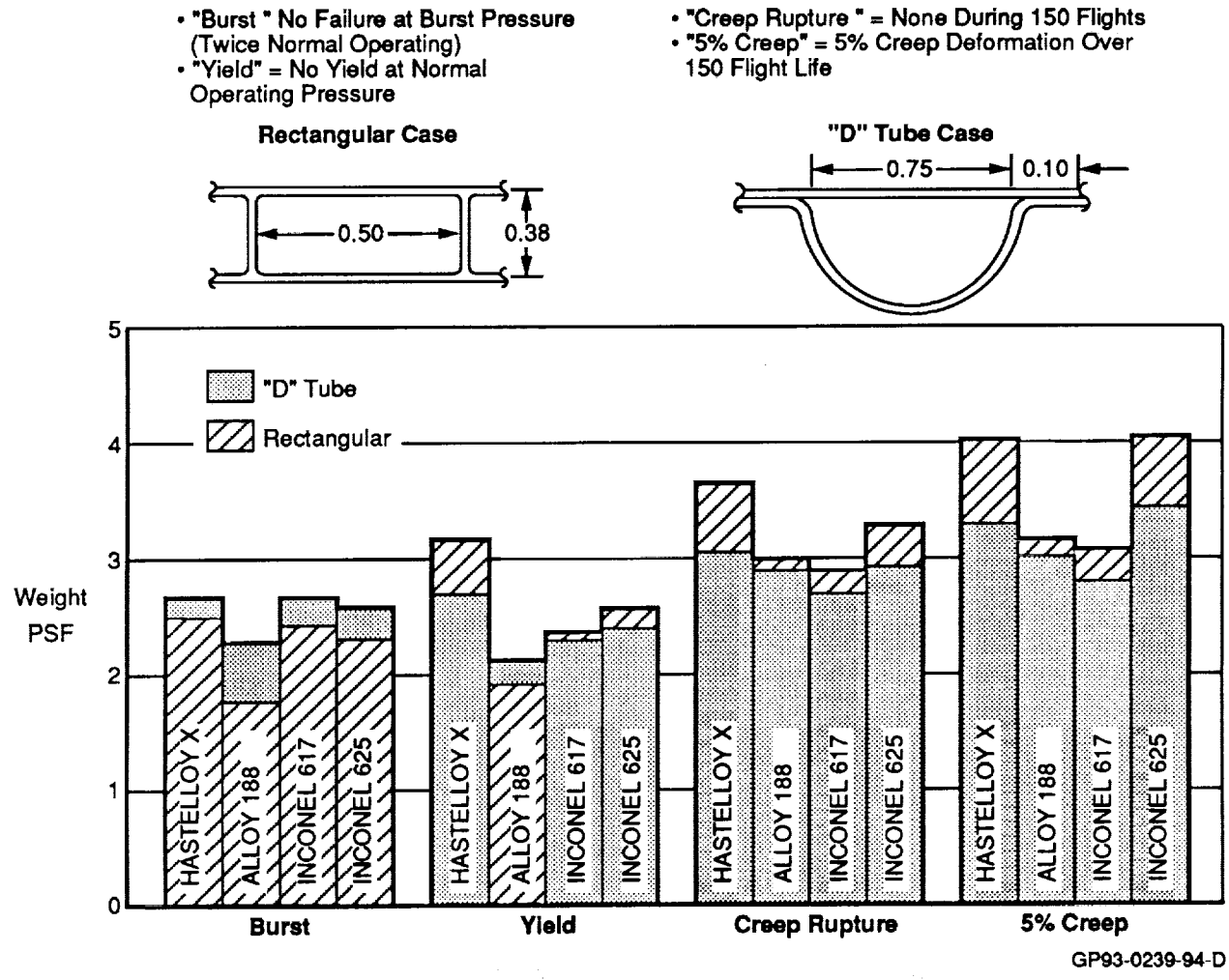

Figure 94. Weight Comparisons of Superalloy Heat Pipes

The rectangular heat pipe configuration results in the lowest weight for short life applications. This is due to the short span between web supports (0.5 inches). However, as life requirements increase, the "D" tube becomes the lower weight configuration. This is because the inner skin carries the pressure efficiently in hoop tension and compensates for the heavier mold line skin required due to the long span between supports (0.75 inches).

Lithium/Molybdenum Heat Pipe - Use of a lithium/molybdenum heat pipe in place of the sodium/Hastelloy X heat pipe for the advanced shuttle application would result in a radically different design. To take full advantage of their properties a lithium/molybdenum heat pipe would operate at a much higher temperature than a sodium/Hastelloy X heat pipe (2400°F vs. 1800°F). As a result the heat pipe would be much shorter (21.7 in. vs. 69.4 in. at the wing tip). Because of the shorter length, the wick requirements are much less and a simpler wick design can be employed. Also, because of its shorter length, the wick could be installed into a one-piece case instead of the current two-piece case. This would allow optimization of the case cross section based on weight (possibly a D-tube design). While a stress analysis of a lithium/molybdenum heat pipe was not performed, the shorter length should be much easier to integrate into a wing leading edge design.

A lithium (working fluid)/molybdenum (case material) heat pipe failure analysis was performed. For simplicity, the cross-sectional geometry was the same as used in the Sodium/Hastelloy X heat pipe analysis. The critical dimension in heat pipe failure analysis is the heat pipe width. So to compare this analysis with previous Sodium/Hastelloy X analysis results, the same width was used. Other dimensions such as depth and wall thickness have a minor effect. The heat pipe length was shortened from 69.4 in. to 21.7 in. in order to operate at higher working fluid temperatures.

The results are shown in Figure 95. The maximum outer mold line increases from 2443°F to 2718°F (locally) due to the heat pipe failure. The sodium/Hastelloy X heat pipe showed an increase from 1882°F to 2538°F which exceeded the Hastelloy X melting temperature. The 2718°F maximum molybdenum temperature is well below its melting temperature but needs to be compared with coating limitations. Therefore, the lithium/molybdenum heat pipe may offer a solution for fail-safe design.

While the lithium/molybdenum heat pipe is attractive because of its higher operating temperature capability and potential for fail-safe design, it is limited by the durability of oxide-resistant coatings. In addition, molybdenum is less ductile than Hastelloy X and may not readily lend itself to being bent to small leading edge radii. Lithium's stringent purity requirements will also effect manufacture of these heat pipes.

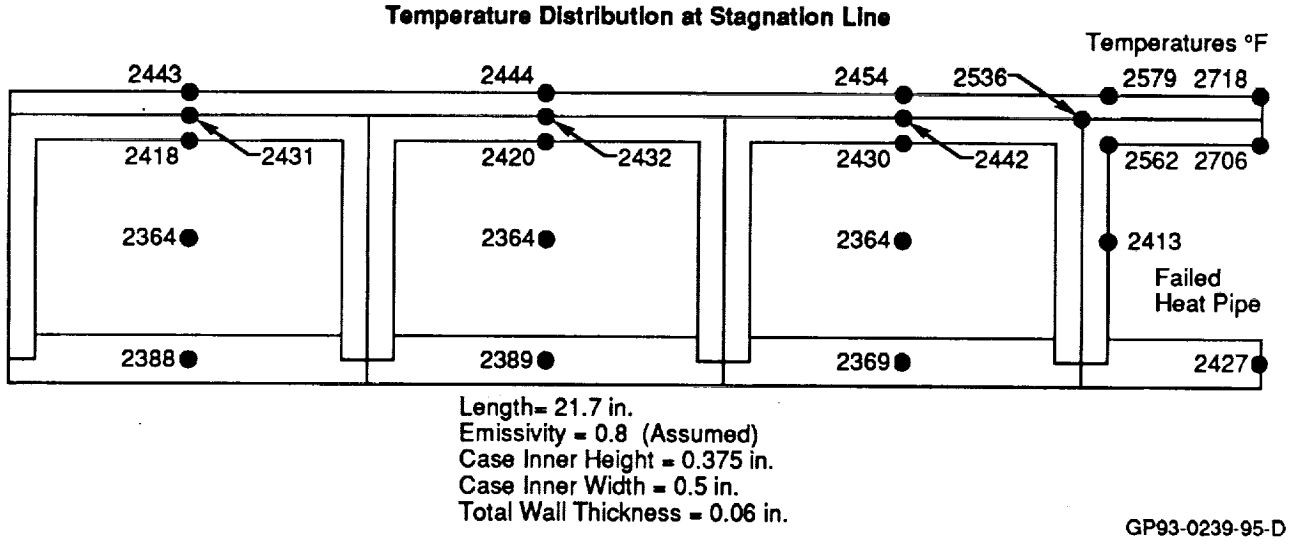

Figure 95. Lithium/Molybdenum Failed Heat Pipe Analysis Results

7.0 TESTING

A test stand capable of testing the single heat pipe was designed and fabricated. The test stand was designed to also test a five heat pipe assembly in which one of the heat pipes could be disabled if NASA elects to pursue this option at a later date. A test plan was formulated to prepare for testing of the single heat pipe. Testing of the test article is planned to be conducted at MCAIR under company funded Internal Research and Development (IRAD), and later at NASA LaRC.

7.1 TEST OBJECTIVES

Objectives of the test program include:

- Demonstrating the heat pipe's performance capability and structural integrity during steady-state and transient operation.

- Gathering test data to increase the understanding of heat pipe behavior during startup and validate current startup prediction methodologies.

Verification of heat pipe startup and operational capability will be achieved by exposing the test article to heating rates up to the maximum values anticipated during the advanced Shuttle re-entry (98 $Btu/s/ft^2$). A graphite heater will be used to radiatively heat the leading edge of the test article at various rates.

The test program will include both steady state and transient tests. In the steady state tests, the heating rate will be increased in finite increments, and the temperature of the test article allowed to approach the steady state after each increment. In the transient tests, the heating rate will be varied with time to simulate an advanced shuttle re-entry heating profile, with the peak heating rate to be increased incrementally for each test up to the maximum expected value.

Instrumentation will be provided to measure test article external surface temperatures, internal vapor temperatures, and pressures. Prior to the heat pipe test, a calorimeter will be used to correlate the incident surface heat flux over the leading edge region with graphite heater power. The total heating rate will be found from measurements of the water flow rate and inlet and outlet water temperatures of a water-cooled calorimeter. This calorimeter will enclose the outer heat rejection surface of the test article, absorbing virtually all of the heat radiated from the heat rejection surface.

Test data will be analyzed to establish surface temperature time and spacial variation, heat pipe heat transport rates versus time, and the velocity at which the high temperature continuum front moves into cooler sections of the test article. Also, time and spacial variations in the internal vapor pressure and temperature, and temperature gradients through the outer skin and wick, will be determined.

After the conclusion of each test, the test article will be examined for evidence of structural changes, corrosion, and fluid leakage before proceeding with the next test.

Conclusions will be drawn regarding the capability of the heat pipe leading edge test article to maintain leading edge temperatures within design limits during the advanced Shuttle re-entry trajectory, while maintaining its structural integrity.

7.2 TEST STAND AND INSTRUMENTATION

The purpose of the test stand is to support the test article and simulate the expected re-entry heat transfer to and from the test article. The test stand, shown schematically in Figure 96, consists of four major components:

- o graphite heater
- o evaporator absorber
- o condenser absorber
- o supports

To prevent oxidation of the graphite heater the test stand must be located in an evacuated or inert atmosphere.

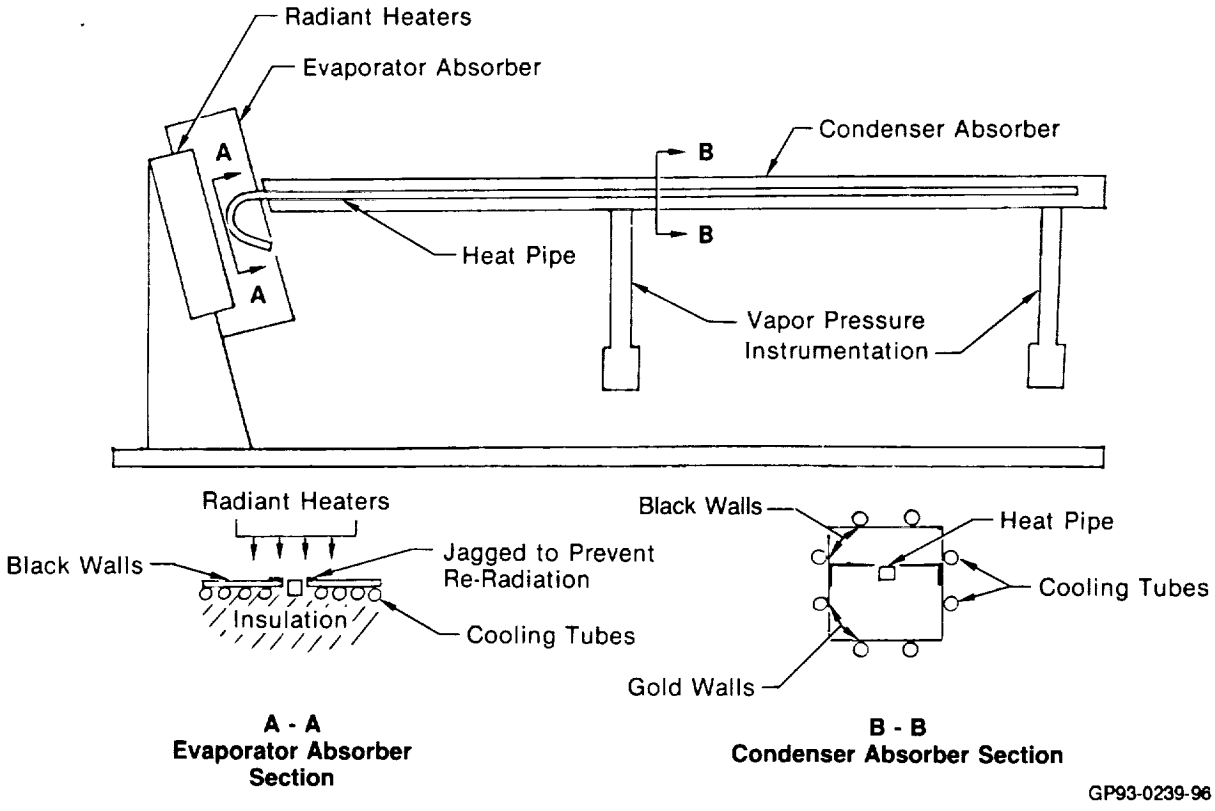

Figure 96. Heat Pipe Stand Simulates Thermal Environment

The graphite heater (Figure 97) will be used to simulate the net heat transfer (aeroheating less radiation-to-space) into the leading edge region of the heat pipe during re-entry. Both the stagnation line heating history and leading edge heating distribution will be simulated. A comparison between the predicted net heat transfer distribution during re-entry (at the time of peak heating) and the predicted net heat transfer distribution from the 5200°F radiant heater spaced 1 inch from the heat pipe is shown in Figure 98. Thus, use of the graphite heater to simulate the aeroheating is feasible. A calorimeter will be used to measure the actual heating rate distribution.

The purpose of the evaporator absorber shown in Figure 96 is to minimize the heat leakage out the back and side of the heat pipe and minimize

re-radiation back to the heaters. Initially, a system to insulate the heat pipe side walls and back face was investigated. However, analysis showed that re-radiation from the insulation back to the heater could result in heater problems. Therefore, a cooled, nickel covered copper plate with cooling tubes is aligned with the heat pipe and spaced 0.030 in. from the side walls. The plated portion of the plate is grooved to prevent re-radiation directly back to the heaters. The gap between the cooled plate and heat pipe prevents significant heat conduction and convection in this area.

GP93-0239-97

Figure 97. Graphite Heater Used in Test Stand

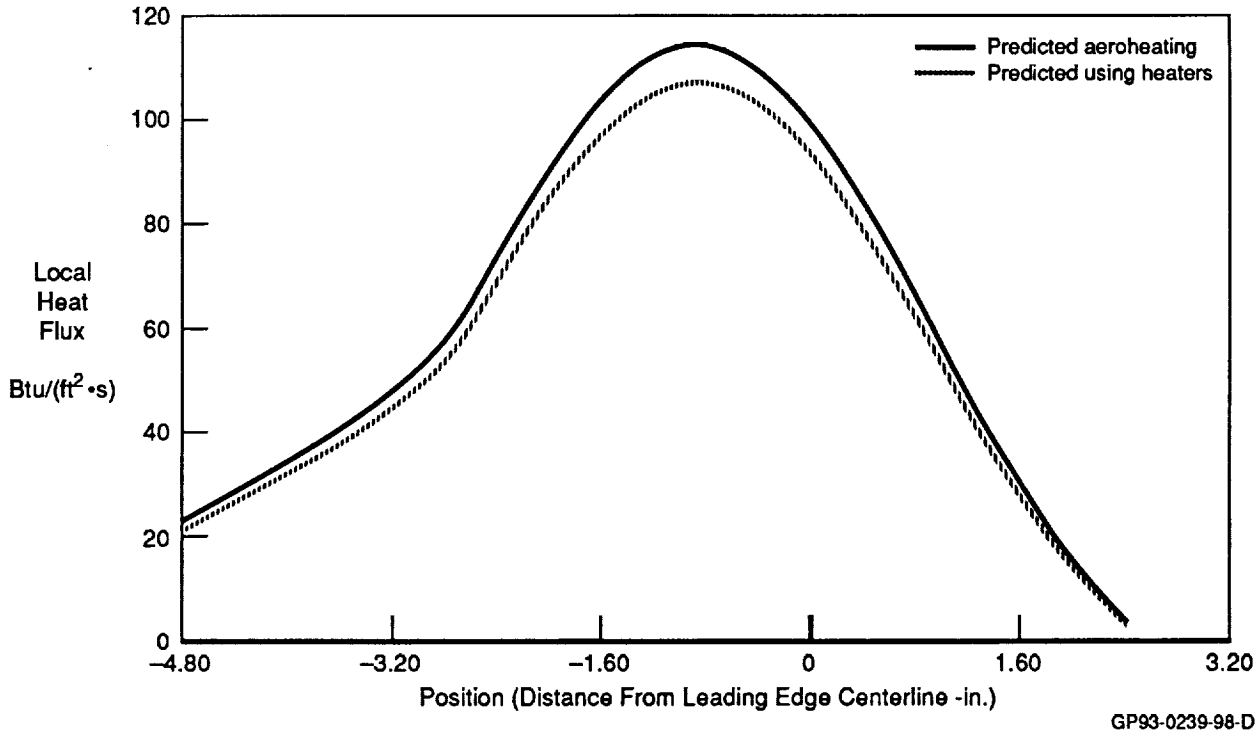

Figure 98. Graphite Heaters Simulate Aerodynamic Heating Distribution

The condenser absorber, shown in Figure 96, acts to simulate radiation from the heat pipe to space during re-entry. Again, to prevent excessive side and back face losses an active system is used. The condenser absorber is a cooled rectangular box. The inner walls, which the side and back of the heat pipe can radiate to, are lined with gold tape to minimize the radiant energy exchange. The wall which the top of the heat pipe can radiate to is lined with a one inch wide gold tape strip. The remaining walls, that the front of the heat pipe can radiate to, are plated black to maximize the radiant energy exchange. The condenser absorber, as will be shown, also serves as a calorimeter to measure the heat rejected by the heat pipe.

The remaining test stand structure serves to support the heat pipe test article, graphite heaters, absorbers, and instrumentation. Photographs of the completed heat pipe test stand are shown in Figures 99-101.

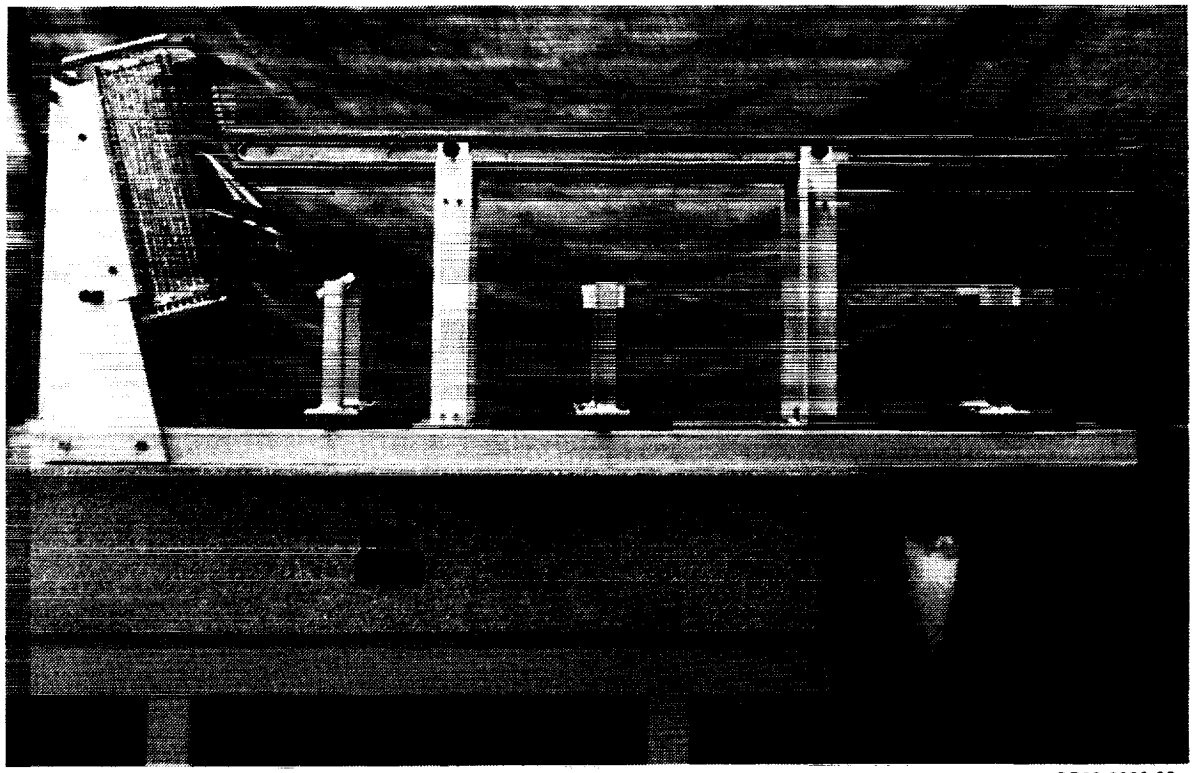

GP93-0239-99

Figure 99. Heat Pipe Test Stand

GP93-0239-100

Figure 100. Heat Pipe Test Stand Evaporator Section

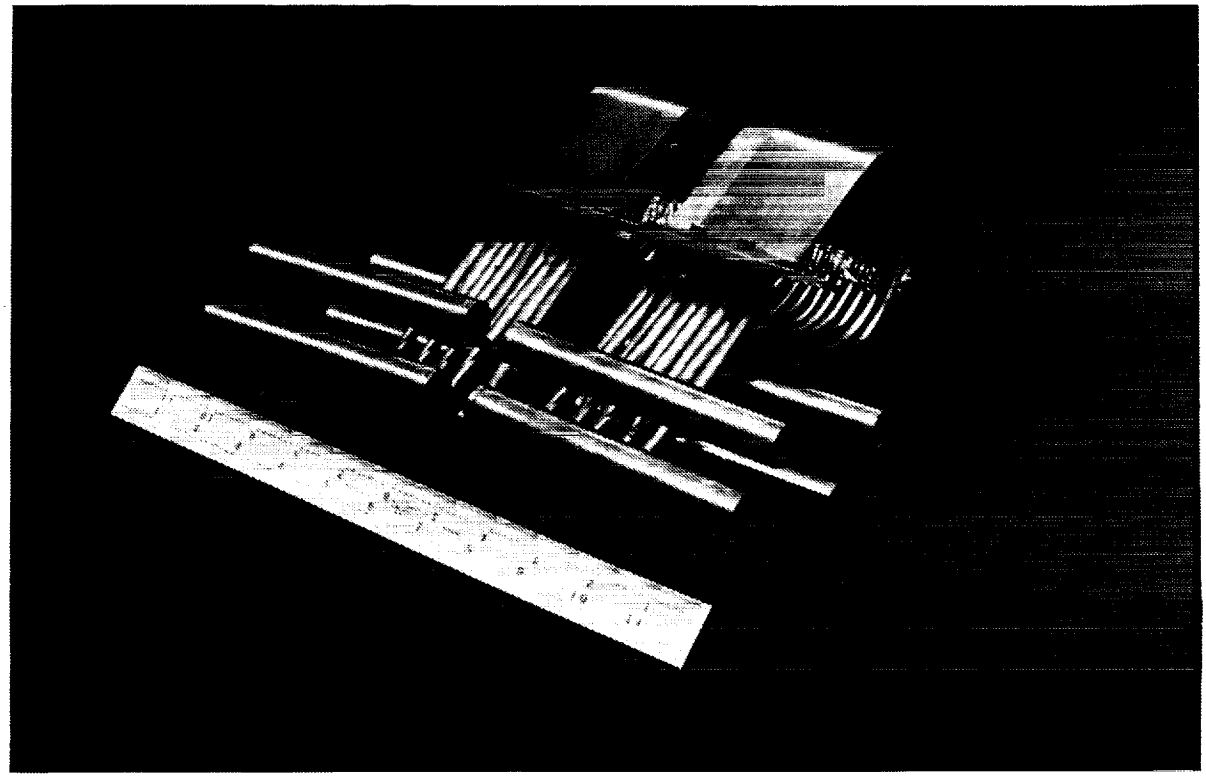

GP93-0239-101

Figure 101. Heat Pipe Test Stand Evaporator Absorber

As discussed in 5.3, the heat pipe test article was internally instrumented with ten thermocouples and three pressure sensors to measure the vapor conditions. This will enable a determination of thermodynamic equilibrium within the heat pipe during startup and steady-state operation. It will also allow determination of the hot continuum front passage during startup. Also the heat pipe was externally instrumented with fifteen thermocouples. These will be used to determine the presence of non-condensible gases, mark the passage of the continuum front, and more accurately determine thermal gradients during startup.

The leading edge heating distribution will be determined by substituting a calorimeter in place of the heat pipe into the test stand. The calorimeter was manufactured by Hy-Cal Engineering and has a 0-120 Btu/sec/ft^2 operating range. It operates on the Gardon principle. This type of calorimeter is fabricated from dissimilar metals. Water cooling is provided on the outer perimeter of the sensor. Incident radiation causes a radial temperature gradient. Due to the selection of metals (copper and constantan) the

gradient provides linear relationship between heat flux and sensor signal. Measurements will be made at various locations around the leading edge at various power levels. This will allow determination of heater power vs. time required to simulate the re-entry heating conditions.

The condenser absorber will serve as an on-line calorimeter. Cooling flow rates and temperatures will be measured to determine the amount of heat transfer radiated away from the heat pipe.

7.3 TEST PLAN DETAILS

A series of steady-state and startup tests are planned. Prior to these, heat flux tests will be performed to characterize the leading edge heating distribution at various heater power levels. Heater power levels which correspond to stagnation line heat fluxes of 20, 40, 60, 70, 75, 80, 85, and 90 $Btu/ft^2/sec$ will be determined. Heating rate distributions at five locations around the leading edge (-4.8 to 2.4 in. relative to the heat pipe centerline) will be determined at these power levels. The distribution will be compared to the analytical model for matching of flight environments.

Steady-state tests will be performed to confirm the test article's operational capability and establish a correlation between the heater power and condenser calorimeter power. Heater power will be increased in steps until the heat pipe is at 1800°F. Thermocouple and pressure response will be recorded and used to determine the continuum front passage, vapor-to-wall temperature changes, and the presence of non-condensible gas.

To perform the transient tests representative of an advanced Shuttle re-entry, the heater power level time variation to correspond to re-entry heating rates will be determined using results of the heat flux tests. Tests will then be performed at 60%, 80% and 90% of this heater power history. After each test, the test article will be examined for evidence of structural changes or leakage before the decision is made to proceed with the next test. Following completion of the 90% power test, a decision will be made whether to conduct a final transient run at 100% power.

Completion of the testing program is expected to establish the capability of the test article to limit leading edge temperatures to specified design limits, while maintaining structural integrity, during a representative advanced Shuttle re-entry trajectory.

Additional information developed in support of this result is expected to include: the heat transport adequacy of the test article design, the extent of spacial isothermality along the test article length, and characterization of the continuum temperature front. Also, the degree of thermal equilibrium in the heat pipe fluid, the vapor pressure distribution along the test article length, and the temperature drop through the wall and wick at the stagnation line will be established.

8.0 CONCLUSIONS AND RECOMMENDATIONS

Wing leading edge heat pipes were conceptually designed for three types of vehicles: an entry research vehicle, aero-space plane, and advanced shuttle. A full scale, internally instrumented sodium/Hastelloy X heat pipe was successfully designed and fabricated for the advanced Shuttle application. Heat pipe manufacturing technology was advanced during this program, including the development of an innovative technique for wick installation. A test stand and test plan were developed for subsequent testing of this heat pipe. The following conclusions were drawn from this investigation:

- Sodium/superalloy wing leading edge heat pipes should be limited to hypersonic vehicle applications where the heating environments are relatively mild and the resulting heat pipe lengths are relatively short.

- Higher temperature capability heat pipes, e.g. lithium/refractory metal concepts, would avoid the major concerns associated with sodium/superalloy heat pipes and increase the applicability of heat pipe designs.

- The structural integrity of high temperature heat pipes is very sensitive to maximum temperature levels and thermal gradients.

- Screen wick designs are feasible for long heat pipes.

Also, from this investigation the following recommendations are made:

- Startup performance of the completed heat pipe test article should be thoroughly evaluated, via testing, to validate design methodologies.

- Innovative heat pipe failure protection concepts should be designed and tested for various failure modes.

- Production manufacturing technology concepts for leading edge heat pipes should be developed.

- Higher temperature heat pipes should be designed, evaluated, and fabricated.

Testing of the heat pipe developed under this contract was performed under a MCAIR independent research and development program. Results of this test are presented in Reference 14.

9.0 REFERENCES

1. Camarda, Charles J., "Analysis and Radiant Heating Tests of a Heat-Pipe-Cooled Leading Edge", NASA TN D-8468, 1977.

2. Camarda, Charles J., "Aerothermal Tests of a Heat-Pipe-Cooled Leading Edge at Mach 7", NASA TP-1320, 1978.

3. Camarda, Charles J., and Masek, Robert V., "Design, Analysis, and Tests of a Shuttle-Type Heat-Pipe-Cooled Leading Edge", ASME-79-ENAS-20, 1979.

4. Camarda, Charles J., and Masek, Robert V., "Design, Analysis, and Tests of a Shuttle-Type Heat-Pipe-Cooled Leading Edge", AIAA 81-4020, 1981.

5. Colwell, G. Jang, H. J., and Camarda, C. J., "Modeling of Startup From the Frozen State", Sixth International Heat Pipe Conference-Grenoble, France, May 1987.

6. Hankey, W. L., Neumann, R. D., and Flinn, E. V., "Design Procedures for Computing Aerodynamic Heating at Hypersonic Speeds", WADC TR 59-610, 1960.

7. Engel, C. D., and Praharaj, S. C., "MINIVER Upgrade for the AVID System", NASA CR-172212, 1983.

8. Thomas, A. C., Perlbachs, A., and Nagel, A. L., "Advanced Re-entry Systems Heat-Transfer Manual for Hypersonic Flight", AFFDL-TR-65-195, 1965.

9. Brennan, P. J., and Kroliczek, "Heat Pipe Handbook", Prepared for NASA Goodard Space Flight Center under contract NAS5-23406 by B & K Engineering, Inc., Towson, MD., N81-70112, June 1979.

10. Dunn, P., and Reay, D. A., Heat Pipes, Pergamon Press, Oxford, 1976.

11. Peeples, M. E., Reeder, J. C., and Sontag, K. E., "Thermostructural Applications of Heat Pipes", NASA CR-159096, 1979.

12. Timoshenko, S. P., and Goodier, J. N., Theory of Elasticity, 3rd ed., McGraw-Hill Book Co., N.Y., 1970.

13. Aerospace Structural Metals Handbook, (Formerly AFML-TR-68-115), MCIC-ASMH, Code 4112, 1988.

14. Boman, B. L., and Herring, R. L., "Testing of a Sodium/Hastelloy X Wing Leading Edge Heat Pipe", MDC Report MDC B1889, December 1989.

NASA
National Aeronautics and Space Administration

Report Documentation Page

1. Report No.	2. Government Accession No.	3. Recipient's Catalog No.
NASA CR-181922		

4. Title and Subtitle	5. Report Date
Heat Pipes for Wing Leading Edges of Hypersonic Vehicles	December 1989
	6. Performing Organization Code

7. Author(s)	8. Performing Organization Report No.
B. L. Boman, K. M. Citrin, E. C. Garner, and J. E. Stone	
	10. Work Unit No. 506-49-11-05

9. Performing Organization Name and Address	11. Contract or Grant No.
McDonnell Aircraft Company P. O. Box 516 St. Louis, MO 63166	NAS1-18144
	13. Type of Report and Period Covered Contractor Report 3/25/86 thru 4/30/89

12. Sponsoring Agency Name and Address	14. Sponsoring Agency Code
National Aeronautics and Space Administration Langley Research Center Hampton, VA 23665-5225	

15. Supplementary Notes

Langley Technical Monitor: Charles J. Camarda
Final Report

16. Abstract

Wing leading edge heat pipes were conceptually designed for three types of vehicle: an entry research vehicle, aero-space plane, and advanced shuttle. A full scale, internally instrumented sodium/Hastelloy X heat pipe was successfully designed and fabricated for the advanced shuttle application. The 69.4 inch long heat pipe reduces peak leading edge temperatures from 3500°F to 1800°F. It is internally instrumented with thermocouples and pressure transducers to measure sodium vapor qualities. Large thermal gradients and consequently large thermal stresses, which have the potential of limiting heat pipe life, were predicted to occur during startup. A test stand and test plan were developed for subsequent testing of this heat pipe. Heat pipe manufacturing technology was advanced during this program, including the development of an innovative technique for wick installation.

17. Key Words (Suggested by Author(s))	18. Distribution Statement
Heat Pipes Thermal Protection Systems Hypersonic Vehicles	Subject Category 34

19. Security Classif. (of this report)	20. Security Classif. (of this page)	21. No. of pages	22. Price
Unclassified	Unclassified	122	

NASA FORM 1626 OCT 86